Chair of Metal Forming

Department Product Engineering
University of Leoben, Austria

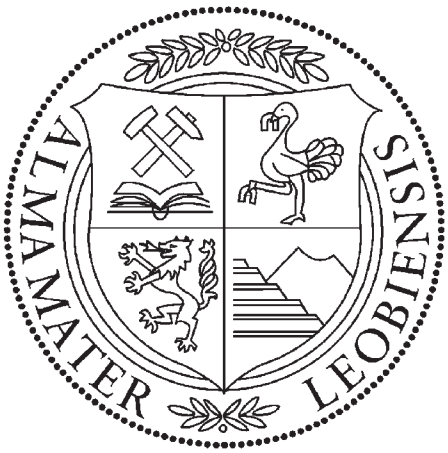

PhD Thesis

Grain structure design of hot formed and annealed multi phase alloys

Supervision
Prof. Dr. Christof Sommitsch

Mirza CANDIC

August, 2010

Affidavit

I declare in lieu of oath, that I wrote this thesis and performed the associated research myself, using only literature cited in this volume.

Leoben, 15 August 2010 Mirza CANDIC, MSc

Acknowledgements

I would like to express my sincere thank to my academic advisor Univ.Prof. Priv.Doz. Dipl.-Ing. Dr. C. Sommitsch for his constant support, encouragement, knowledge and friendship. I also thank my superior Univ.Prof. Dr. R. Pippan for his guidance and discussion during this work.

I am especially grateful to DDr. Tian Baohui for his invaluable advice on the experimental and theoretical advice throughout the project. My thanks also to many technicians in the Chair of Metal Forming in Leoben and Institute for Materials Science and Welding in Graz. I also grateful acknowledge the support of Dr. M. Kamaya from Institute of Nuclear Safety System in Sata (Japan).

Finally, I would like to express my sincere gratitude to my family for their ceaseless encouragement and unswerving loyalty over the years. To my wife Gurbet for making sure that I put all my time and energy in my PhD work and to my daughters Lejla and Alena for giving me a lot of fun.

Abstract

The aim of the presented PhD thesis is to develop a deterministic and a probabilistic Cellular Automata (CA) model to reflect the grain growth process for the solution annealing of austenitic stainless steel 304L (18-9 Cr-Ni, balance Fe). This uncontrolled exaggerated grain growth results in a negative influence on mechanical properties, e.g. strength, of the material.

In order to define what exactly launches the process of abnormal grain growth and what factors come into play, un-deformed cylindrical specimens were annealed at different temperatures (900°C-1200°C). At higher temperatures the start of abnormal grains occurred earlier. The un-deformed homogenized initial grain structures investigated by transmission electron microscopy proved the occurrence of faceted and rough grain boundaries, explaining higher mobilities during annealing of some grain boundaries and occurrence of abnormal grain growth. The solution annealing was carried out at 900°C, 1000°C, 1100°C and 1200°C for annealing times up to 40 hours. Abnormal grain growth started at 1200°C after 120 minutes, at 1100°C after 8 hours, at 1000°C after 12 hours and never at 900°C, due to grain boundary pinning resulting from the carbide precipitations on grain boundaries.

Simulated and experimental grain structures are comparable, and simulated results are very close to the underlying physics. Many physical parameters can be taken into account in both CA models. The grain growth process is not only demonstrated qualitatively but also used for a quantitative analysis of grain growth phenomena. Beginning from the predictions of average normal and abnormal grain sizes, then defining the grain sizes separating normal and abnormal grains, and an accurate description of grain size distributions are demonstrated. In the analysis of the simulated grain structures, the start of abnormal grain growth and improved definition of exact fraction of abnormal grains is evaluated. Especially an improved description of grain size distributions by incorporating a two parameter approach for the evaluation of grain size separating normal and abnormal grains, paves the way for an exact description of the grain growth process.

Kurzfassung

Das Ziel der vorliegenden Arbeit ist die Entwicklung eines deterministischen und eines probabilistischen Zellulären Automaten Modells. Während des Lösungsglühens von austenitischem Stahl 304L (18-9 Cr-Ni, Matrix Fe) sind die beiden Modelle in der Lage das normale und das abnormale Kornwachstum zu beschreiben. Dieses unkontrollierte Kornwachstum resultiert in einer negativen Beeinflussung der mechanischen Eigenschaften (z.B. Festigkeit) des Materials.

Um den Beginn und die Einflussfaktoren für abnormales Kornwachstum zu bestimmen, wurden unverformte zylindrische Proben lösungsgeglüht (900°C-1200°C). Mit steigender Temperatur kam es zu einem früheren Beginn des abnormalen Kornwachstums. Die mittels Transmissionselektronenmikroskopie untersuchte homogenisierte Anfangskornstruktur zeigte facettierte Konrngrenzen, die aufgrund höherer Mobilität während des Lösungsglühens das Auftreten des abnormalen Kornwachstums erklären. Das Lösungsglühen, das bis zu 40 Studen dauerte, wurde bei 900°C, 1000°C, 1100°C und 1200°C durchgeführt. Das abnormale Kornwachstum trat bei 1200°C nach 120 Minuten, bei 1100°C nach 8 Stunden und bei 1000°C nach 12 Stunden Glühzeit auf. Aufgrund der Ausscheidungen und der niedrigen Treibkräfte wurde bei 900°C kein abnormales Konrnwachstum fest gestellt.

Die Simulationen und die Experimente führten zu vergleichbaren Ergebnissen. Eine Vielfalt der physikalische Ansätze kann in den entwickelten Zellulären Automaten Modellen wiedergespiegelt werden. Der Kornwachstumsprozess wurde nicht nur in einer hohen Qualität gezeigt, sondern wurde auch dazu benutzt, quantitative Kornwachstumsphänomene zu erklären. Die Vorhersage der durchschnittlichen Korngröße des normalen und abnormalen Kornwachstums, die Definition der Korngröße die das normale und abnormale Korngefüge limitiert, beziehungsweise die exakte Beschreibung der Kornstrukturverteilung können dabei hervor gehoben werden. Durch die Analyse des simulierten Korngefüges, kann der Beginn des abnormalen Kornwachstums und die Verbesserung der metallographischen Definitionen des Anteils der abnormalen Körner am Gesamtgefüge gezeigt werden. Die verbesserte Beschreibung der Korngrößenverteilungen durch die Implementierung einer zwei Parameter Annäherung für das normale Kornwachstum, macht es möglich, die Kornentwicklung besser zu verstehen.

Contents

Acronyms

AGG	Abnormal Grain Growth
CA	Cellular Automata
CAS	Cellular Automata Step
CSL	Coincidence Site Lattice
DAM	Domain Averaging Method
DRX	Dynamic Recrystallization
EBSD	Electron Back Scatter Diffraction
FCC	Face Centered Cubic
FEM	Finite Element Method
HV	Vikers Hardness
MC	Monte Carlo
MCS	Monte Carlo Simulation Step
MCD	Modified Crystal Deformation
NGG	Normal Grain Growth
OPS	Oxid Polishing Suspension
PFM	Phase Field Modelling
REF	Reference Specimen
REG	Regression
SIC	Silicon Carbide
SRX	Static Recrystallization

List of symbols

A	area
A_0	initial average grain area
A_{growth}	grain growth constant
a_{jump}	jump distance of atoms
$\alpha - phase$	ferrite phase in steels
C	number of corners of a grain
C_1, C_2, C_3	constants
D_{rex}	diameter of grain after recrystallization
D_{gb}	diffusion coefficient for grain boundary
D^0_{gb}	constant for grain boundary diffusion
d_k	average grain diameter
d_c	distance of the MC lattice system
D_{max}	maximal grain size
ΔD	change in grain size
d_p	diameter of second phase particles
d^0_p	starting diameter of second phase particles
δ	grain boundary thickness
E	number of edges of a grain
E_{barr}	energy barrier
E_{GB}	grain boundary energy
E_n	net energy accompanying grain growth
f	fraction of second phase particles
G	shear modulus
h	step hight
γ	grain boundary energy
$\gamma - phase$	austenitic phase in steels
k	constant
k_{boltz}	Boltzman constant
M	mobility
M_0	constant

M_{Taylor}	Taylor factor
L	mean grain intercept
n	grain growth exponent
n_i	number of atoms i
P	number of polygons of a grain
$p_{boundary}$	pressure on grain boundary
p_{curv}	pressure on grain boundary resulting solely from grain curvature
p_{ret}	retarding force
p_{strain}	pressure on grain boundary resulting solely from strain
q	number of states in MC simulation
Q_{act}	activation energy for grain growth
Q_b	activation energy for bulk diffusion
R	radius of a grain
r	radius of a second phase particle
r_{nbh}	radius of neighborhood for the random automata modelling
R_0	initial grain radius
R_{AG}	radius of abnormal grains
R_{Cr}	critical grain radius
R_{cu}	radius of grain curvature
R_i	radius of grain `i`
R_t	radius of grain after time t
R_{gas}	universal gas constant
R_Z	Zener radius of grain
R_R	Rios radius of a grain
$\overline{R}$	average grain radius
$\widehat{R}$	grain growth rate
r	radius of a second phase particle
ρ_a	geometrically necessary dislocations
ρ_{total}	total dislocation density
ρ_m	dislocation density of the matrix

ρ_d	dislocation density of a dynamically recrystallized grain
$\rho_{spheres}$	number of spheres
σ_f	flow stress
$\sigma(T)$	step edge free energy
σ_{ij}	stress
ΔS_a	activation entropy
T	temperature
T_m	melting temperature
$T_{Helmholtz}$	Helmholtz surface free energy
t	time
t_0	initial or starting time
Θ_B	strain defined by Briant
τ_{disl}	dislocation line energy
V	molar volume
v_{gb}	grain growth velocity
v_{Atom}	the atomic vibration frequency
ΔX	grain boundary displacement
Z	ratio of radii of growing grain and matrix grain

1 Introduction

The aim of this PhD thesis is to develop a simulation set-up which reflects the solution annealing process of austenitic stainless steel 304L (18-9 Cr-Ni, balance Fe) when abnormal grain growth can occur. The solution annealing process defines the mechanical properties, e.g. toughness, over large areas and thus determines the possibilities for extensive field of application for metallic materials. Knowledge of the microstructural changes, e.g. grain growth, which takes place during the annealing process is of great importance for the evolution of the final structural condition of the material. The grain growth kinetics are strongly influenced by the grain structure topology, annealing temperature, precipitations, stored deformation energy and the grain boundary energy.

Depending on the growth behavior of the grains, grain growth can be classified into two types, shown in figure 1.1: normal or continuous grain growth and abnormal or discontinuous grain growth. The latter has also been termed exaggerated grain growth or secondary recrystallization and leads to an inhomogeneous distribution of material properties [1].

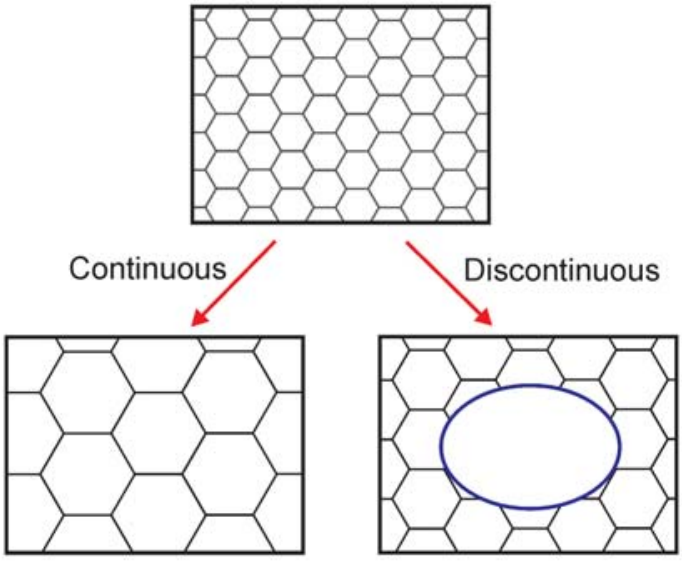

Figure 1.1: The distinction between continuous (normal) grain growth, where most grains grow at roughly the same rate, and discontinuous (abnormal) grain growth, where one or more grains grow at a much higher rate than its neighbors [2].

The grain size is directly related to many properties of the final product, and the control and prediction of the grain size is a major concern in the materials engineering field. With the development of computer technology it becomes possible to reproduce the grain growth process. But simulation of microstructural evolution is complex and difficult, because many factors affect the process and there are strict topological requirements. At present, only normal grain growth can be modelled quantitatively. Compared to other modelling methods, Cellular Automata (CA) is believed to have the greatest potential to model the microstructural evolution qualitatively. This method will be used for predicting both normal and abnormal grain growth in the following work.

The theoretical background of this work is given in the first chapter (Fundamentals) describing the properties of austenitic stainless steel and grain structure changing during solution annealing process. Additionally, the possibilities of modelling grain growth on local scale, especially by CA methods is described.

In the following chapter (Experimental Part), an exact description of experimental results containing of the metalographical preparation of the specimens, then the evaluation of grain sizes and fractions of abnormal grains, and the grain size distributions are provided. A discussion of the grain growth kinetics of normal and abnormal grain growth are followed.

The chapter Cellular Automata Modelling presents both deterministic and probabilistic modelling set-ups, followed by the validation of both models in the presence of precipitations and stored deformation energy. The model characteristics and the simulation results of normal grain size, abnormal grain size, fraction of abnormal grains, separating grain size between normal and abnormal grain size, grain size distributions and grain growth kinetics are discussed and compared to the experimental results.

A summary of the most important results can be found in the final chapter, entitled Conclusions.

2 Fundamentals

2.1 Austenitic Stainless Steels

Austenitic stainless steels are used wherever high strength and corrosion resistance is needed. They are widely used in the petrochemical, marine, food and nuclear industries, but may also be used for heat exchangers, pipework, machinery parts and in the manufacture of milder chemicals. The microstructure can be ferritic, martensitic, ferritic-austenitic or austenitic and depends largely on the alloying elements.

By altering their chemical composition, different types of austenitic stainless steels have been developed.

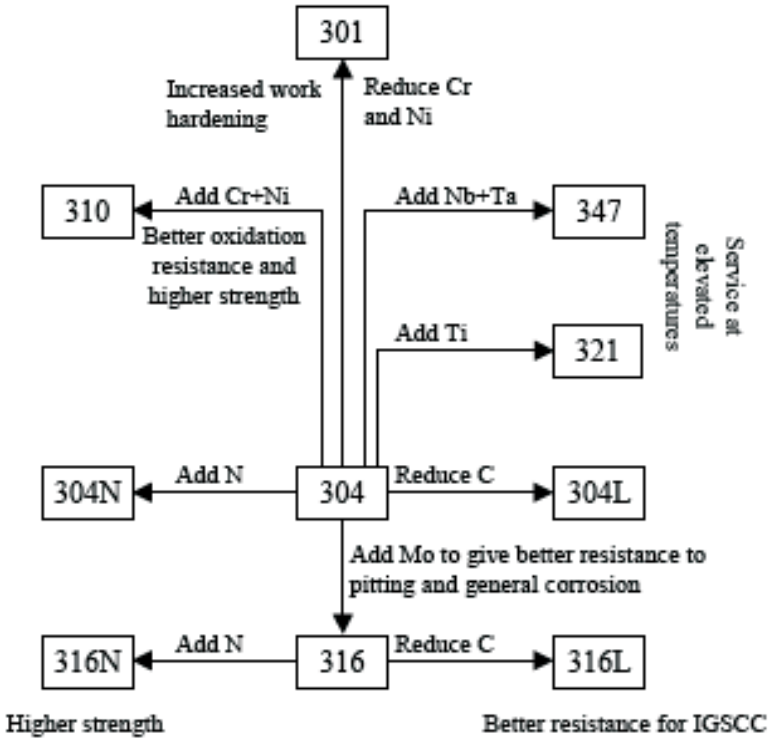

Figure 2.1: Compositional modifications of 18Cr-8Ni steels [3].

Austenitic grades [4] are those alloys which are commonly in use for stainless applications and are shown in figure 2.1 and 2.2. The austenitic grades are not magnetic. The most

common austenitic alloys are iron-chromium-nickel steels and are widely known as the 300 series. The austenitic stainless steels, because of their high chromium and nickel content, are the most corrosion resistant of the stainless group providing unusually good mechanical properties. They cannot be strengthened by heat treatment, but can be strengthened significantly by cold-working.

Further, the so called L-grades are used to provide extra corrosion resistance after welding. The letter L after a stainless steel type indicates low carbon (as in 304L). The carbon is kept up to 0.03 % to avoid carbide precipitations. Heating at critical range temperatures leads to the precipitation of carbon [5] with chromium gathering on the grain boundaries. This deprives the steel of the chromium in solution and promotes corrosion adjacent to the grain boundaries. By controlling the amount of carbon, this type of corrosion can be minimized.

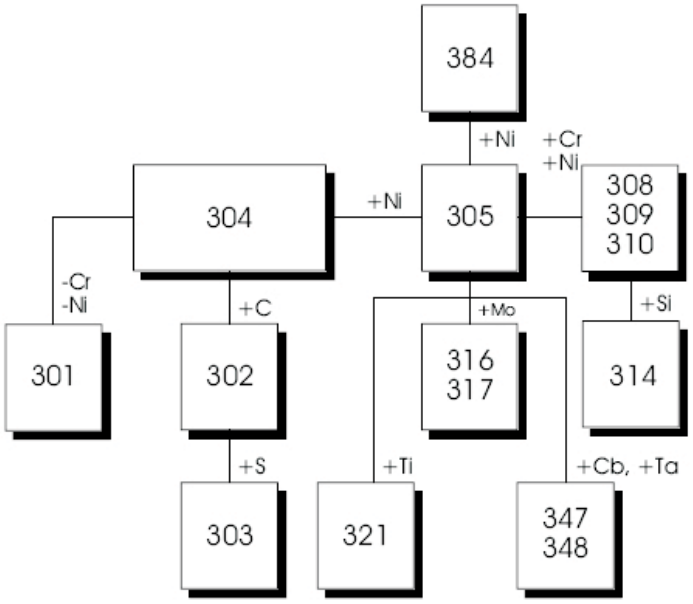

Figure 2.2: Austenitic Group [4].

In this study the austenitic stainless steel 304L (X2CrNiMo17-12-2 or 1.4404) is used exclusively where the chemical composition is given in Table 2.1.

Elements:	C	Si	Mn	P	S	Cr	Mo	Ni
Percent:	max. 0,03	max. 1,00	max. 2,00	max. 0,045	max. 0,030	16,50-18,50	2,00-2,50	11,00-14,00

Table 2.1: Chemical composition of the stainless steel 304L in weight percent [6].

The alloy composition [3] is often characterized by use of Cr- and Ni-equivalents. The first group stabilizes the α-phase and the second one the γ-phase. The ferritic α-phase has a body centered cubic (bcc) and the austenitic γ-phase has a face centered cubic crystal (fcc) structure. The low carbon content affects the flow behavior by modifying the stacking fault energy [7].

Diffusion-Controlled Precipitation

In the absence of stabilizing elements, $M_{23}C_6$ is the predominant carbide formed in austenitic stainless steel and is mainly composed of chromium carbide [3, 8]. The principal practical consequences of precipitation are degradation of intergranular corrosion resistance and reduction in tensile properties, especially ductility and toughness. Precipitation occurs very rapidly on the ferrite-austenite interfaces, followed by precipitation on other non-coherent boundaries including inclusions, grain and twin boundaries. Other types of precipitation are MC, M_6C, M_7C_3, i.e. carbonitrides and other intermetallic phases.

The austenitic stainless steel are usually annealed between 1000-1150°C and thereafter quenched quickly to avoid carbide formation. The austenitic structure is for some steel types metastable at room temperature and can form martensite by deep cooling and/or plastic forming operations.

2.2 Development and Properties of Grain Structure during Solution Annealing

Grain growth is the term used to describe the increase in grain size which occurs during annealing a polycrystalline aggregate after primary recrystallization is completed. Two different types of grain growth phenomena, namely normal grain growth and abnormal grain growth are distinguished [9] and shown schematically in figure 2.3. The main driving

force is the decrease in free energy which accompanies reduction in total grain boundary area and hence in total grain boundary energy.

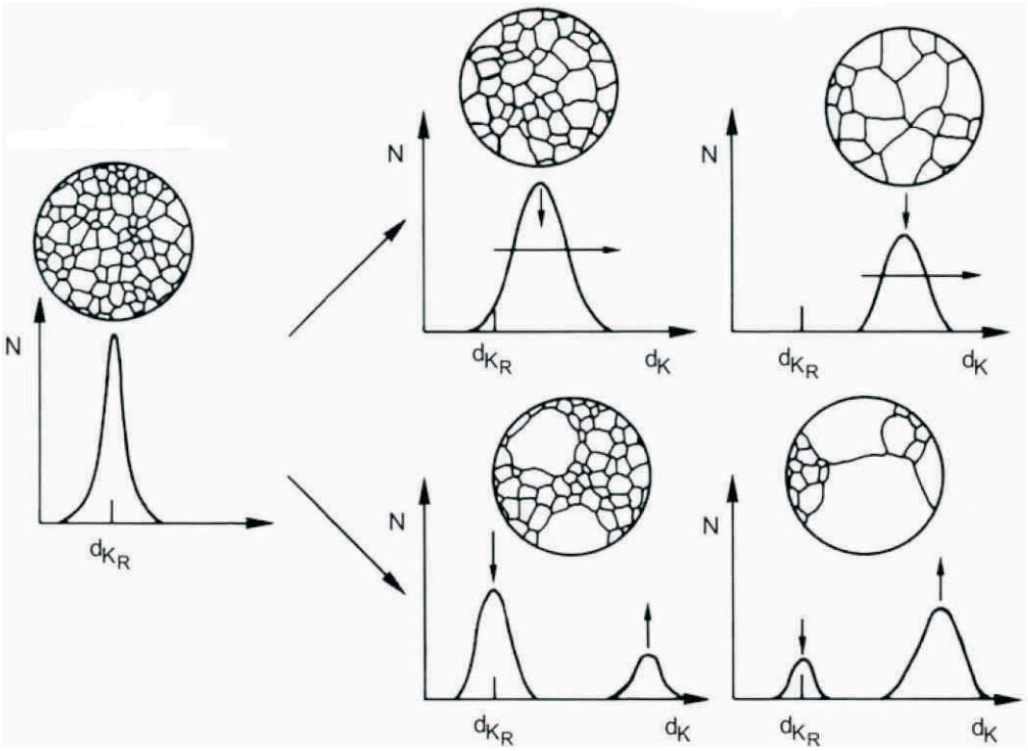

Figure 2.3: Difference between normal (top) and abnormal (bottom) grain growth. N = probability, d_K = grain size diameter and d_{KR} = average initial grain size diameter [10].

2.2.1 Energy of Polycrystalline Materials

Each grain boundary in a polycrystalline material may be regarded as a sink or source for atoms within the total system. Atoms in the vicinity of a particular grain boundary will have a driving force to diffuse towards that boundary and will diffuse if the temperature is sufficiently elevated resulting in an equilibrium condition where creation and absorbtion of atoms are constant. During this process, the boundary may move from its original location, resulting in the growth of certain grains at the expense of neighboring grains [11, 12].

The disorientation (figure 2.4) between grains will determine the manner in which a particular grain boundaries may act as a sink or source, and migrate. The disorientated or inclined low-angle grain boundaries can move only by the climb of primary dislocations in the boundary plane which have a Burgers vector, b, component normal to the plane

[13]. High angle grain boundaries act as sources and sinks by the climb of secondary dislocations in the boundary plane [14].

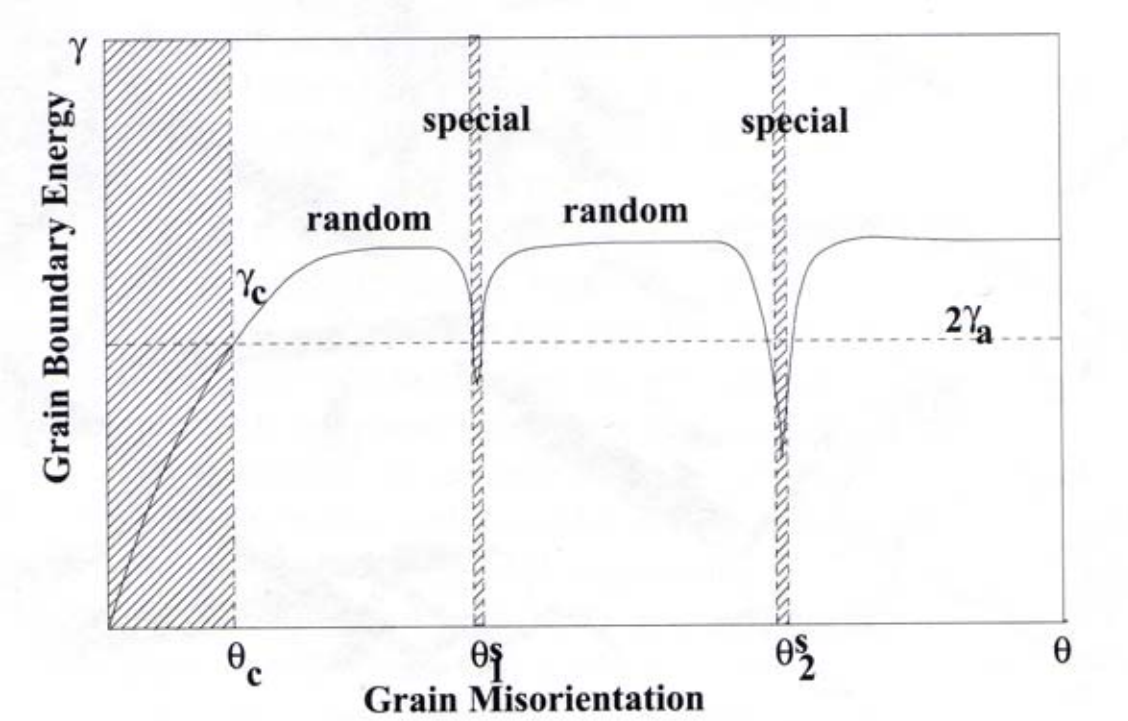

Figure 2.4: Variation of grain boundary energy as a function of misorientation between adjacent grains [11].

When two grains come in contact, one may grow at the expense of the other to reduce the total energy of the system. For this to occur, the driving force comes from the difference of chemical potentials across the boundary, even if all other factors are equal (curvature, stored energy, elastic strain, temperature, impurity content or second phase particles).

2.2.2 Grain Growth Kinetics

The grain growth belongs to a thermally activated process, thus the final grain size depends on time and temperature. Other factors, such as crystallographic texture and second phase particles, which can exert a frictional drag on the moving boundary, also can influence the migration of grain boundary. Burke and Turnbull [15] put forward a simple parabolic relationship for the grain growth kinetics with the following assumption

1. the grain boundary energy is independent of grain size and time and is the same for all boundaries
2. the radius of curvature R_{curv} is proportional to the mean radius of an individual grain, and
3. the boundary velocity dR/dt is proportional to the driving pressure $p_{boundary}$, so that $dR/dt = C_2 p_{boundary}$, where C_2 is a constant.

Under isothermal annealing conditions they obtained the following equation:

$$R_t^2 - R_0^2 = kt \tag{2.1}$$

where R_t is the mean grain radius at time t. R_0 is the initial mean grain radius and k is a constant determined by the boundary mobility, energy and temperature [16, 17].

Sellars and Whiteman [18] analyzed published grain growth data of low carbon-manganese steels and arrived at the following expression:

$$D^{10} - D_{rex}^{10} = A_{growth} \cdot t \cdot exp\left(-\frac{Q_{act}}{R_{gas}T}\right) \tag{2.2}$$

where A_{growth} is a constant which depends on material composition and process conditions, Q_{act} is the activation energy for grain growth, R_{gas} is the gas constant and D_{rex} is the grain size after recrystallization.

Yoshie presented an empirical approach to predict grain growth of austenite in an as-cast C-Mn steel [19]:

$$D^2 - D_0^2 = k_2 t \tag{2.3}$$

where

$$k_2 = \frac{\gamma V D_{gb}}{\delta R_{gas} T} \tag{2.4}$$

and

$$D_{gb} = D_{gb}^0 exp\left(-\frac{Q_b}{R_{gas}T}\right) \tag{2.5}$$

where D_{gb} is the diffusion coefficient at a grain boundary, Q_b is the activation energy for grain boundary diffusion and δ is the thickness of the grain boundary.

In general, the grain growth can be described by the grain boundary mobility and the activation energy for the grain growth. Therefore, the determined grain sizes can be

evaluated according to the grain growth law from [5], which is described in the equations 2.6 - 2.9.

$$D = t^n Mob \tag{2.6}$$

$$D = \left[Mob^{\frac{1}{n}} t + D_0^{\frac{1}{n}} \right]^n \tag{2.7}$$

$$Mob = Aexp\left(\frac{-Q_{act}}{R_{gas}T}\right) \tag{2.8}$$

$$D = \left[\left(Aexp\left(\frac{-Q_{act}}{R_{gas}T}\right) \right)^{\frac{1}{n}} t + D_0^{\frac{1}{n}} \right]^n \tag{2.9}$$

The symbols used in the equations above stand for

- D = grain diameter after a particular annealing time
- D_0= initial grain diameter
- Mob = grain boundary mobility
- A = constant
- Q_{act} = activation energy for grain growth
- R_{gas}= universal gas constant
- T = temperature
- n = grain growth exponent

Although there is a wealth of experimental evidence accumulated over many years, in many cases the results are contradictiously and no clear pattern emerges. Experimental studies of grain coarsening in metals often show that n was generally below 0.5 and it varied with temperature and composition [20, 21].

Much effort has been expended in trying to explain why the measured grain growth exponents differs from the theoretical value of 0.5. Since both boundary mobility and energy are known to be functions of misorientations, solute segregations and temperatures, the grain growth kinetics in real materials are unlikely to conform the equation 2.1. Furthermore, the boundary mobility varies with boundary velocity, and the velocity is not linearly proportional to the driving pressure except for very low or very high boundary

velocity [22].

The application of computer simulations have been put forward to model grain growth kinetics. The Exxon group using the Monte Carlo method predicts the grain growth exponent to be 0.41 [23–27]. Fan and Chen using Continuum Field model found a n value of 0.5 [28, 29]. Liu using the CA method got a n value of 0.45 [30].

Particle dissolution occurring during grain growth affects the grain size evolution. Smith included an analysis of Zener on the pinning force exerted on the grain boundaries due to particles, defining a limiting, i.e. impeding, grain radius R_Z for grain growth, and stated the following relationship [31]:

$$R_Z = \frac{4r}{3f} \tag{2.10}$$

where r is the radius of second phase particles and f is the fraction of of the same in the whole system.

Gladman adopted a more realistic approach by considering that there exists a critical point where the rate of release of energy per unit displacement of the grain boundary during grain coarsening is equal to the rate of increase in energy due to the unpinning process [32, 33]:

$$R_G = \frac{\pi r}{6f}\left(\frac{3}{2} - \frac{2}{Z}\right) \tag{2.11}$$

where Z lies between 1.4 and 2 and defines the ratio of the radii of the growing grain and matrix grains R/R_0.

Rios considered an interface bending around the particle and derived an equation to predict the limiting grain size [34]:

$$R_R = \frac{r}{6f} \tag{2.12}$$

Elst developed a model to accommodate elongated particles, a bimodal particle distribution and a distribution of grain boundary precipitates based on equation 2.11 [35]:

$$R_E = \frac{4r}{3\beta f}\left(\frac{3}{2} - \frac{2}{Z}\right) \tag{2.13}$$

where β is a function of R/r.

2.2.3 Topological Requirements for Grain Growth

Many studies have been conducted to evaluate the shape of grains, where the grain must exhibit a shape that is space filling and the interface between grains must conform to the law of governing the grain boundary energy. In any array of 2D space filling polygons, where three of more polygons meet, there is a simple relationship between the number of corners, the number of edges and the number of polygons in the array, which can be stated as:

$$P - E + C = 1 \tag{2.14}$$

where P, E and C are the number of polygons, edges and corners, respectively.

Smith´s [36] experimental observations on soap froth lead to an average number of edges per face of 5.06 and average number of faces per grain of 12.48. The edges between 2D grains are influenced by the boundary energies associated with the atomic lattice distortion between grains. Geometric adjustments of the boundary will occur to minimize the boundary area and hence the total boundary energy, given that there is adequate boundary mobility to affect such short range boundary movement. For a 2D structure, in which all boundaries have the same surface tension, the equilibrium angles at a vertex are 120°. It is assumed that grains with more than 6 sides have boundaries convex towards their centers, those with less than six sides concave toward their centers, and those with exact six sides have straight boundaries. All grains with less than six sides are unstable and tend to shrink in size, while those with more than six sides tend to grow in size. The shrinkage of 5-sided grains leads to 4-sided grains, which than continue to shrink and undergo a similar transformation to become 3-sided grains, and then the grain vanishes completely.

The study of Gladman considered that the energy of the system is increased by the expansion of the interfaces but at the same time decreases by the elimination of the grain interfaces of the grains which are absorbed by the growing grains. The net energy change (ΔE_n) accompanying grain growth is given by [32, 33]:

$$\Delta E_n = \frac{\Delta D \gamma}{R}\left(\frac{2}{Z} - \frac{3}{2}\right) \tag{2.15}$$

where ΔD is the change in grain size. When Z <1.33, there is an increase in the grain boundary area, and when Z >1.33, there is a decrease in the grain boundary area. This explains why large grains grow at the expanse of small grains.

Although, the topological rule for grain growth is very important for understanding the process, it tells us nothing how quickly topological transformations and overall grain growth can occur [9]. In contrast, grain growth kinetics by Burke and Turnbull [15, 37] are not defining the space-filling network thus its influence on the grain boundary migration, which can be approached by computer modelling.

2.2.4 Normal Grain Growth

One of the structural characteristics during normal grain growth is that the grain-size and grain-shape distributions are essentially time invariant [38]. During normal grain-growth the average grain size increases, but the size and shape distributions of the grains remain essentially the same before and after the growth, differing only by a scale factor [26, 39, 40].

Driven by the grain boundary energy reduction, the local grain boundary movement during grain growth is governed by grain boundary energy and grain boundary mobility.

The velocity of the grain boundary depends on the net pressure acting on the grain boundary:

$$p_{boundary} = \frac{2\gamma}{R_{cu}} \tag{2.16}$$

The pressure on the grain boundaries acts in such a way that it forces the grain boundary to move towards the center of the curvature, where a grain with a convex grain boundary grows and a grain with a concave grain boundary shrinks.

The grain boundary displacement, ΔX, in a single time increment, Δt, is a function of the pressure, and the mobility of the grain boundary and is given by:

$$\Delta X = M p_{boundary} \Delta t \tag{2.17}$$

The grain boundary mobility depends on temperature and activation energy:

$$M = M_0 exp\left(\frac{-Q_{act}}{R_{gas}T}\right) \tag{2.18}$$

Despite the importance of grain growth, the details of the process are not well understood.

The reason is that boundary migration involves atomistic processes under conditions which are far from equilibrium, especially at high temperatures. It is quite difficult to observe and measure boundary migration experimentally. It is generally accepted that the driving force for grain growth lies in the grain boundary energy of the grain boundaries. As the grains grow in size and their numbers decrease, the grain boundary area diminishes and the total grain boundary energy is lowered accordingly [34, 41–48].

2.2.5 Abnormal Grain Growth

A second type of grain growth phenomenon which can occur after recrystallization is abnormal grain growth [26, 40]. In general, it is defined as a rapid increase in size of a few grains in the recrystallized microstructure such that the topology is not time invariant and the maximum grain size increases at a rate much faster than the arithmetic mean.
It is commonly observed, that secondary recrystallization requires normal grain growth to be strongly impeded, with the exception of a few grains which act as nuclei for secondary recrystallization. Inhibition of normal grain growth is attributed to a number of mechanisms:

- Grain boundary grooving in the case of thin films and sheet materials on the surface
- Particle pinning of boundaries
- Texture inhibition in a material with strong preferred orientation
- Impurity inhibition

The driving force is generally assumed to be provided by associated reduction in total grain boundary energy, as for normal grain growth. However, an additional driving force has been experimentally demonstrated in thin films and sheet materials, which arises from orientation dependance of the gas-metal surface energies [49]. The start of secondary recrystallization has some common characteristics [50]:

- The grains that grow large are not newly nucleated but it is part of the primary structure.
- The very large grains initially grow slowly, followed by rapid growth to sizes of the order of centimeters in some cases.
- The grains that coarsen possess many sides.

2.2.5.1 The Influence of the Starting Microstructure

For 316L stainless steel it is observed that during heat treatment, abnormal grain size develops depending strongly on the initial grain size after the primary recrystallization (figure 2.5) [51].

When decreasing the initial grain size, abnormal grain growth begins earlier during the heat treatment, and if the initial grain size is large only slow grain growth occurs without any distinct abnormal grain growth. The extremely slow grain growth with initially large average grain size is attributed to the low grain boundary velocity limited by the boundary step nucleation or growth.

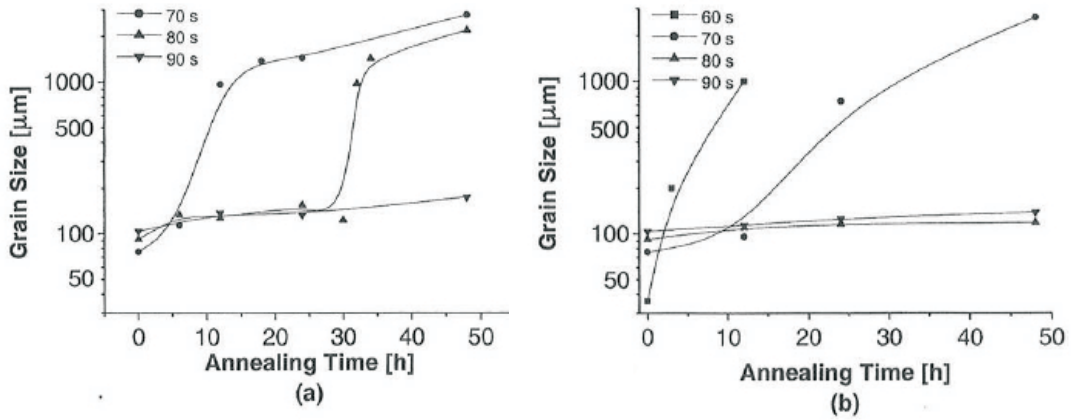

Figure 2.5: Illustrations of the grain growth at different annealing temperatures and different initial grain sizes in a 316L austenitic steel. Lee produced at 1300°C different initial grain sizes and afterwards annealed the structure at (a) 1150°C and (b) 1100°C. Different initial grain sizes were produced by different pre-annealing times. Exemplarily annealing for 70s results in a lower initial grain size than annealing for 80s [51].

2.2.6 Faceted Grain Boundaries

Abnormal grain growth is often marked with occurrence of faceted grain boundaries. Grain boundary phase transformations based on the observation of an apparently discontinues change of the energies of grain boundaries generated during the annealing process at different annealing temperatures (e.g. $0.73T_m$ for Pb) [52].

The faceting of grain boundaries have been observed in many metals and oxides, and

impurities and additives as O in Ni or Ag, Bi in Cu, Te in Fe, and CaO or SiO_2 in Al_2O_3 have been observed to induce the grain boundary faceting [53, 54]. It has also been observed that at high temperatures close to the melting point in a carburizing atmosphere, the grain boundaries of a Nickel based alloy become de-faceted, producing curved shapes that have an atomically rough structure. In contrast, normal grain growth occurs at low temperatures. At high annealing temperatures faceted grain boundaries are developed and abnormal grain growth occurs.

In an experimental study [55] in stainless steel 316L, the first heat treatment at 1100°C leads to an AGG structure but afterwards heat-treated again at 1300°C results in a NGG structure. This time the fine matrix grains coarsened but the large grains did not grow abnormally, and a normal grain size distribution was reached. It is shown that with changing the growth mechanism due to producing rough grain boundaries, the abnormally grown grains did not continue to grow.

The dependence of abnormal grain growth on the annealing temperature in the range between 600°C and 1050°C has also been observed in pure bulk Cu specimens [56]. The incubation time for AGG decreases and the number of density of abnormally large grains increases with decreasing initial grain size and increasing annealing temperature. At low temperatures, most of the grain boundaries were faceted. With increasing temperatures, the grain boundaries become de-faceted and atomically rough. The observed grain-growth behavior appears to be qualitatively consistent with the movement of faceted grain boundaries by two dimensional nucleation of boundary steps. The temperature dependence appears to be consistent with roughening of grain boundaries. Before the onset of AGG, stagnant growth of the grains occurs at low rates, probably limited by slow two-dimensional nucleation of boundary steps.

Both general grain boundaries and grain boundaries with well-defined geometrical characteristics such as the coincidence site lattice (CSL) relations were observed to have faceted grain structures, which are often associated with impurities and additives [53], depicted in figure 2.6.

These faceted grain boundaries can move by two-dimensional nucleation of steps or on existing steps produced by dislocations (figure 2.7), as proposed by Gleiter [52, 57]. The grain-boundary migration rate will then increase progressively with the driving force, causing rapid growth of only large grains and, hence, AGG [8]. If the grain boundaries

have an atomically rough structure, the migration rate will increase linearly with the driving force, thus normal grain growth will occur [56].

If the faceted grain boundaries migrate by growth on the steps produced by dislocations, the migration at low driving force will be substantially higher than that by two-dimensional nucleation, as shown by dashed curve in figure 2.7. But at high driving forces, the growth can still occur by two-dimensional nucleation, and, with either type of non-linear migration behavior with driving force, AGG can occur in the system of many grains [56].

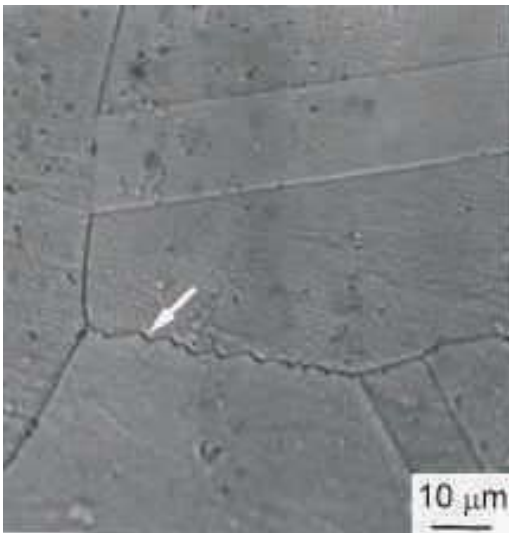

Figure 2.6: A faceted grain boundary in silver [54].

With growth by two-dimensional nucleation of boundary steps, the growth rate ($\widehat{R}$) depends on the step-edge free energy ($\sigma(T)$) and the change of driving force (Δg)

$$\widehat{R} \propto exp\left(\frac{-\pi V \sigma(T)^2}{h \Delta g k_{boltz} T}\right) \tag{2.19}$$

where h is the step height. As in most of the grain-growth theories, it may be assumed that (Δg) is approximately given by

$$\Delta g\left(\overline{R}, R_i\right) = \beta_{geo} V \gamma \left(\frac{1}{\overline{R}} - \frac{1}{R_i}\right) \tag{2.20}$$

where β_{geo} is a geometric factor and $\overline{R}$ is the average size of the grains surrounding it, which may be assumed to be the average size of all grains. For abnormal grain growing in

the matrix of fine grains, $\overline{R}$ will represent the average size of the matrix grains. Writing $R_i = \overline{R}\alpha_i$ the following equation is derived

$$\Delta g_i\left(\overline{R}, R_i\right) = \frac{\beta_{geo} V\gamma}{R}\left(\frac{\alpha_i - 1}{\alpha_i}\right) \tag{2.21}$$

Therefore, the driving force must be large enough to exceed the critical driving force, depicted in figure 2.7.

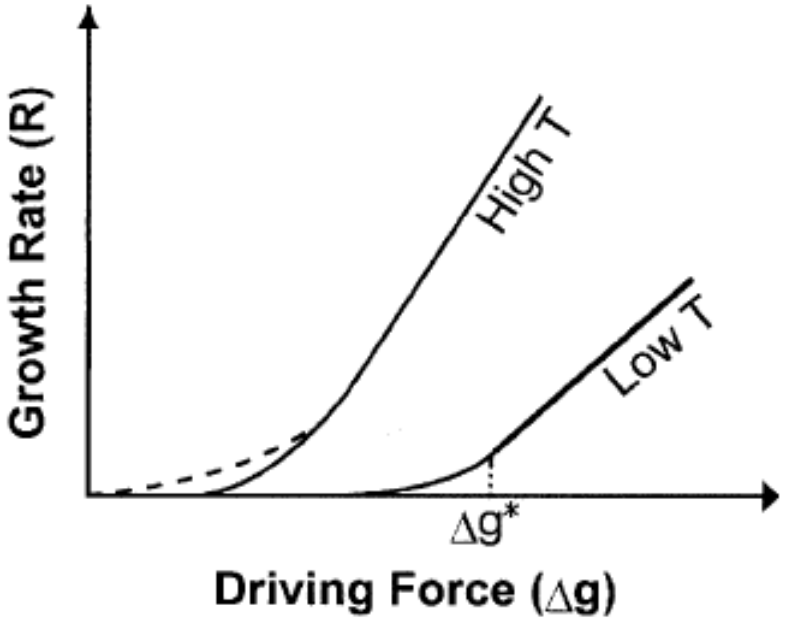

Figure 2.7: Schematic variation of the rate of grain growth by two-dimensional nucleation with the driving force at high and low temperatures with the dashed curve for the dislocation growth mechanism at high temperatures [56].

The equation 2.19 for $\widehat{R}$ as a function of (Δg) is plotted schematically in figure 2.7 at two temperatures. Because this equation describes the growth by mono-nucleation, it is expected to be valid for relatively low driving forces. As the driving forces increases, poly-nucleation is expected to occur with slightly different dependence on (Δg), and above (Δg^*), $\widehat{R}$ is expected to increase linearly with (Δg), because the growth will be limited by the rate of the atom jump across the boundary [56].

If initially none of the grains are large enough to exceed Δg^*, which is required for AGG, then all the grains will grow at very low rates in the very low-driving-force range shown in figure 2.7. Such a slow growth limited by nucleation of steps is known as stagnant

growth. During stagnant growth, large grains can grow relatively faster than the increase of the average size because of the nonlinear variation of the growth rate with the driving force, and when the large grains attain the critical sizes required to exceed Δg^*, they will undergo accelerated growth to produce AGG. If the initial $\overline{R}$ value is smaller, the time required for the large grains to exceed Δg^* will be shorter, thus the incubation time for AGG will be shorter which is in agreement with experimental results [56].

2.3 Modelling of Grain Growth

At present, many simulation methods have been put forward to reflect grain coarsening process, which can be classified into statistical methods and direct simulations. Statistical methods deal with ensemble probabilities for a collection of grains and the computer solves a series of equations for a collection of grains in order to explain the behavior of grain growth (e.g. grain size). Direct simulations construct a boundary network and can be classified into deterministic, defining subsequent configurations exactly, and probabilistic models [9]. The following chapter focuses on direct simulation methods.

2.3.1 Monte Carlo Method

Since Srolovitz [23–27] applied the Monte Carlo method to model grain coarsening which allows topological constraints to be taken into account, the Monte Carlo method has gained much attention and has been applied to many metallurgical phenomena, such as solidification, recrystallization and grain growth.

In the Monte Carlo method, the grain structure is mapped onto a discrete triangular or square lattice. Each lattice site is assigned a number between 1 to q corresponding to the orientation of the grain in which it is embedded. If q is large, grains with same orientation impinge infrequently. A grain boundary is defined to lie between sites of unlike orientation and the grain boundary energy is also specified. The Hamiltonian for the system energy, E_{system}, is written as:

$$E_{system} = \frac{1}{2} \sum_{i=1}^{N_{sites}} \sum_{j=1}^{n_{neighbors}} E_{q_i q_j}(1 - \delta_{q_i q_j}) \tag{2.22}$$

where $n_{neighbors}$ is the number of neighbors, N_{sites} is the total number of sites, q_i is the state of the grain at site `i`, q_j is the nearest state of the grain at site j and $\mathrm{E}_{q_i q_j}$ is the

neighbor interaction energy between neighbors located at site i and j, and $\delta_{q_i q_j}$ is the Kronecker delta function. Thus the only energy considered in the simulation is the interfacial energy and all unlike neighbors contribute one arbitrary unit of energy to the system.

The kinetics of the boundary motion is simulated by selection of a lattice site at random and a new trial orientation is chosen at random from one of the other $q-1$ possible orientations. The change in energy is calculated by the equation 2.22. The transition probability for the change in the energy caused by change in orientation of $\Delta E < 0$ is 1 and for $\Delta E > 0$, the transition probability is defined as $exp\left(-\Delta E/k_{boltz}T\right)$. Successful transition at the grain boundaries to orientations of nearest neighbor grains correspond to boundary migration. The unit of time defined is as 1 Monte Carlo step (MCS) per site, which corresponds to N_{sites} re-orientation attempts.

Saito [58, 59] adopted the Monte Carlo Method and developed a conversion of MCS to real time on the basis of diffusion controlled mechanism by

$$MCS = \frac{d_{cell}^2}{6D_{gb}q} \tag{2.23}$$

where d_{cell} is the distance of the MC lattice system and q the number of states.

2.3.2 Continuum Field Model

The special features of the Continuum Field method is that it describes the grain boundary with some thickness [28, 29]. A continuum grain boundary structure is mapped onto a discrete, square lattice using a set of order parameters, which is allowed to evolve with time at each lattice to simulate the grain structure evolution. The driving force for the grain structure evolution is the reduction of total free energy of the system. Kinetics for grain structure evolution is introduced by the time-dependent equation:

$$\frac{d\eta(r,t)}{dt} = -L_i \frac{\delta F(r,t)}{\delta \eta_i} \tag{2.24}$$

where F(r,t) is the free energy for the system, L_i is the kinetics rate coefficient related to the interface mobility and diffusivity. The starting grain structure for this study initialized by assigning small random numbers for each order parameters at each site at time $t = 0$. Once the grain structure is initialized, grain growth is simulated by solving the equation 2.24 by using numerical methods.

2.3.3 Front Tracking Method

For the curvature driven Front Tracking method, the velocity of each grain boundary segment is proportional to the local curvature and the grain boundary mobility. At grain boundary triple junctions, a local force balance is enforced, so that grain boundaries meet at 120°. In the simulation, time is measured in dimensional units as $\tau = tM/A_0$, where A_0 is the initial average grain area as presented in [60]. The same author also modeled abnormal grain coarsening due to the free surface energy variation in thin films.

Humphreys developed a model in which the grain structure consisting of a two-dimensional network of grains and subgrains is constructed, where the subgrains are represented by the node points N_j and each grain and subgrain is given a number g_j, representing its crystallographic orientation. As the orientations of adjacent boundaries are known, the boundary misorientation angle is also known, thus the boundary energy can be calculated. Incorporating the Read-Shockley equation for low angle grain boundaries, the grain boundary energy for high angle grain boundaries is taken to have a constant value. Each node is subjected to forces arising from the three boundaries which intersect it. The boundaries are assumed to bow to configurations determined by the positions of the adjacent nodes and the boundary energies. The line tension forces at a node are summed to give the driving force on the node. The velocity of the node is then determined by the mobility of the boundaries moving in the direction of the driving force, and this is obtained from an average of the mobilities of the moving boundaries, weighted by the boundary lengths resolved perpendicular to the direction of motion. The node is then moved a small distance proportional to its velocity and the cycle is repeated [61].

2.3.4 Cellular Automaton Method

A Cellular Automaton is an algorithm that describes the discrete spatial or temporal evolution of the complex system by applying local deterministic or probabilistic transformation rules to the cells of a lattice. The lattice is typically regular and its dimensions can be arbitrary. In general CA modelling utilizes a regular 2D or 3D lattice that is divided into cells of equal size, usually square in 2 dimensions or cube in 3 dimensions. Each cell is characterized by different states (e.g. temperature, orientation,..). By taking into account the states of cells of its neighborhood, the state of the cell can be made to change by time stepping according to transition rules [62–64].

The CA evolution takes place through the application of certain transition rules. These rules determine the state of a cell as a function of its previous state and the state of neighboring cells. The transition rule can be designed as deterministic or probabilistic. The flexibility of CA method allows the use of mathematical expressions as variables and can incorporate any kind of element and rule that are assumed to be relevant [65].

The CA evolves in discrete time steps, after each time interval, the values of the state variable are simultaneously updated for all cells. The CA is a dynamical system in which space and time are discrete, which is similar to the Monte Carlo method, but with the difference that CA looks only on those sites with the potential to take part in the transformation. CA performs a simultaneous state update whereas the MC method carries out a sequential state variable update. Within the MC method, the state transition is achieved by the energy difference before and after reorientation, whereas in the CA model, the new states comes from its neighbors cells according to the set of transition rules. In addition, MC simulation is computationally more intensive compared to the CA model. The CA method can involve a huge variety of possible transition rules, enabling for subsequent refinements to the model. The standard form of the MC method does not result in a linear relationship between migration rate and stored energy. [30, 65, 66].

Hasselbarth tried to use CA method to simulate the recrystallization process [67]. Simulation of solidification has produced satisfactory results in the CA method by Gandin [68–70]. The cellular automata are also used for simulation of austenite-ferrite phase transformation [71].

Relatively little work has been done to simulate grain growth. Liu applied the CA method to simulate normal grain coarsening by using Von Neumann‘s definition of neighboring cells with deterministic transformation rules, where the following assumptions based on grain growth theory are made [30]:

1. If three cells among the four surrounding cells have the same state as the central cell, the state of the central cell will definitely keep its original state at the next time step.

2. A cell must overcome an energy barrier to reach its new state.

3. Each state of a cell represents the orientation of its grain in a simulated microstructure.

4. Boundary energy is homogenously distributed.

The process explained in assumption 1 is equivalent to the grain boundary migration due to curvature effect. The assumption 2 is directly connected with temperature, and according to statistical mechanics, the probability of atoms which can overcome an energy barrier is written as:

$$p_{boundary} = exp\left(-\frac{E_{barr}}{k_{boltz}T}\right) \tag{2.25}$$

where E_{barr} is the energy barrier.

The author assumed [30] that the temperature is high enough and all the cells are successful in their state transition, that is P= 1. The simulation is proceeded using a matrix of $200x200$ cells, and a time step is defined when all cells have proceeded an attempt of state transition. Periodic boundary is introduced in order to represent infinite grain structure and the simulations performed until 20000 steps. The simulation gives an average growth exponent of 0.45 and the distribution of grain sides a high reorientation frequency at 6 grain sides.

In the probabilistic model of Yu [72–76], at each step, every cell is scanned, and its state will change according to the following integrated rules (figure 2.8) considering Moore's neighborhood of 9 cells:

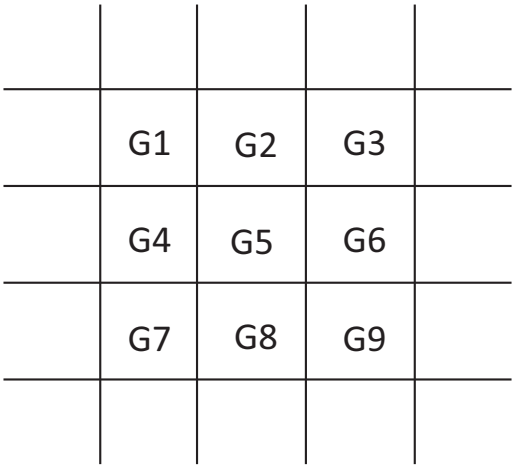

Figure 2.8: Moores neighborhood [30].

1. If all 8 cells around the G5 have the same state as G5, then G5 will keep its state at the next time step.

2. (a) If any three of the states G2, G4, G6, G8 are the same integer (grain identification number), for example equal to A, then G5 is A. Similarly, if this does not hold, then (b) if any of the three states G1, G3, G7, G9 are the same integer, for example equal to an integer B, then G5 is B.

3. The distribution of grain boundary energy is homogenous. A cell must overcome an energy barrier to change its state: if any of the eight surrounding cells have different state from G5, then G5 has the possibility to change its state. In this case, the probability is the same for all grains and is set to be $P_{boundary}$.

If the state of a cell can meet any of these conditions, then the following condition will be ignored. For example, the condition (1) is actually to judge if this cell is in the interior or on the boundary. If it is in the interior, it must maintain its state and the following conditions do not need considerations any more and the next cell will be checked subsequently. If not, the cell must be on the grain boundary and then the computer will check if its state can meet condition (2a) and so on.
On the integrated rules given above, the second rule simulates the grain curvature effect, where the grain boundary would tend to form a straight line due to the grain boundary tension requirement. The reason to use the Moore configuration considering both the nearest and next-nearest neighbors is to make a grain boundary move in any direction.
The third rule simulates the effect of grain boundary energy, which is vital to keep the boundaries move and make small grains vanish. It reflects the effect of mobility on the grain growth, which includes the temperature dependance.The deterministic CA models work with exact calculation of grain boundary displacement by evaluating the grain boundary curvature and temperature dependence of grain growth, defined by the mobility of grain boundary [77, 78].

A two-dimensional cellular automaton algorithm developed by Lan [79, 80] defines the velocity of grain growth as

$$M = M_0 exp\left(-\frac{Q_a}{R_{gas}T}\right) = \frac{b^2 D_b}{k_{boltz}T} exp\left(-\frac{Q_a}{R_{gas}T}\right) \tag{2.26}$$

In his study Lan reduced the mobility at the triple points from $8.929 \cdot 10^{-11}$, of normal cells, to $1.488 \cdot 10^{-11}$ for the cells in a triple point.

In the CA model of Yazdipour, a comprehensive range of thermo-mechanical conditions

were considered and compared with experimental data for the type 304 austenitic stainless steel [81]. Each cell in the model was categorized by three variables: an orientation which is the same for all cells located in the same grain, the´dislocation density which represents the stored energy due to the deformation and grain boundary energy which is zero for the cells located away from the grain boundaries and calculated for the cells next to the grain boundaries (e.g. for high angle grain boundaries $\gamma = 8.35 \cdot 10^{-7}\ mJ/m^2$). For the austenitic stainless steel 304 the mobility of the grain boundaries is defined as follows:

$$M = \frac{\delta_{gb} D_b b}{k_{boltz} T} exp\left(\frac{-Q_b}{R_{gas} T}\right) \tag{2.27}$$

where $\delta_{gb} D_b = 1.1 \cdot 10^{-13}\ m^3/s$, $b = 2.5 \cdot 10^{-10}\ m$ and $Q_b = 174\ kJ/mol$.

Simulation experiments of Janssens [82] illustrate that the random grid base of an automaton eliminates the dependence of the model on grid symmetry as observed in conventional cellular automata, made for recrystallization and grain growth. For irregular automata the number of cells per unit area varies from position to position in the grid. The local variation of the resolution of the automata influences the simulation in two ways. The precision of the computations varies locally, which means that local conclusions about the results of a simulation involve some form of statistical analysis. Further, the local density of the random grid must be observed when making statements about accuracy. It is a well known fact that the shape of the neighborhood, which is closely related to the grid, has a major influence on e.g. the way grain boundaries move in the simulation of grain growth. This implies that the automaton directly influences the outcome of the calculation. This problem is solved when using a random grid but the cost for this advantage is that for each cell the neighborhood must be computed and stored.

3 Experimental Work

3.1 Annealing and Quenching

For the annealing tests cylindric specimens of 304L with a diameter of 10 mm and a height of 5 mm were used. The geometry of the specimen was finished at Böhler Edelstahl, Kapfenberg, Austria.

Furnace

The specimens were heated in a laboratory furnace *RHF* 14/35 from Carbo Light shown in figure 3.1. In order to achieve the aimed annealing temperature, a charge time of 4.5 minutes (for 900°C and 1000°C) and 3 minutes (for 1100°C and 1200°C) were defined from temperature measurements on the specimens. That means for example, if the annealing time is 20 minutes at 1200°C the specimen would be in the furnace for 23 minutes, where the 20 minutes are an absolute time value for the annealing without charging and cooling.

Figure 3.1: Left: Carbo Light furnace *RHF* 14/35. Right: Magnification of the heating chamber.

The temperature in the center of the furnace chamber (figure 3.1) was used to control the annealing temperature. The specimen needs a fireclay base to get near to the center area of the chamber.

The specimens were charged only once to a specific temperature inside the furnace, then quenched. The charging temperatures used were: 900°C, 1000°C, 1100°C and 1200°C. The REF specimens are the reference material without any annealing. These were used to classify the initial grain sizes. The x in table 3.1 shows the annealing temperatures and times for the specimens.

Time [s]	*REF*	*900°C*	*1000°C*	*1100°C*	*1200°C*
0	xx				
1200					x
2400					x
3600					x
4800					x
7200					x
10800					x
14400		x	x	x	
18000					x
28800		x	x	x	
36000					x
43200		x	x	x	
57600		x	x	x	
72000		x		x	
86400		x	x	x	
115200		x	x		
144000		x	x		

Table 3.1: Annealing specimen table.

Quenching

After annealing, the grain structure of the specimen had to be fixed so that subsequent evaluations could be carried out. The small scale of the specimen meant that on removal from the furnace it could be immediately quenched in cold (≈10°C) water.

3.2 Metallography

Once the annealing procedure was completed, the specimens were embedded, descaled, polished and etched electrolytically to resolve the grain structures [38, 83, 84].

3.2.1 Embedding

The specimen was placed in a hot mounting press, resin was added, and processed under heat and high pressure.

Hot Mounting Press and Resins

For hot mounting a Struers Cito Press 10 [84] was used with two different resins. For the polishing side a Struers MultiFast Black (phenolic resin with wood flour filler) and on the top side Struers ConduFast (acrylic conductive resin with iron powder filler) was used.

Process Parameters:
Diameter: 40 mm
Quantity MultiFast: 15 ml
Quantity ConduFast: 30 ml
Pressure: 250 bar
Temperature: 180°C
Heating Time: 4.5 min
Cooling Time: 3.0 min
Cooling Rate: High (Full Flow)

3.2.2 Grinding and Polishing

The purpose of the grinding is to planarise the specimen and to remove material approaching the area of interest. Soft ferrous metals like 304L are relatively easy to grind where a 180 grit SiC abrasives provide a good initial start with subsequent use of 320, 600, 800, 1200 and 2500 grit SiC.

Polishing is the most important step in preparing a specimen for microstructural analysis. For the 304L only a 3μm step with Struers monocrystalin diamond suspension on a MD-NAP was necessary. The fine polishing was done with OPS (0.05μm) and a Struers MD-Chem towel.

For grinding and polishing a single wheel ATM- Saphir 550 was used. Working wheel: Ø300 mm; Single pressure: 5 - 100 N; Motor: 1.2 kW; Speed: 50 - 600 rpm.

In total, during grinding and polishing at least 150 μm of the material was removed.

3.2.3 Electrolytic Etching

The Struers LectroPol 5 uses a two-electrode design (anode and cathode) with acids or bases for the electrolyte and it is an apparatus [84] for automatic, micro-processor controlled electrolytical polishing and etching of metallographic specimens. With a scanning function for easy determinations of parameters, built-in safety features, and a database with methods for various materials, short polishing times and maximum reproducibility are achieved.

Setup:
Acid Temperature: 22 °C
Flow Rate: 10
Voltage: 1.0 V
Time: 30 - 400 sec (depends on the annealing time)

Electrolyte:
60 % nitric acid

3.3 Grain Size Evaluation

The etched specimens were recorded with an Olympus light microscope in different magnifications. The microstructure pictures were printed on A3 or A4 for editing. The traced grain boundaries were digitized and evaluated with a Software Package from Digital Imaging Solution.

3.3.1 Microscopy

The grain boundaries were recorded in different magnifications from 5x (50 fold extension), 10x, 20x, 50x and 100x. From each sample a 5x and a 10x picture was taken and if the magnification was too small for evaluation, pictures with better resolution were taken.

For example, figures 3.2 shows a picture taken in 10x magnification of the annealed specimen: firstly homogenized at 1200°C for 20 minutes and then solution annealed at 1000°C for 12h.

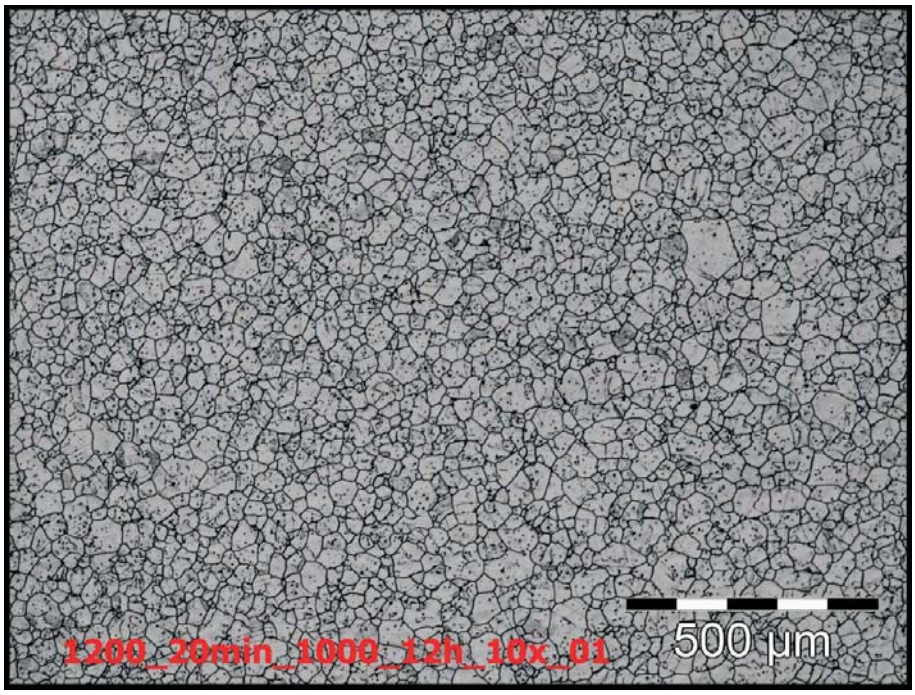

Figure 3.2: Micrographs annealed at 1200°C and 20min: high magnification.

3.3.2 Data Edit

Evaluation of the grain size is difficult because of etching artefacts, twin boundaries and other irregularities. It would have taken longer to check and correct the detected grain boundaries than to trace them to a transparency film, so all pictures of the annealed specimen were printed to paper format A4 and traced onto transparency films. For a correct evaluation of the grain size of each sample a minimum of 300 grains had to be detected. If there were fewer grains on a micrograph, a second picture or more had to be taken and traced. For correct transmission of small grains some of the micrographs were printed on A3 paper format. In figure 3.3 the traced micrograph of figure 3.2 is shown.

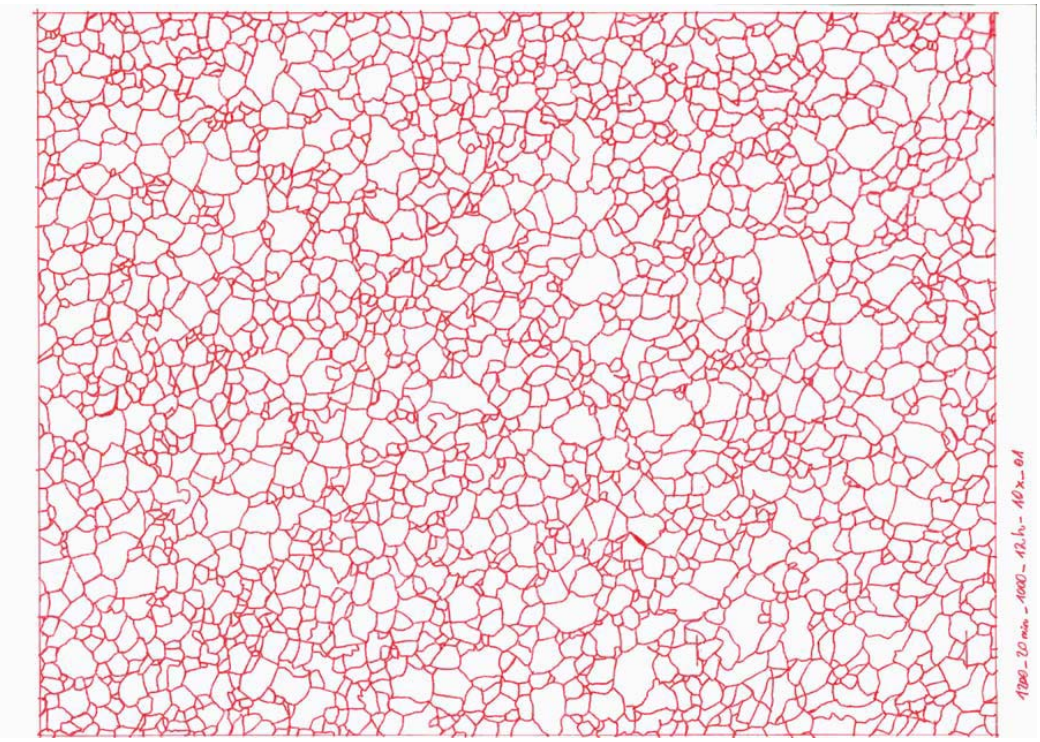

Figure 3.3: Illustration of a traced micrograph.

3.3.3 Grain Size Evaluation

Preparatory work

The traced and scanned digital micrographs were converted into a gray scale picture. During this converting process a lot of detailed information was lost, but to restore the information an intensity adjustment was made. The adjustment gave greater accuracy to the various gray lines and thus provided a more detailed outline of the grain boundaries. An additional problem was to detect the intersection points of the grain boundaries. This problem was minimized through using the software tool NxN-filter. The filter produced a relatively blurred image, but one which enabled more precise detection of the intersection points.

Evaluation of Grain Sizes

After the preparatory work the real evaluation starts. The first step is to produce a decollator picture. The decollator is a contour detection software tool to find all traced grain boundaries. This tool detects the different grey scales and defines the boundaries.

Once this process was complete the boundaries which had been discovered were edited again to correct any mistakes and the picture geometry was trimmed and calibrated. The result is shown in figure 3.4. For every single grain, the software's grain module calculates the surface area, diameter, elongation and any other user-defined parameters. For this work the quantity, diameter and the surface of all grains were detected. The grains in the border area were excluded from the evaluation.

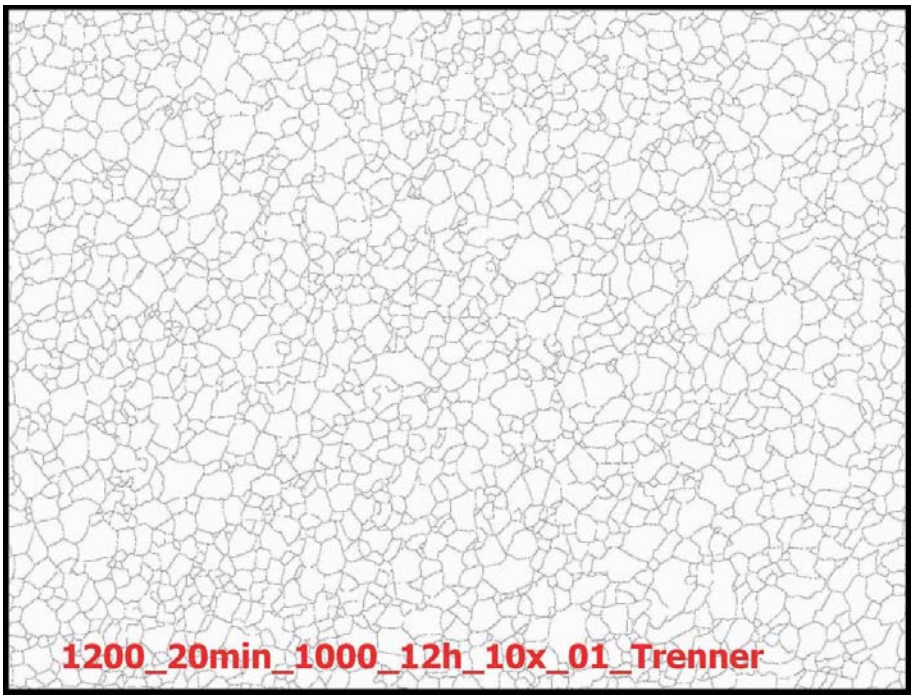

Figure 3.4: Decollated micrographs annealed at 1200°C and 20min.

3.3.4 Evaluation of the Grain Size Separating Normal and Abnormal Grains

The grain size separating normal and abnormal grain growth was defined according to an optical method. The smallest abnormal grains were measured and the average grain size was defined as the grain size separating normal and abnormal grains. With the aim of increasing the accuracy to define such a value, a second definition was employed: the sizes of all single grains belonging to a particular specimen were sorted and graded from the smallest to the largest. To find a step between consecutive grains the actual value over the preceding value was calculated. The factor usually has a value between 1.00 and 1.02. In the area of the optical defined regions with normal grown grains the value may rise to 1.20 or more. For the last grains on the list, in the area of abnormal grain growth,

values of up to 1.50 are possible.

With the grain size separating normal abnormal grains the area fractions of the normal and abnormal grains can be evaluated and also the average grain size diameter of the normal and abnormal grains.

Small abnormalities may induce large errors in the calculated values for the fraction of abnormal grains. If the area fraction of abnormal grains was less than 10 %, it was assumed that no abnormal grown grain was observed and the value to separate the grains was not taken into account.

3.4 Definition of Grain Size Distributions

In the presented work, the size of each grain at a given time was directly calculated from the grain structure and the average grain size was obtained. But for an accurate description of grain growth process the grain size histograms were used. Due to the analysis of all grain structures evaluated, the definition of upper and lower grain sizes which are separating the grain size classes are illustrated in the table 3.2.

Class	*Lower class grain size [µm]*	*Upper class grain size [µm]*
1	0	15
2	15	25
3	25	35
4	35	45
5	45	55
6	55	65
7	65	75
8	75	85
9	85	95
10	95	1000

Table 3.2: Definition of classes of grain sizes by upper and lower grain size limit used for all annealing time steps.

3.5 Experimental Results

In this section the measured average grain sizes and grain size distributions for the annealing process are given. All grain structures analyzed were evaluated at leats for 300 grains. The grain sizes distinguishing normal and abnormal grains and the area fractions of abnormal grains are then evaluated [85].

In the following section, all diagrams are sequenced as follows:

- Firstly, the results of normal grain growth for all temperatures are shown (figure 3.5).
- Secondly, the results of abnormal grain growth are shown (figure 3.6).
- Thirdly, the fixed grain sizes separating normal and abnormal grain growth (section 3.3.4) are illustrated in figure 3.7.
- Fourthly, figure 3.8 shows the part of surface of abnormal grains versus the annealing time.
- Fifthly, according to the definitions in table 3.2, the grain size distribution for all temperatures and times are given in figures 3.9, 3.10, 3.11 and 3.12.

Figure 3.5 displays the normal grain sizes versus the annealing time for the annealing process. The diagram clearly illustrates the high influence of annealing temperature on the development of grain size.

For the annealing temperature of 900°C, the grain size doubles at 14400 seconds and then remains constant for 36 annealing hours. It is assumed that this is caused by impeding of grain growth by precipitations. The small variation of 4 μm is not significant, because there was only one specimen at each annealing time evaluated. The annealing temperatures of 1000°C and 1100°C lead to a higher grain growth rate. The 1200°C samples show a huge increase in grain size during the short annealing period.

The huge increase in grain size at high temperatures and short annealing times stimulate the development of abnormal grain growth. Figure 3.6 shows the abnormal grain sizes at different annealing temperatures. For the 900°C the forces for abnormal grain growth are to weak due to low temperature and precipitations, thus no abnormal grain

growth occurs. At higher annealing temperatures the forces for secondary recrystallization are high enough for exaggerated grain growth to develop. With higher temperatures abnormal grain growth starts earlier. For 900°C there is no abnormal grain growth even after 40 hours of annealing time, but for 1200°C abnormal grain growth is evident after just 7200 seconds. At 1100°C abnormal grain growth needs 28800 seconds (three times that of 1200°C and the 1000°C specimen needs 43200 seconds, which is almost double that at 1100°C and six times that at 1200°C.

The area fraction values in figure 3.8 for the 1000°C annealing specimen decline after 115200 seconds. A possible reason for this phenomenon is associated with the evaluation of the separating grain size between the distribution of abnormal and normal grains. At long annealing times over 24 hours and high temperatures the distribution of the grains overlap and the separating grain size reduces and so the fraction rises. At 1000°C and 115200 seconds annealing time the separating grain size was fixed at 200 μm and the result of the fraction of abnormal grains was 41 %. At 144000 seconds the separating grain size was 250 μm and the fraction 45 %. The fraction of abnormal grains rises to 55 and 69 % when the separating grain sizes are reduced to 100 and 120 μm. When the distribution overlaps and develops more than one peak the separating grain sizes are difficult to define after this scheme (see chapter 3.3.4).

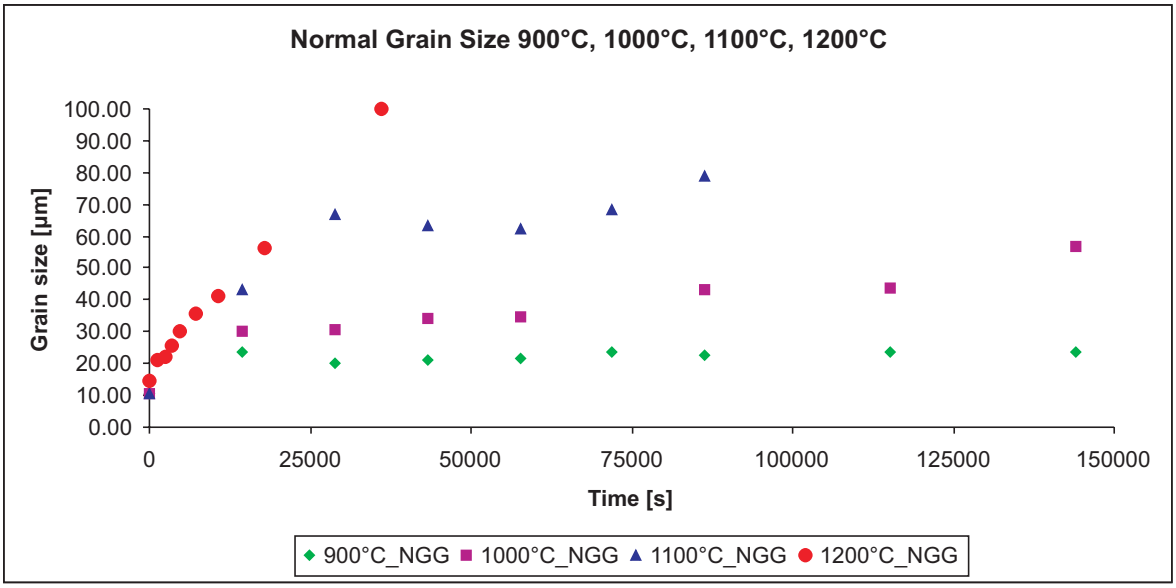

Figure 3.5: Grain size as a function of time for normal grain growth during the solution annealing process at different annealing temperatures.

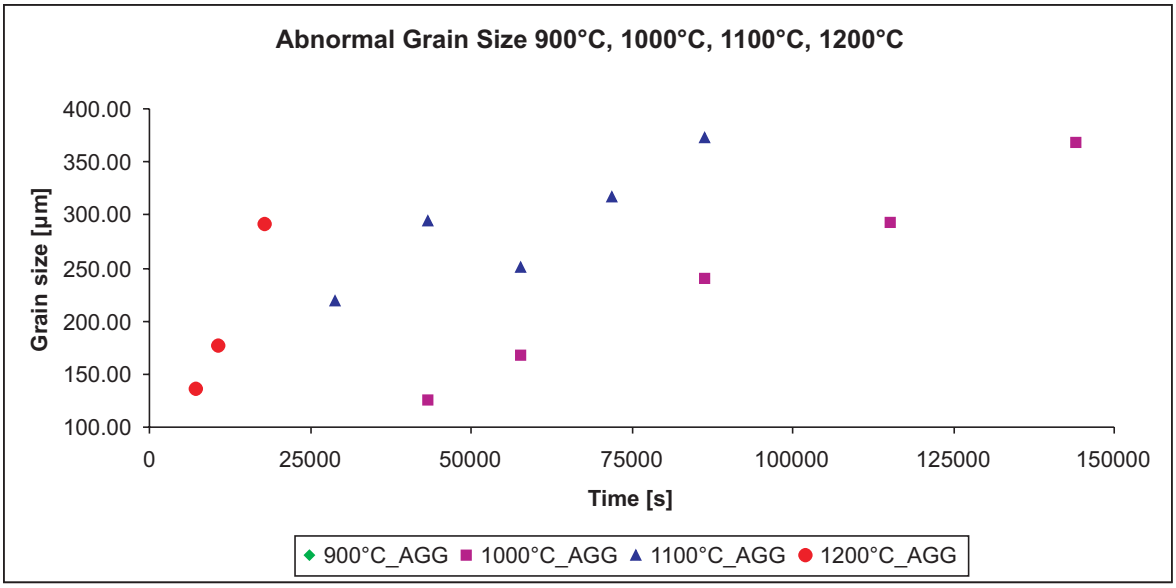

Figure 3.6: Abnormal grain size vs. annealing time for the solution annealing process at different temperatures and times.

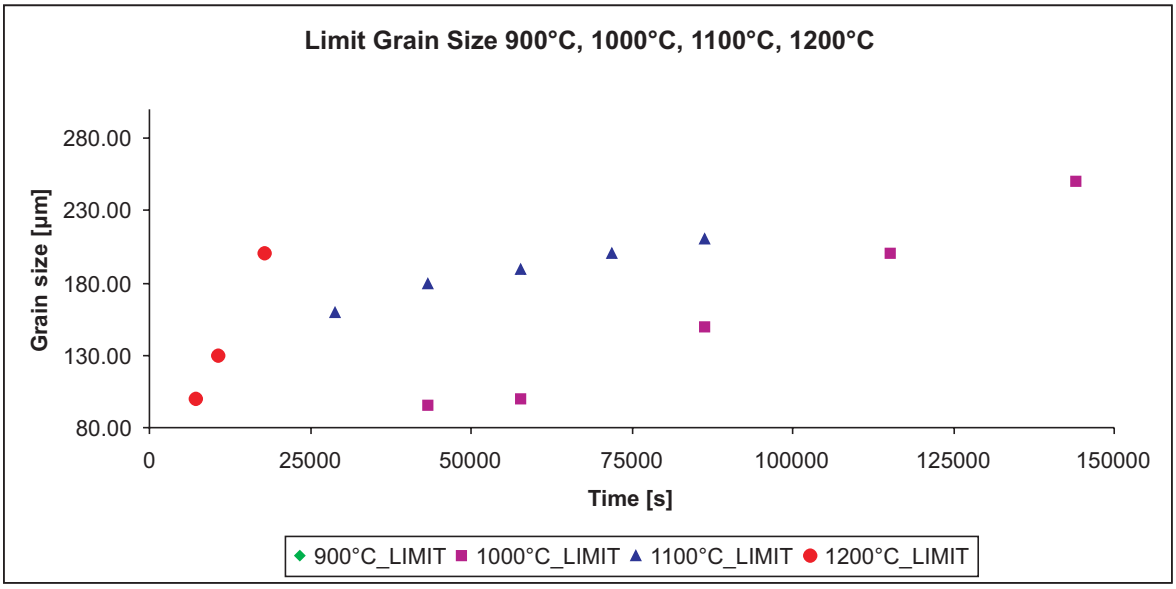

Figure 3.7: Evaluation of the defined grain size separating normal and abnormal grain growth vs. annealing time for annealing process at different temperatures and times.

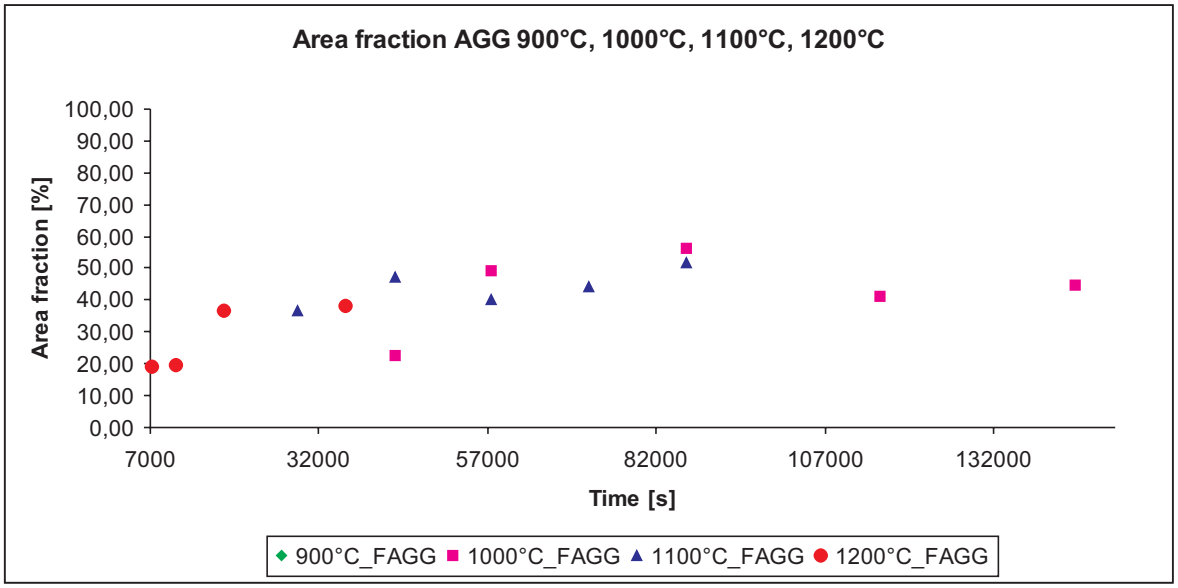

Figure 3.8: Illustration of area fraction for abnormal grain growth vs. annealing time for the annealing process at different temperatures.

The histograms for solution annealed specimens at the temperatures of 900°C, 1000°C, 1100°C and 1200°C are shown in the figures 3.9, 3.10, 3.11 and 3.12. The definition of upper and lower limits of grain classes are explained in chapter 3.4.

At the beginning of annealing process the upper histogram classes were not filled. Due to the limiting grain growth at 900°C there are no grains above the histogram class 8, even at long annealing time steps.

For 1000°C at least above the annealing time steps of 12h, all histogram classes are filled. For higher temperatures, despite the reference specimens, all histogram classes were filled for all annealing time steps. In order to validate the modelling setups and for a better understanding of abnormal grain growth, the grain size distributions were also predicted by application of cellular automaton simulations. Especially, the prediction of grain size separating normal and abnormal grains helped to eliminate erroneous results evaluated from optical metallography.

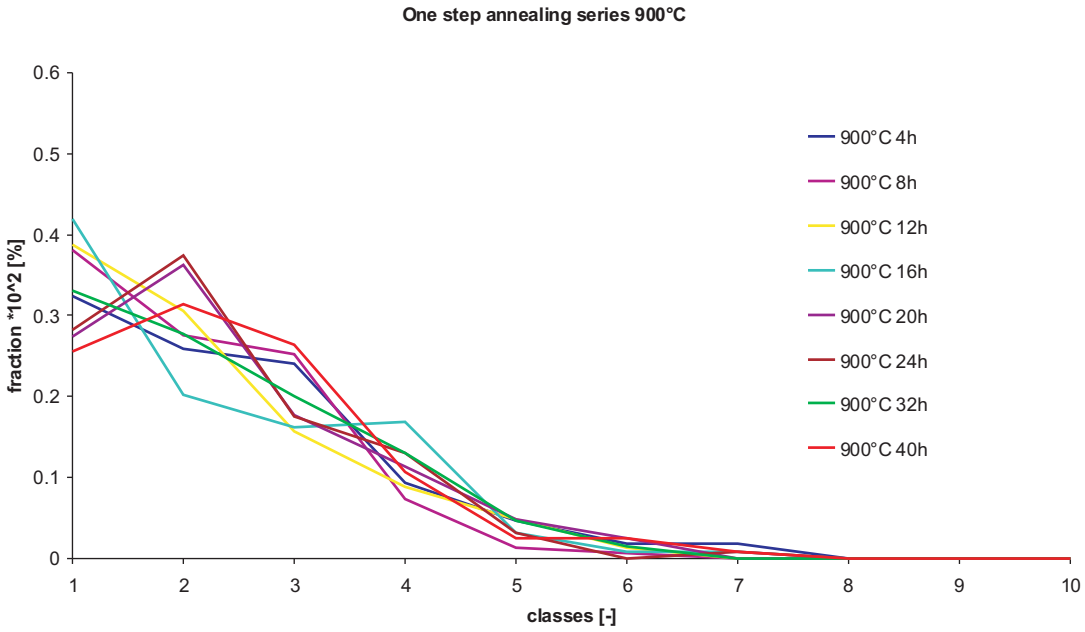

Figure 3.9: Histograms of the fraction of grain classes for the solution annealing at 900°C for different time steps.

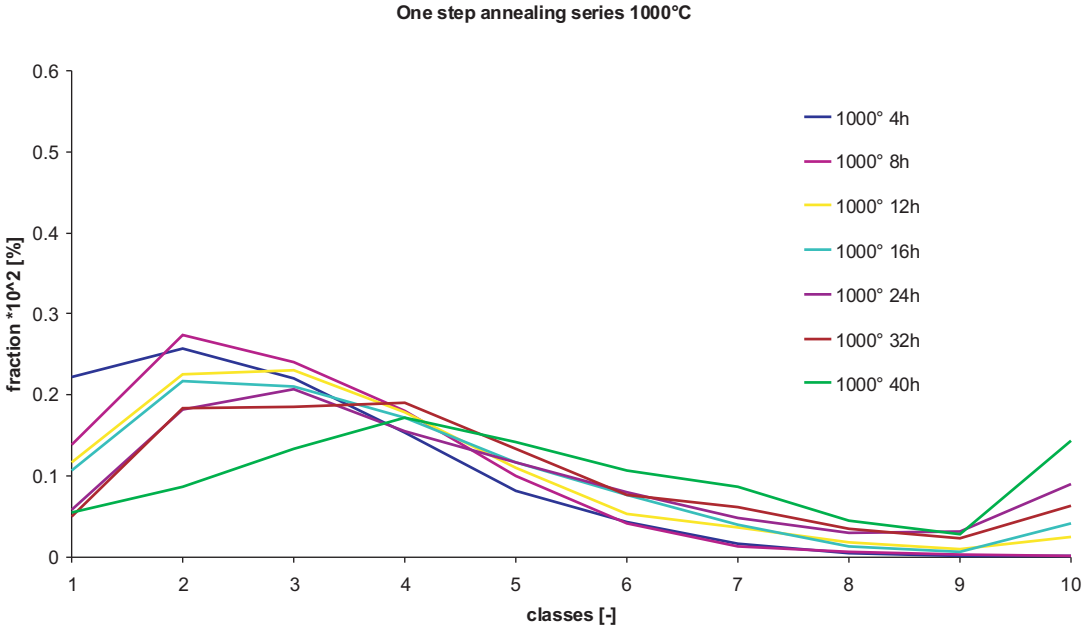

Figure 3.10: Histograms of the fraction of grain classes for the solution annealing at 1000°C for different time steps.

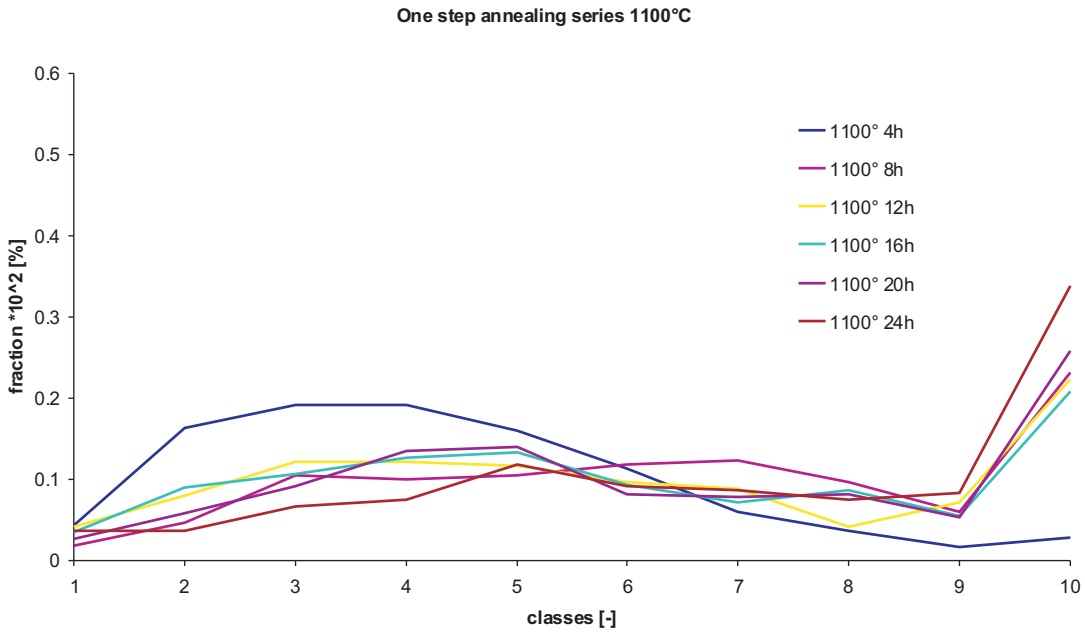

Figure 3.11: Histograms of the fraction of grain classes for the solution annealing at 1100°C for different time steps.

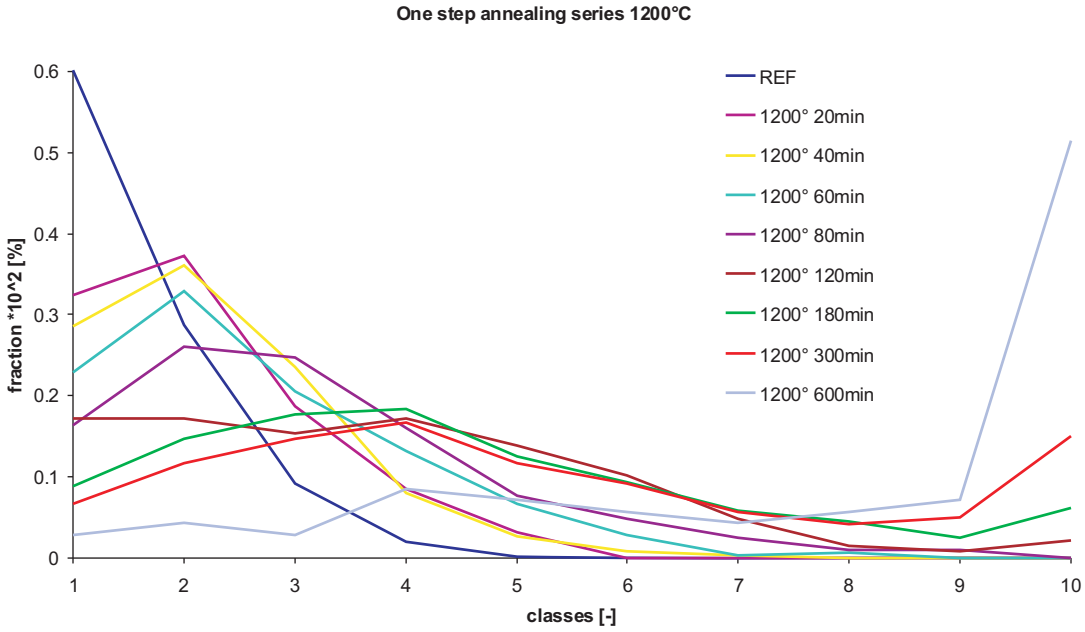

Figure 3.12: Histograms of the fraction of grain classes for the solution annealing at 1200°C for different time steps.

3.6 Evaluation of the Grain Growth Kinetics

In the following section the results of the evaluation of normal and abnormal grain sizes are analyzed. The well known equation $D = [(Aexp(-\frac{Q_{act}}{R_{gas}T}))^{\frac{1}{n}}t + D_0^{\frac{1}{n}}]^n$ was used and regressed (Software Statistica and TableCurve) in order to calculate the grain growth constants n, A and Q_{act}. For a useful regression at least three measurement points at the same annealing temperature are required. The received n-values, illustrated in table 3.3, for the regression of the annealed specimens are below 0.5, which corresponds to the literature value given in [86] and [87]. The activation energy Q_{NGG} is constant for normal grain growth at 62314.6 J/Kmol.

Temperature	*n [-]*	*A [-]*	*Q_{NGG} [J/Kmol]*
1000°C	0.31	0.00376	62314.6
1100°C	0.37	0.00494	62314.6
1200°C	0.43	0.00569	62314.6

Table 3.3: n, A and Q_{act} values for normal grain growth: regression results.

For the abnormal grain growth, the calculated results for the grain growth exponent n are higher than the values evaluated for normal grain growth due to a higher growth rate (table 3.4). The activation energies for normal and abnormal grain growth are assumed to be constant, but the value of Q_{AGG} is lower and equals 33682.7 J/Kmol.

Temperature	*n [-]*	*A [-]*	*Q_{AGG} [J/Kmol]*
1000°C	0.75	0.00217	33682.7
1100°C	0.80	0.00242	33682.7
1200°C	0.89	0.00297	33682.7

Table 3.4: n, A and Q_{act} values for abnormal grain growth: regression results.

Figure 3.13 summarizes the complete regression values of the annealing process. In order to compare the regression data, results of grain coarsening treatments for a type 304L steel of [5] are regressed in the same way. The evolution of the grain sizes of the literature are shown in table 3.5 and the n, A and Q_{act} values in table 3.6.

Time [s]	*1000°C*	*1050°C*	*1100°C*
0	7 μm	7 μm	7 μm
60	9 μm	14 μm	28 μm
120	13 μm	19 μm	31 μm
240	17 μm	30 μm	40 μm
600	25 μm	40 μm	49 μm
1200	31 μm	48 μm	62 μm

Table 3.5: EU Commission paper [5]: grain sizes of normal grain growth.

Temperature	*n [-]*	*A [-]*	*Q_{NGG} [J/Kmol]*
1000°C	0.36	0.0105	58329,6
1050°C	0.39	0.0152	58329,6
1100°C	0.42	0.0203	58329,6

Table 3.6: n, A and Q_{act} values for normal grain growth: regression results.

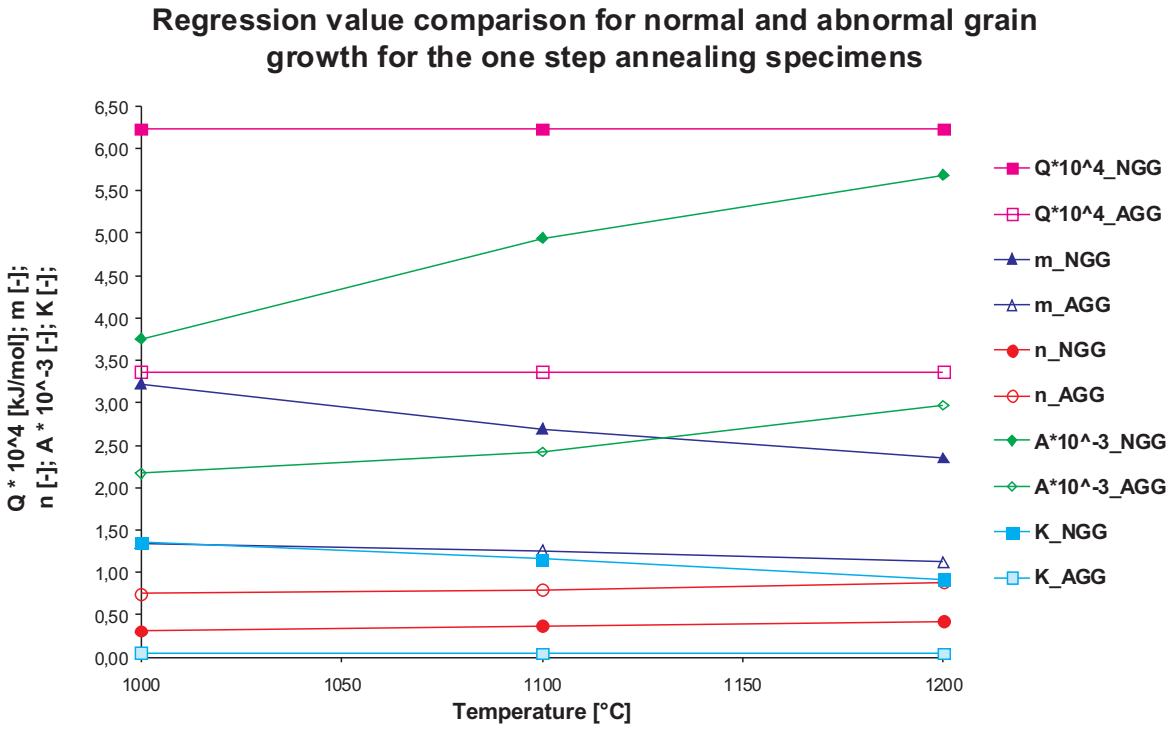

Figure 3.13: Comparison of all regression values for the annealing process.

3.7 Discussion of Experimental Assessments

Abnormal grain growth is observed earlier at higher annealing temperatures. The revealed grain structures showed abnormal grains for 1200°C at 7200 seconds, for 1100°C at 28800 seconds, for 1000°C at 43200 seconds and for 900°C never. The grain growth rate increases with annealing temperatures and abnormal grain growth occurs earlier. It is also stated that the activation energy for grain growth was much lower for abnormal grains than for normal grains.

Using TEM (Transmission Electron Microscopy) investigations with a very high resolution of grain structure, the reference specimen showed some faceted grain boundaries, where the biggest part composed of rough grain boundaries (figure 3.14). Faceted grain boundaries are often associated with abnormal grain growth, but it is not clear if faceted grain boundaries move faster than rough grain boundaries or vice versa. According to the literature survey, opposite explanation can be evaluated [52, 57].

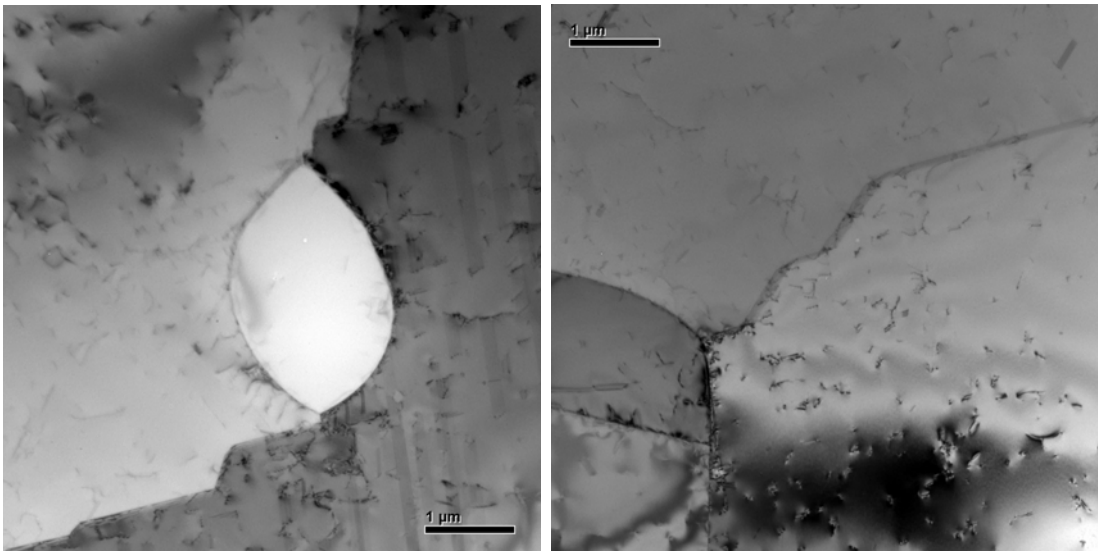

(a) (b)

Figure 3.14: Faceted Grain boundaries: results from Transmission Electron Microscopy. (a) and (b) represent different grain boundaries.

Gleiter [52, 57] explains that faceted grain boundaries start to grow earlier and became the candidate grains for abnormal grain growth. An exponential growth rate is stated in the beginning of solution annealing process for the grains with faceted grain boundaries,

where after a critical driving force is reached all grain boundaries (faceted and rough) move linearly with the same velocity, depicted in figure 2.7. Therefore, if some candidate grains are larger in size compared to the rest of the matrix grains, abnormal grain growth can be observed. It is noticeable, that until the candidate grains become relatively large, they can not be differentiated from normal matrix grains by optical metallography. So, it is assumed that faceted grain boundaries move with a higher mobility than grains with a rough grain boundary structure. It is assumed that the roughening of grain boundaries with annealing time could be the reason for the linear increase of grain boundary velocity.

Additionally, a preheating of reference specimens was performed, in order to test the influence of initial, i.e. starting, grain size on the development of abnormal grain growth. At 1000°C abnormal grain growth started after 43200 seconds of annealing time. A preheating time of reference specimens, with a significant change of initial grain size from 15 μm to 30 μm, led to a prolonging onset time for the start of abnormal grain growth where the first abnormal grains occurred at 86400 seconds of annealing time at the same annealing temperature of 1000°C. A higher starting grain size leads to growth rates, which were lower compared to the non preheated specimens, for both faceted and rough grain boundaries. Assumed that the growth rates of faceted and rough grain boundaries are still different but this time with a lower driving force, i.e. higher initial grain size, a much longer onset time for abnormal grain growth can be expected. Metallographically, much longer annealing times have to be performed for an accurate differentiation of grain structures. An other explanation could be the dissolution of faceted grain boundaries. The grain growth enhanced by two dimensional nucleation of grain boundaries may also be changed by lowering step-edge free energies or step heights. This can also result in a lower driving force of faceted grain boundaries.

4 Cellular Automata Modelling

This chapter focuses on the description of development and application of cellular automaton models for the prediction of normal and abnormal grain growth. Based on a literature survey, the cellular automaton method was chosen as an appropriate tool to incorporate topological features into a computer simulation and to give an improved space-time description of grain size distribution during grain growth. The provided measured initial grain size distributions purpose a modelling of discretized space, time and state of the physical system by using a rule set of incremental time steps where the state of dependent variables is determined at each of these discrete spatial locations.

Therefore, a deterministic CA model, where the equations for the grain boundary velocity due to grain boundary curvature, boundary energy and temperature are solved to calculate the net displacement of the boundary, and a probabilistic CA model, where the movement of a boundary is based on the stochastic majority rules, were developed.

The rule sets that govern the transition of the state of the cell are critical in determining the final microstructure and the degree to which these rules correspond to physical reality.

4.1 Deterministic Model

The calculation domain is divided into regular, square cells, where each cell represents a definite space in the material (i.e. grain identification) with periodic boundary conditions. In the first possible state of a cell, the entire cell represents a portion of a grain and is associated with the uniform property of the same. The other possible state is that of a grain boundary, where the cell can have fractions of two or even three grains, i.e. triple points, with the respective properties of the grains it belongs to [88, 89]. The schematic of the CA model domain comprising cells with grains and grain boundaries is shown in figure 4.1 based on models published earlier [77, 78].

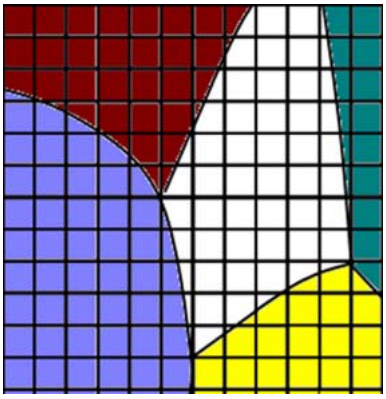

Figure 4.1: Grains with different crystallographic orientations (colors) in a CA model.

4.1.1 Modelling Setup

In order to simulate the grain boundary movement, the cells belonging to grain boundaries are identified at first and the displacement of the grain boundary is calculated. In contrast to earlier models [77, 78], the calculation of boundary displacement is performed for each boundary cell. The velocity of the grain boundary depends on the net pressure $p_{boundary}$ acting on the grain boundary:

$$p_{boundary} = \frac{2\gamma}{R_{cu}} f\left(\Delta\rho\right) \tag{4.1}$$

where γ is the grain boundary energy and R_{cu} is the local radius of the curvature of the grain boundary, calculated by using the height function technique, which is explained in chapter 4.1.1.1. The pressure on the grain boundaries acts in such a way that it forces the grain boundary to move towards the center of the curvature, hence the grain with a convex grain boundary grows and the grain with a concave grain boundary shrinks. It was assumed that the influence of deformation energy $f(\Delta\rho)$, described by variable deformation values evaluated by Electron Backscatter Diffraction, explained extensively in the chapter 4.1.1.2, decreases exponentially with annealing time.

The grain boundary displacement, ΔX, in a single time increment, Δt, is a function of the grain boundary pressure, and the mobility of the grain boundary:

$$\Delta X = M p_{boundary} \Delta t \tag{4.2}$$

The grain boundary mobility, M, is dependent on temperature (T) and activation energy for the grain coarsening Q_{act}:

$$M = M_0 exp\left(\frac{-Q_{act}}{R_{gas}T}\right) \tag{4.3}$$

where M_0 is a constant.

For the precipitations kinetics, firstly the limiting grain size of each grain D_{lim} is calculated according to the following equation, defined by Zener [90]:

$$D_{lim} = \frac{2d_p\,(t)}{3f\,(t)} \tag{4.4}$$

where d_p is the diameter of the particles (underlying Ostwald ripening) evaluated by the $MatCalc$® calculations [91] and updated during the whole simulation procedure by

$$d_p(t) = 2\left\{\left[kt^{\frac{1}{3}}\right]^3 + \left[\frac{d_p^0}{2}\right]^3\right\}^{\frac{1}{3}} \tag{4.5}$$

where k is a constant and d_p^0 is the diameter of the particles at the beginning of the simulation (see also chapter 4.1.3). During annealing the fraction of precipitates, $f\,(t)$, is assumed to decrease with time following

$$f\,(t) = f_0 - k_1 t \tag{4.6}$$

where k_1 is a constant and f_0 is the fraction at beginning of the simulation process.

4.1.1.1 Calculation of the Grain Boundary Curvature [77]

The grain boundary can either move forward or backward, depending on the sign of ΔX in equation 4.2. The fraction of a grain in a cell increases or decreases, and once the fraction in a cell becomes 1.0 or 0.0, the neighboring cells of different orientations (identification number) are captured to form a new grain boundary cell. The area swept by the boundary in a given cell is obtained from ΔX and the angle of normal, which is the line connecting the cell of interest with the center of mass of a grain in a circular area ($7x7$ cell diameter), shown in figure 4.2.

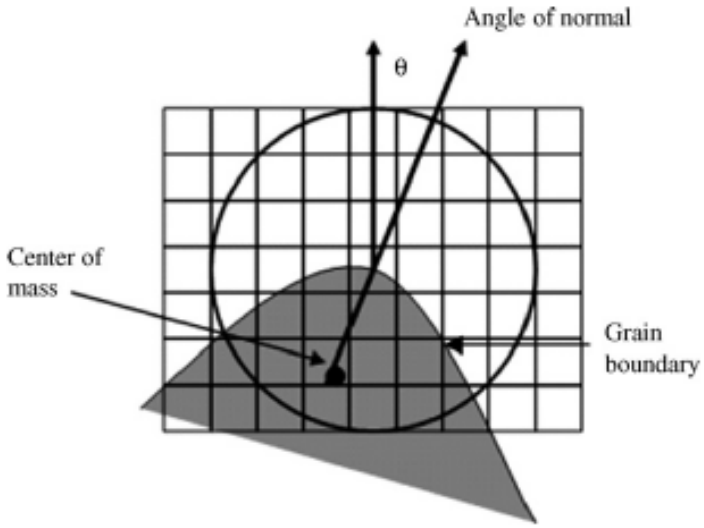

Figure 4.2: A schematic illustration of the calculation of the angle of the grain boundary normal [77].

In order to calculate the grain curvature the height technique is used, which was originally proposed by [92]. Thus, a region of $7x3$ cells is constructed around the cell of interest, i.e. grain boundary cell, and depending on the angle of normal, n, a vertical region is considered if the angle of normal is less than 45° and a horizontal region if the angle of normal is greater than 45°, depicted in figure 4.3.

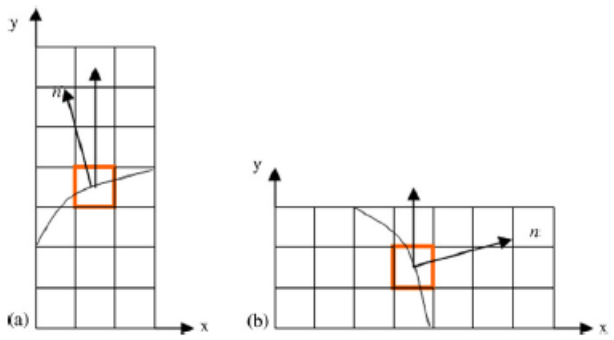

Figure 4.3: A schematic illustration of the cells to be considered if (a) the angle of normal is less than 45° and if (b) the angle of normal is more than 45° [77].

The sum of fraction of the grain of interest in each row or column is calculated to evaluate the height function, depicted in figure 4.4.

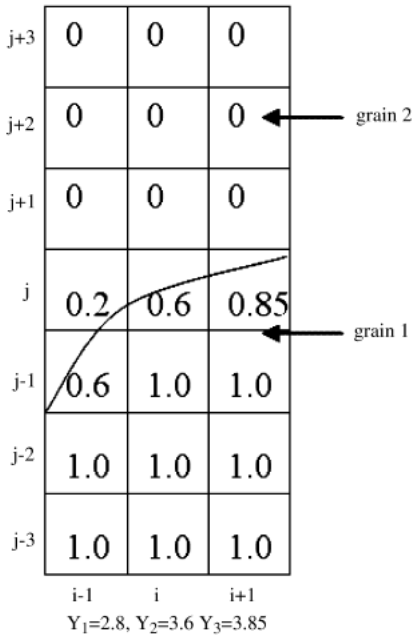

Figure 4.4: A schematic illustration of the calculation of the height function; The numbers in the boxes indicate the fraction occupied by grain-1 [77].

The curvature of every cell is calculated following

$$\kappa = -\frac{Y_{xx}}{\left[1 + \left(Y_x\right)^2\right]^{\frac{3}{2}}} \tag{4.7}$$

where the first, Y_x, and second, Y_{xx}, derivatives of the height function are used.

4.1.1.2 About the Consideration of Deformation Energy

Electron Back Scatter Diffraction (EBSD) is widely used for characterizing the grain structure of engineering materials by determining the crystallographic orientation. Therefore three different methods for the description of the induced plastic strain, namely the CD, MCD and M_{aver} values were used. All values were developed by Kamaya [93], and also calculated by himself for our purposes in this thesis.

Crystal Deformation (CD) and Modified Crystal Deformation (MCD)

Using EBSD in conjunction with scanning electron microscopy, a parameter, which quanti-

fies the spread of the crystal orientation within individual grains arising due to dislocation accumulation during plastic deformation, is correlated with imposed plastic strain. The parameter is called crystal deformation (CD) and is determined from the spread in misorientation from the mean grain orientation [93].

Further in [94], Kamaya explains that the accuracy of the measurements of misorientation was improved by the technique called the Domain Averaging Method (DAM). It is shown that DAM reduces the error in misorientation and enables us to obtain a clear distribution of misorientations. The distribution followed a log-normal distribution and its mean value correlated linearly with the macroscopic plastic strain induced in the specimens. By using the correlation between misorientation and the plastic strain, the distribution of local plastic can be estimated defining the so-called Modified Crystal Orientation (MCD), which was another value used in this work.

Firstly, the misorientation distribution was represented by the log-normal distribution for both strained and un-strained material. Then, the mean of the log-normal distribution was defined as the modified crystal deformation (MCD):

$$MCD, CD = exp \frac{\sum_{k=1}^{n_g} \left(ln \left\{ \beta(m_{k,i}) \right\} \right)}{\sum_{k=1}^{n_g} n_k} \tag{4.8}$$

where $\beta\ (m_k, i)$ denotes the misorientation between the central orientation, m, of the k-th grain and the point i that belongs to the k-th grain, and n_k is the number of points included in the grain.

The parameters explained above and used in this work have good correlation to the degree of the plastic strain and they are independent of the measurement conditions such as the EBSD system used for the measurements, number of data and step size in the crystal orientation map, electron beam condition, grain size and material.

Averaged Misorientation (M_{aver})

A spatial distribution of the local change in the crystal orientation corresponds to the averaged misorientation angle β between neighboring points p and is named the local

misorientation. The calculation of local misorientation in the grain interior (figure 4.5 a) is performed as

$$M_L = \frac{1}{4}\{\beta(p_0, p_1) + \beta(p_0, p_2) + \beta(p_0, p_3) + \beta(p_0, p_4))\} \tag{4.9}$$

and on the grain boundary (figure 4.5 b) as

$$M_L(p_0) = \frac{1}{2}\{\beta(p_0, p_2) + \beta(p_0, p_3))\} \tag{4.10}$$

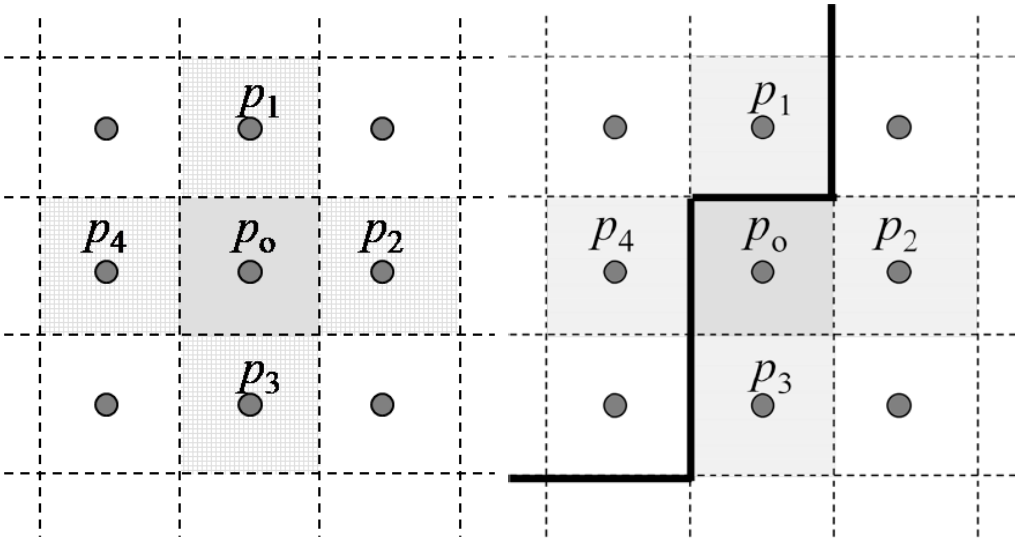

Figure 4.5: Illustration of the consideration of local orientation for the calculation of local misorientation in a grain (a) and at a grain boundary (b).

Exemplarily in the figure 4.6, it is shown that the degree of the local misorientations tends to be large near the grain boundaries. From earlier publications it is known that local misorientations correlate well with the degree of local dislocation density [93–102].

As a reference, the evaluated average value of all local misorientations, M_{ref}, of an undeformed homogenized specimen is used and compared to the values of M_{aver} for deformed specimens, described as:

$$f(\Delta\rho) = \frac{M_{aver}}{M_{ref}} \tag{4.11}$$

The same procedure can be performed by using the CD or MCD value.

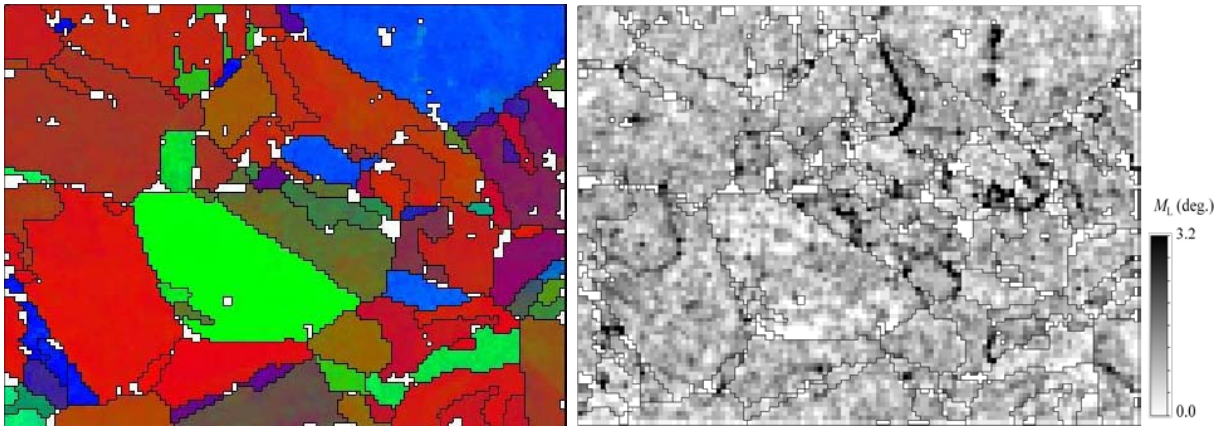

(a) (b)

Figure 4.6: Illustration of (a) an orientation map and (b) a local misorientation map of a deformed specimen.

4.1.2 Effect of Lattice Cell Number on Simulation Time

For the evaluation of simulation time depending on the grain structure resolution, the simulation was repeated for different number of cells. In this study the influence of precipitates or and deformation energy was not considered. A higher resolution of the grain structure led to increasing simulation times, as visible in the table 4.1.

dimensions	**number of cells**	$\Delta t_{simulation}$ [s]
$200x200$	40000	1
$283x283$	80000	2.5
$400x400$	160000	5.3

Table 4.1: The influence of the resolution on simulation time for the deterministic model. For the comparison of simulation times, the lowest resolution of the grain structure was defined arbitrary to have a simulation time of 1.

The simulation time of the deterministic model depends strongly on the number of grain boundaries in the simulated grain structure. As grains grow, the number of grain boundaries decreases with simulation time, thus the time for one reorientation loop of all cells

decreases with simulation time. For the evaluation of the results in the table 4.1, the same initial grain structures were used.

4.1.3 Modelling Results for Normal Grain Growth in the Presence of Second Phase Particles

When the pressure on a grain boundary due to the particle pinning is equal to the driving pressure for grain growth, the growth is impeded and the limiting grain size for grain growth is reached. $M_{23}C_6$ is the predominant carbide formed in the austenitic stainless steel 304L which dissolutes very quickly at the austenitic grain boundaries during the solution annealing process, explained extensively in chapter 2.1. In order to validate the influence of precipitates for the deterministic CA model, starting at 900°C for 5h, a heating up with $10°C/h$ and a final solution annealing at 1000°C for 5h was experimentally conducted and compared to the simulation results. The precipitations kinetics were evaluated by MatCalc® calculations and compared to the results of the deterministic CA model incorporating Ostwald ripening (equation 4.5) and the fraction of precipitates (equation 4.6) which is decreasing during the solution annealing process (figure 4.7).

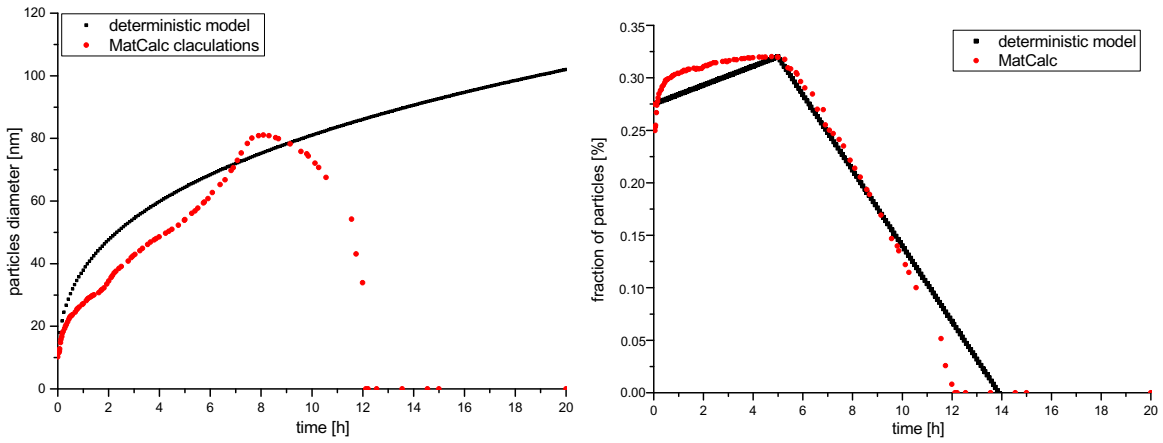

(a) (b)

Figure 4.7: Comparison of precipitations kinetics during solution annealing evaluated by MatCalc®, fitted empirical model, and used in the deterministic CA model.

Different approaches of limiting grain sizes described in chapter 2.2.2 were tested and compared with experiments, depicted in figure 4.8.

The slow increasing of limiting grain size defined by Gladman (D_G) at different Z-values,

namely 1.43, 1.70 and 2.0, led to strong and inaccurate impeding of grain boundary movement and was therefore not adapted in the deterministic model for the description of precipitation kinetics.

In contrast to the results of Gladman, the application of limiting grain size defined by Elst (D_E) predicted a much higher grain size. Similar results were obtained by D_R and D_S, defined by Rios and Smith.

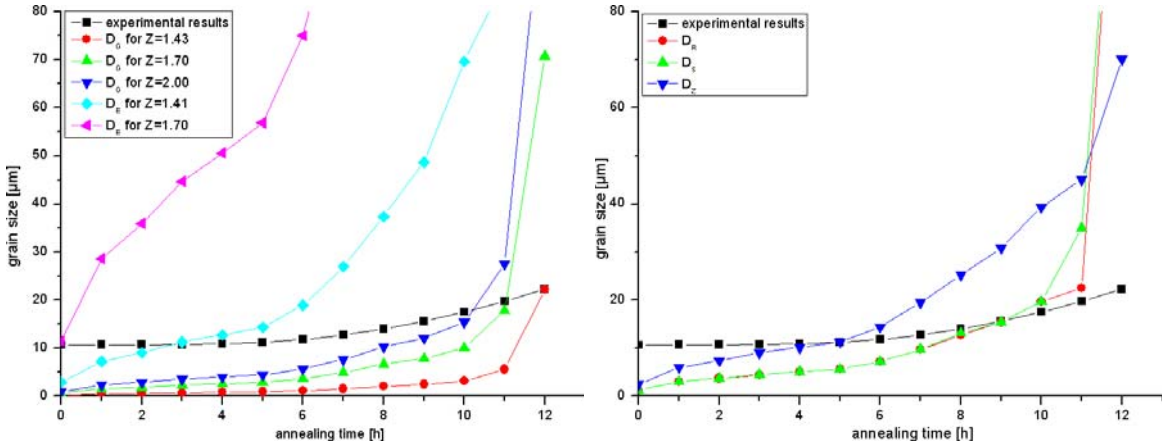

(a) (b)

Figure 4.8: Comparison of the experimental results for average grain size and evaluation of limiting grain size by (a) Gladman (D_G) and Elst (D_E) for different Z-values and (b) by Rios (D_R), Smith (D_S) and Zener (D_Z).

For the comparison of the modelling predictions and the experimental results, the definition of limiting grain size by Zener was evaluated as an appropriate solution. Therefore the deterministic model defines the limiting grain size as

$$D_{lim} = \frac{2d_p\,(t)}{3f\,(t)} \tag{4.12}$$

where the starting conditions (particles diameter, fraction of particles) are defined by MatCalc® calculations.

The dissolving of particles started after an annealing time of 6h resulting in a growing of the limiting grain size and therefore increasing of average grain sizes. The obtained simulation results corresponded well to the evaluated experimental results, depicted in figure 4.9.

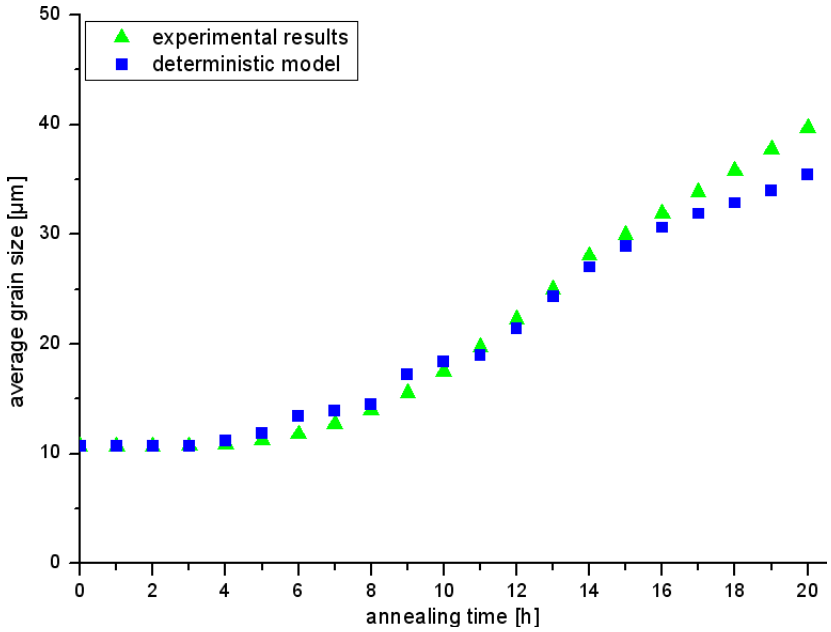

Figure 4.9: Prediction of grain growth in the presence of second phase particles (deterministic model). The solution annealing began at 900°C for 5h, afterwards heated up with $10°C/10h$ and a final solution annealed at 1000°C for 5h. Precipitations diameter and fractions were evaluated by MatCalc®, and limiting grain size is according to the definition by Zener [90].

4.1.4 Modelling Results for Normal Grain Growth

Experiments and simulations of homogenized, un-deformed, specimens were performed between 900°C and 1200°C for up to 144000 seconds (40h) of annealing time, explained in chapter 3.5. The values of grid size and time step were chosen accurately for the desired resolution of the microstructure after a testing of grid size and time step sensitivity. Due to long processing times of the deterministic model, the resolution of 40000 (200x200), thus a calculation domain of 225x225 μm with the grid size of 1.13 μm was defined.

Exemplarily, the developing grain structure from the deterministic CA model for the normal grain growth are shown in figure 4.10. Many features of normal grain coarsening can be seen in the simulated grain structures, beginning from microstructure evolution driven by the excess free energies associated with the grain boundaries resulting in an increase of the overall grain size, the growth of larger grains at the cost of smaller ones and the evolution of grains towards stable six-sided configurations and preferred configurations of triple points at 120°.

(a) t=1h (b) t=3h (c) t=5h (d) t=10h

Figure 4.10: Results of the simulated grain structures as a function of time for the annealing process at 1200°C (deterministic model).

The area of each grain at a given time step is directly calculated from the microstructure by counting the number of cells within a grain. The grain size D is obtained from the area by assuming a circular shape for all grains, therefore $A = D^2\pi/4$. The average grain diameter at a given time step is then obtained by averaging over all the grains in the system. The results are shown in the figure 4.11.

In the chapter 3.5 "Experimental Results" the grain growth kinetics of the austenitic stainless steel 304L for all four simulated solution annealing temperatures (900°C, 1000°C, 1100°C, 1200°C) were described in detail. Evaluated MatCalc® results for precipitation kinetics proved a strong impeding of grain growth for the annealing cycle at 900°C, which can be seen in the figure 4.11a. The simulation parameters incorporating precipitation kinetics, defined in the deterministic CA model, predicted a good correspondence of average grain sizes between simulation and experiments for 900°C. In the beginning of the simulation the grains with $D < D_{lim}$ are growing until the limiting grain size (D_{lim}) is reached. All other grains $D > D_{lim}$ are not growing until the limiting grain size changes, due to the defined precipitation kinetics. The end of solution annealing cycle defined the limiting grain size as 22.9 μm, d_p of 110 μm and f of 0.32 %, which results in strong impeding of normal grain growth, depicted in figure 4.11a.

According to the MatCalc® results, for annealing temperatures 1000°C, 1100°C and 1200°C all precipitations dissolved very quickly. Therefore, without any impeding of grain boundaries, the grain growth depends solely on the temperature dependent mobility M defined in CA model. An appropriate definition of mobilities resulted in a good correspondence of normal grain growth, depicted in figures 4.11 b-d.

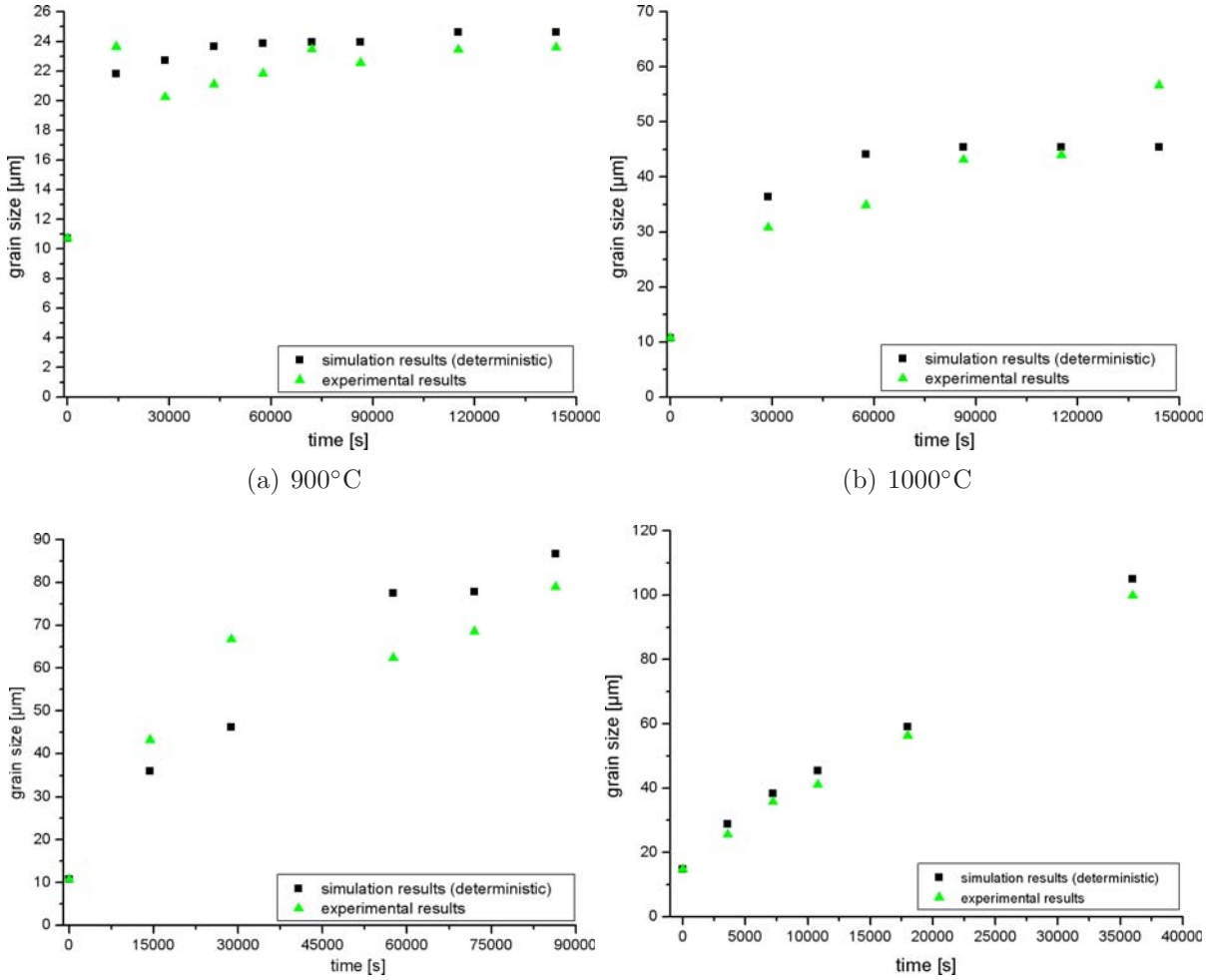

(a) 900°C (b) 1000°C

(c) 1100°C (d) 1200°C

Figure 4.11: Comparison of experimental and simulated results for solution annealing process at different annealing temperatures (deterministic model).

The grain size distributions are presented in figures 4.12, 4.13 and 4.14 for the solution annealing temperatures 1000°C, 1100°C and 1200°C at different annealing time steps. Due to the strong impeding of grain growth at 900°C, the grain size distributions of different time steps were not changing significantly and therefore not presented. Although the average grain size corresponded well with simulation results, the grain size distribution showed some offset comparing to the experimental results. Therefore, the topological rearrangements play an important role in the evolution of grain structures where the rate of change of grain size of an individual grain rather depends on the topological class then just on the curvature.

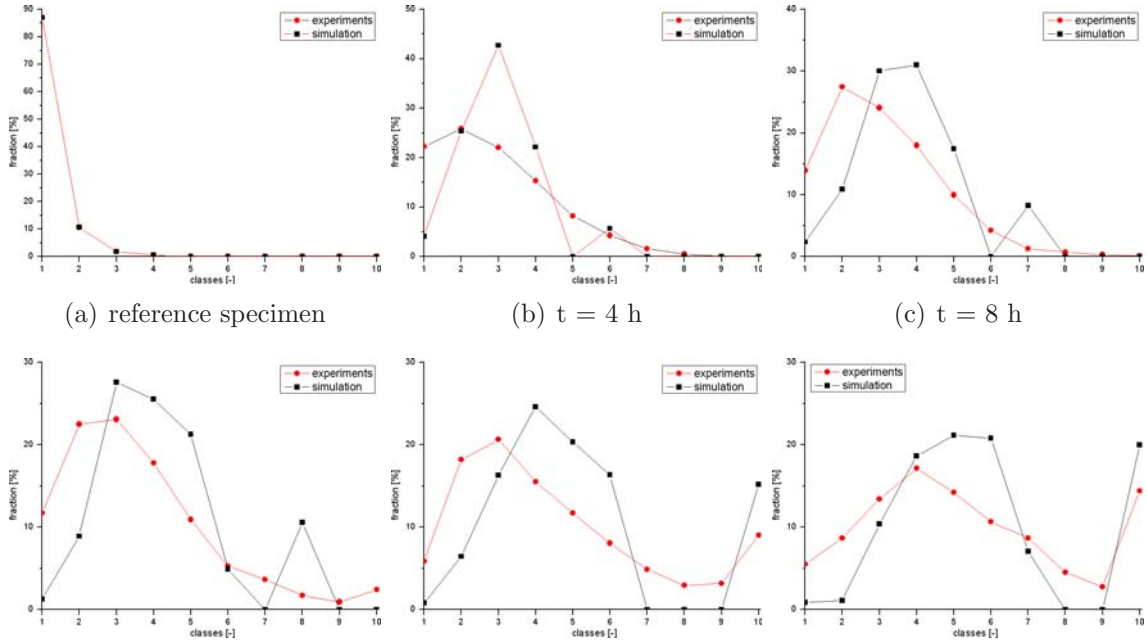

(a) reference specimen (b) t = 4 h (c) t = 8 h

(d) t = 12 h (e) t = 24 h (f) t = 40 h

Figure 4.12: Grain size distributions (deterministic model) for normal grain growth at 1000°C and annealing times of (a) 0, (b) 4, (c) 8, (d) 12, (e) 24 and (f) 40 hours.

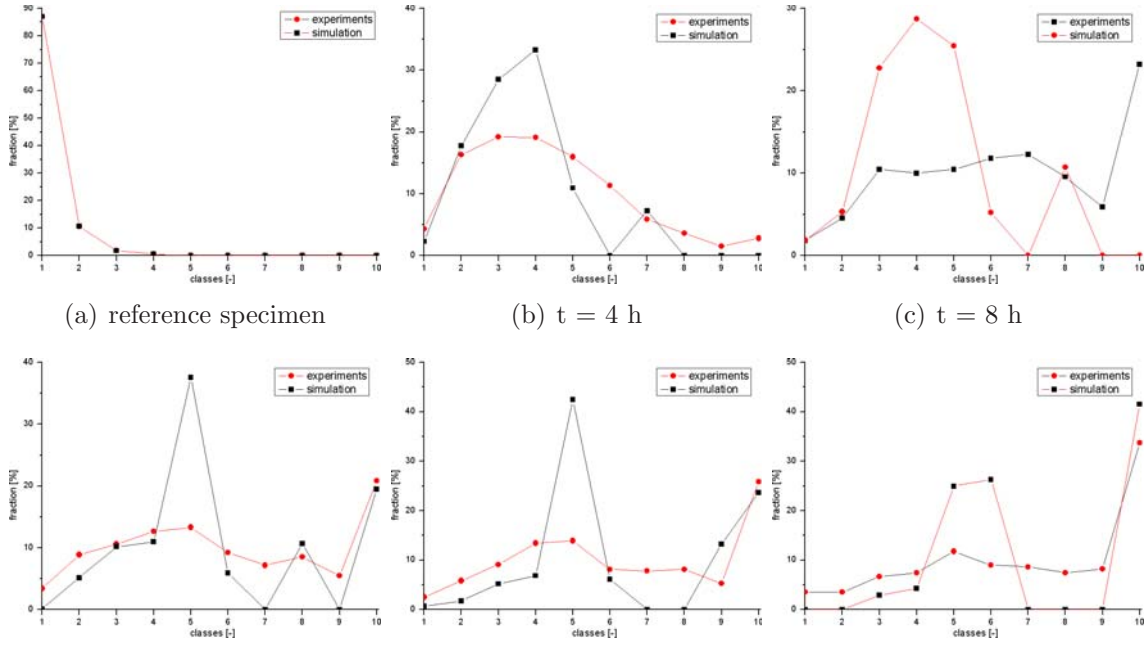

(a) reference specimen (b) t = 4 h (c) t = 8 h

(d) t = 16 h (e) t = 20 h (f) t = 24 h

Figure 4.13: Grain size distributions (deterministic model) for normal grain growth at 1100°C and annealing times of (a) 0, (b) 4, (c) 8, (d) 16, (e) 20 and (f) 24 hours.

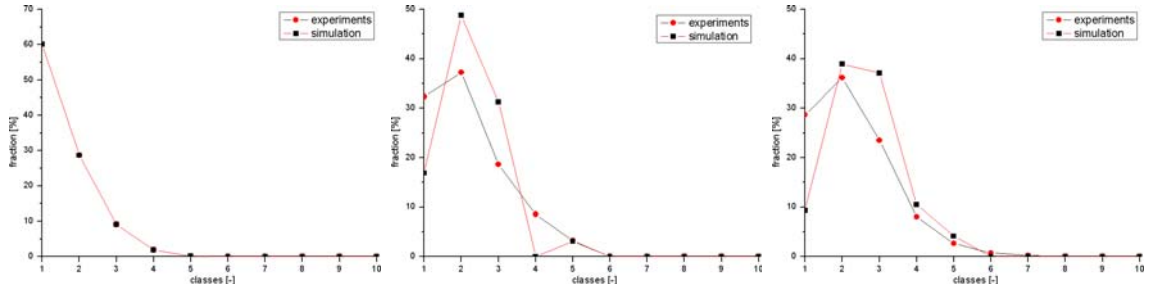

(a) reference specimen (b) t = 20 min (c) t = 40 min

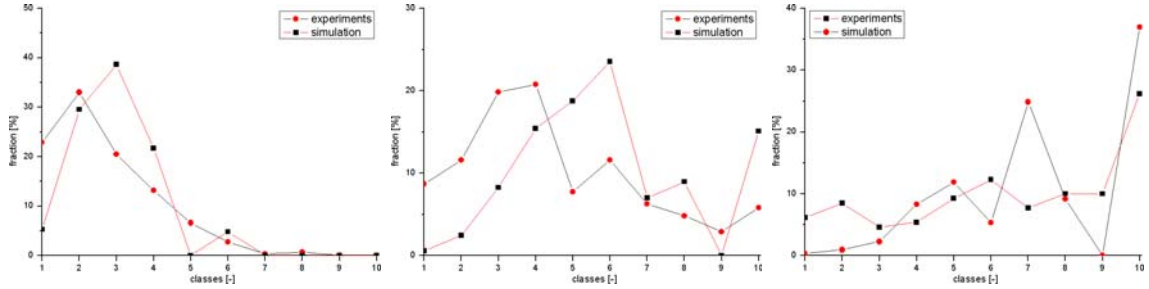

(d) t = 60 min (e) t = 300 min (f) t = 600 min

Figure 4.14: Grain size distributions (deterministic model) for normal grain growth at 1200°C and annealing times of (a) 0, (b) 20, (c) 40, (d) 60, (e) 300 and (f) 600 minutes.

According to the simulation results of Raghavan [77, 78] and Lan [80] explained in chapter 2 entitled "Fundamentals", the mobility of grain boundaries is temperature dependent and is often found to obey the Arrhenius type relationship, discussed in the chapter 3.6 entitled "Evaluation of the Grain Growth Kinetics". The regressed experimental results defined an activation energy for normal grain growth of 62.3 kJ/mol.

For the regression of the grain growth mobility in the deterministic model, a constant grain boundary energy, γ, of 0.5 $[J/m^2]$ was defined as in [61]. Depending on the used grain structure resolution, the mobility is related to the atom-scale thermally activated process which controls the boundary migration [88] and was fitted as

$$M = M_0 exp\left[-\frac{Q_{act}}{R_{gas}T}\right] = 0.000136 exp\left[-\frac{83338}{R_{gas}T}\right] \tag{4.13}$$

presented in figure 4.15.

The dependance of grain growth mobility on annealing temperature (figure 4.15) led to the evaluation of activation energy for normal grain growth (Q_{act}=83.3 kJ/mol).

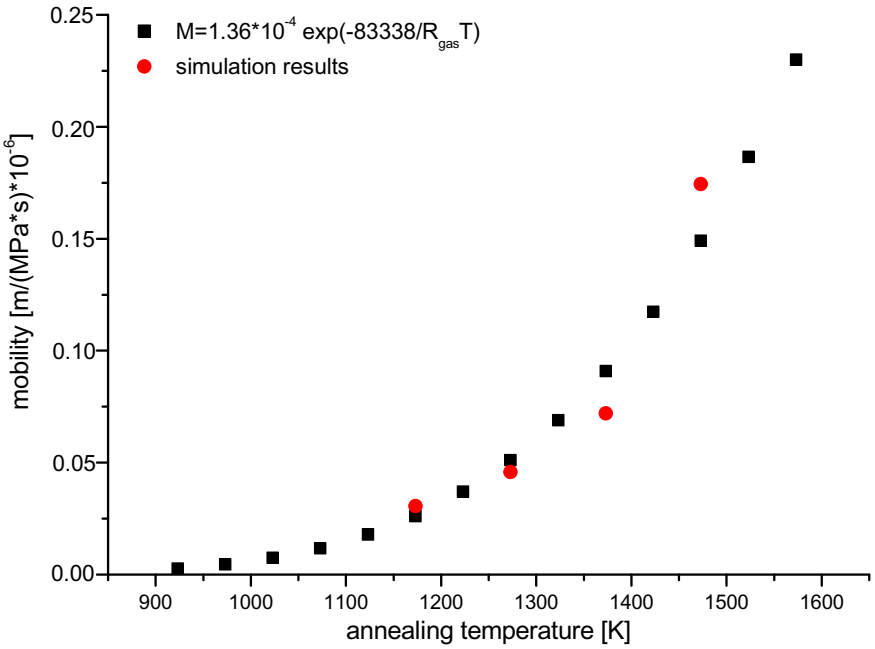

Figure 4.15: Simulation results and corresponding values of equation 4.13 for normal grain growth in the deterministic model.

The calculation of the grain boundary curvature bases on the number of cells describing the topology of grains. So, a grain described by high number of cells possess a low grain boundary curvature, thus a lower grain boundary velocity or mobility. Therefore, the description of grain growth kinetics, e.g. activation energy, depends on the defined grain structure resolution and the space-time relation of modelling parameters.

Defining the Burgers vector of $b = 2.5 \cdot 10^{-10}\ m$ [103] and using the evaluated value for the activation energy of normal grain growth ($Q_{act} = 83.3\ kJ/mol$), the boundary diffusion term $\delta_{gb}D_b$ can be derived as

$$\delta_{gb}D_b = \frac{M_0 k_{boltz} T}{b} \tag{4.14}$$

The defined $\delta_{gb}D_b$-values for each temperature of $8.8{\cdot}10^{-15}\ m^3/s$, $9.6{\cdot}10^{-15}\ m^3/s$, $1.0{\cdot}10^{-14}\ m^3/s$ and $1.1 \cdot 10^{-14}\ m^3/s$ for 900°C, 1000°C, 1100°C and 1200°C corresponded to the values presented in other publications [81], explained in chapter 2.3.4 entitled "Cellular Automaton Method".

4.1.5 Modelling Results for Abnormal Grain Growth

The procedure employed in the simulation of abnormal grain coarsening was nearly identical to those developed in modelling of normal grain growth, presented in chapter 4.1.4. The main difference was that a larger domain area of 182399 μm^2, a grid size of 1.42 μm and 90300 (350x258) cells were used, which was necessary for an accurate description of evaluated experimental results. Therefore a fraction of candidate grains with a higher mobility was defined for incorporating of an advanced grain boundary velocity describing abnormal grain growth.

Especially for high grain structure resolutions, the deterministic model requires long calculation times. Therefore, the calculations of abnormal grain growth were just performed until the first occurrence of abnormal grains in the grain structure. The simulations aimed for corresponding average grain sizes of normal grains, abnormal grains and fraction of abnormal grains for the last annealing time step. The last simulation time step was defined as the first annealing time step where abnormal grain growth occurred. The simulations were performed at 1000°C, 1100°C and 1200°C for 43200 seconds, 28800 seconds and 7200 seconds.

For the grain structures developed, similar features were observed as for simulation of normal grain growth in the deterministic model, explained in chapter 4.1.4. The candidate grains are growing at the cost of smaller grains but posses more than six sided topologies and preferred configuration of 120°. In the figure 4.16 the initial, i.e. starting, grain structure and the grain structure at the first occurrence of abnormal grains are demonstrated.

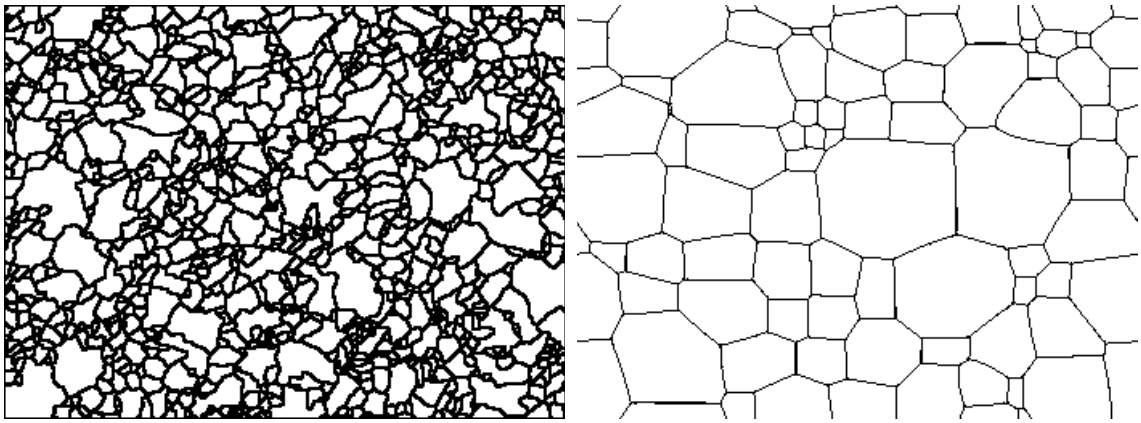

(a) reference specimen (b) t = 120 min

Figure 4.16: Simulation of abnormal grain growth: grain structures for 1200°C at (a) 0 and (b) 120 minutes (deterministic model).

Due to different space-time relation, the used simulation parameters were different from that simulation parameters evaluated in the simulation of normal grain growth (chapter 4.1.4). The mobility of grain boundaries is temperature dependent and is different for normal and abnormal grain growth, presented in equations 4.15 and 4.16, where a constant grain boundary energy (γ) of 0.5 $[J/m^2]$ was defined [103]. The results proved the different values of activation energies for grain growth between normal and abnormal grain growth process. The mobility is related to the atom-scale thermally activated process which controls the boundary migration [88] and is described for normal grain growth as

$$M = M_0 exp\left[-\frac{Q_{act}}{R_{gas}T}\right] = 0.0048 exp\left[-\frac{75400}{R_{gas}T}\right] \tag{4.15}$$

and for abnormal grain growth as

$$M = M_0 exp\left[-\frac{Q_{act}}{R_{gas}T}\right] = 0.0048 exp\left[-\frac{33700}{R_{gas}T}\right] \tag{4.16}$$

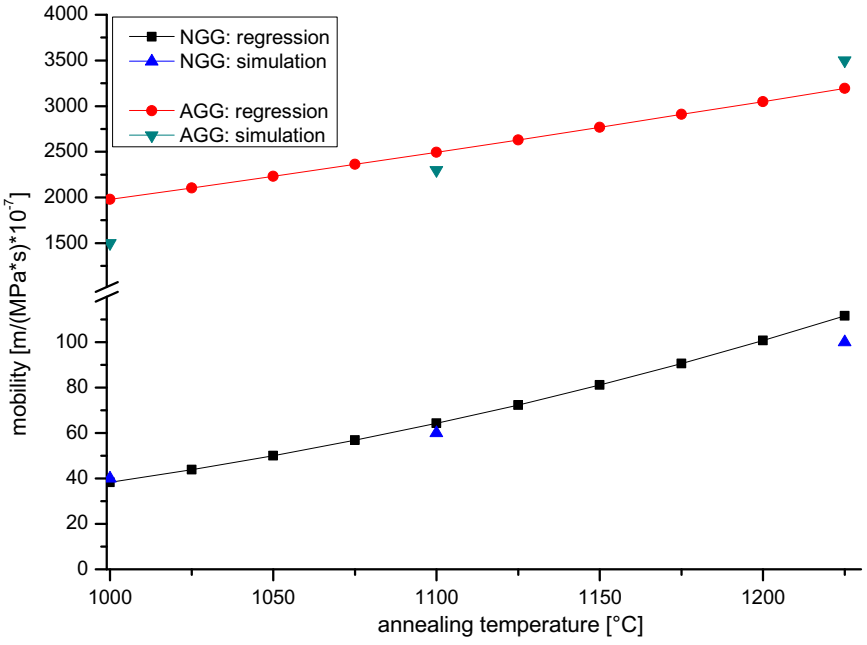

Figure 4.17: Illustration of the results of mobility vs. annealing temperature for the deterministic model: normal and abnormal grain growth.

The simulated grain structure helped for the definition of the fractions and mobilities of both normal and abnormal grain growth phenomena. The fraction of abnormal grains

was defined to be 0.1 % and equal for all annealing temperatures simulated. Therefore, only a very low fraction of grain boundaries grows with an approximately 35-times higher mobility, resulting in abnormal grain growth, which is depicted in figure 4.17.

4.1.6 Modelling Results for Normal Grain Growth in the Presence of Deformation Energy

In order to validate the stored deformation energy of the deterministic model, one-hit upsetting tests were carried out on the computer-controlled dynamic system Gleeble ^{TM} 3800 [104–106]. Samples employed were cylindrical of 10 mm diameter and 12 mm length. Before compression, all specimen were homogenized for 20 minutes at 1200°C and air cooled afterwards, resulting in an initial grain size of 21.3 μm. The specimens were heated up to the testing temperature, held at this temperature until stabilization and then compressed. Hot deformation was performed at $T_{def} = 750$, a strain rate of $1.0s^{-1}$ and φ_{global} of 0.8, resulting in a deformed un-recrystallized grain structure. After deformation, the samples were solution annealed at 1000°C for 1h. The short annealing times were chosen due to the strong recovery of deformation energy at 1000°C.

Afterwards, EBSD measurements were carried out and CD value, MCD value, M_{aver} value were evaluated. In the chapter 4.1.1.2 entitled "About the Consideration of Deformation Energy" all three methods are described. All evaluated deformation values showed an approximately five times higher stored energy term in the deformed specimen compared to the homogenized un-deformed specimen, which is presented in the table 4.2.

specimen	CD value	MCD value	M_{aver} value
un-deformed	1.22	0.87	0.37
deformed	6.55	5.30	1.74
ratio (deformed/undeformed)	5.36	6.09	4.7

Table 4.2: CD, MCD and M_{aver} values obtained from EBSD data of undeformed and deformed 304L steel.

Based on a literature survey [56, 107–110], deformation can lead to an accelerated grain growth. In comparison to homogenized un-deformed samples, the evaluated misorientation values described in average an approximately five times higher grain boundary pressure of deformed samples. Therefore, it is assumed that in average all cells of the sim-

ulation area posses the same reinforcements of grain boundary pressure when deformed. Due to the irregularity of EBSD scanning (e.g. measurement errors due to high local deformations), the local evaluation of deformation energy could not be performed, thus a global application of the EBSD methods (table 4.2) was used for the simulation procedure. For the recovery of deformation energy during the solution annealing process, it is assumed that the influence of deformation energy declines exponentially until the end of annealing time.

By using the same simulation parameters (mobility, resolution) of normal grain growth (chapter 4.1.4), the simulation without considering the deformation energy results in a lower average grain size. Therefore, considering the M_{aver}-value of 1.74 of deformed specimens, which is 4.7-times higher than the M_{aver}-value of un-deformed specimens and incorporating an exponential declination of $f(\Delta\rho)$ from initially 4.7 to 1 at 60 minutes, defined in equation 4.1, was performed. The simulation results corresponded well to results obtained by experiments, depicted in figure 4.18.

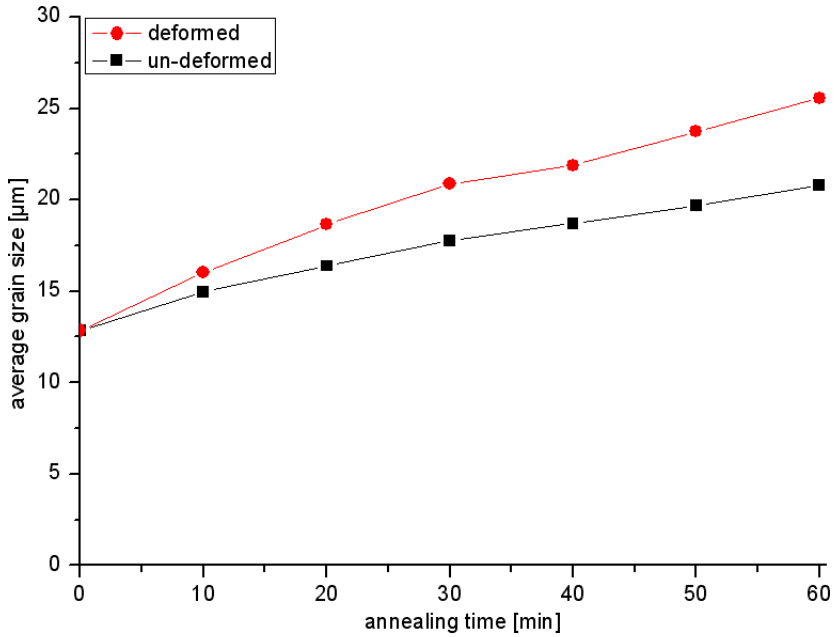

Figure 4.18: Prediction of normal grain growth for deformed and un-deformed specimens during the annealing process at 1000°C and for 60 minutes (deterministic model).

The results also show that starting with an elongated initial grain size of 13 μm, the average grain size of deformed specimen led to almost circle shaped grains of 25 μm after

the annealing process. The evolution of the topology of simulated grain structures is depicted in figure 4.19.

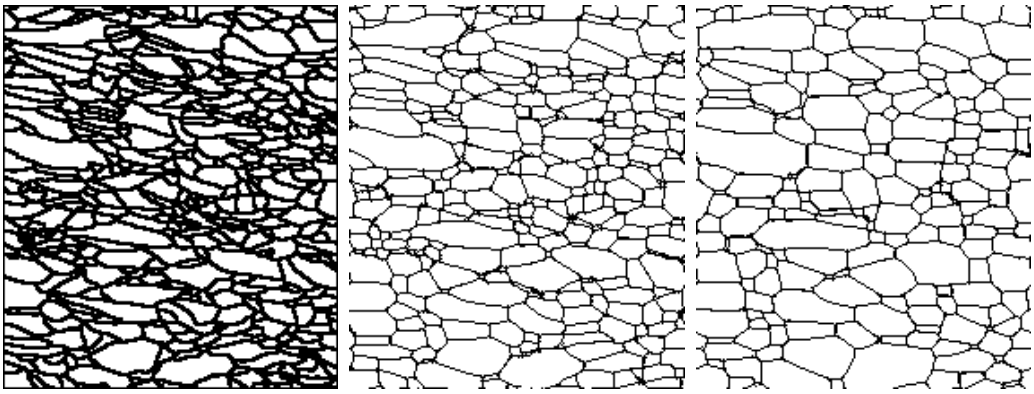

(a) reference specimen (b) t = 20 min (c) t = 60 min

Figure 4.19: Grain structure development under consideration of deformation energy at 1000°C and annealing times of (a) 0, (b) 20 and (c) 60 minutes.

4.2 Probabilistic Model

While deterministic cellular automata directly perform continuous change of a cell and corresponding cell neighbors in accordance with the underlying rate equations, probabilistic cellular automata calculate the switching (transition) probability of each lattice point. Switches are in cellular automata algorithm performed as a function of the previous state and the state of neighboring lattice points.

4.2.1 Modelling Setup

In general, the space is divided into a regular network of cells with periodic boundary conditions. Every lattice cell represents one part of a grain and is marked with a grain identification number. Lattice cells which are adjacent to neighboring cells with different grain identifications are regarded as being part of the grain boundary, while the cells surrounded by cells with the same grain identification are in the grain interior. In order to make the boundary move in any direction, Moore´s neighborhood configuration is considered where both the nearest and next-nearest neighbors are used. One cellular automaton step (CAS) corresponds to one loop of re-identification attempt at defined transition probability where the cell state of each step is updated simultaneously [88, 89].

The calculation of the transition probability $P_{transition}$ is performed as

$$P_{transition} = P_a \left\{ P_{temp} P_{\Delta\rho} \right\} \tag{4.17}$$

where P_a is the probability influenced by the dissolution of the precipitates and P_{temp} is the probability influenced solely by the temperature dependence of grain growth at a defined grain resolution of the CA model.

The stored deformation energy is an additional term which accelerates the grain boundary movement. In the probabilistic model its influence is described as

$$P_{\Delta\rho} = f\left\{\Delta\rho\right\} (\geq 1) \tag{4.18}$$

where $f(\Delta\rho)$ is a function describing stored energy as a ratio of CD, MCD or M_{aver} values between deformed and un-deformed specimens. $f(\Delta\rho)$ is defined to be equal or greater than 1.

The impact of the temperature on grain growth is described by:

$$P_{temp} = A_{temp} exp\left(\frac{-Q_{temp}}{R_{gas}T}\right) \tag{4.19}$$

where Q_{temp} is the activation energy for bulk diffusion at a given grain structure resolution and A_{temp} is a constant [72].

The dissolving of the precipitations during the grain growth is assumed to follow

$$P_a = 1 - exp\left(-C_a t\right) \tag{4.20}$$

corresponding to the influence that precipitations have on the grain growth mechanism where P_a has a value between 0 and 1, depicted schematically in figure 4.20. C_a is a temperature dependent constant. MatCalc® calculations were used for the definition of precipitation kinetics, i.e. simulation steps at which the dissolution of precipitations starts and ends.

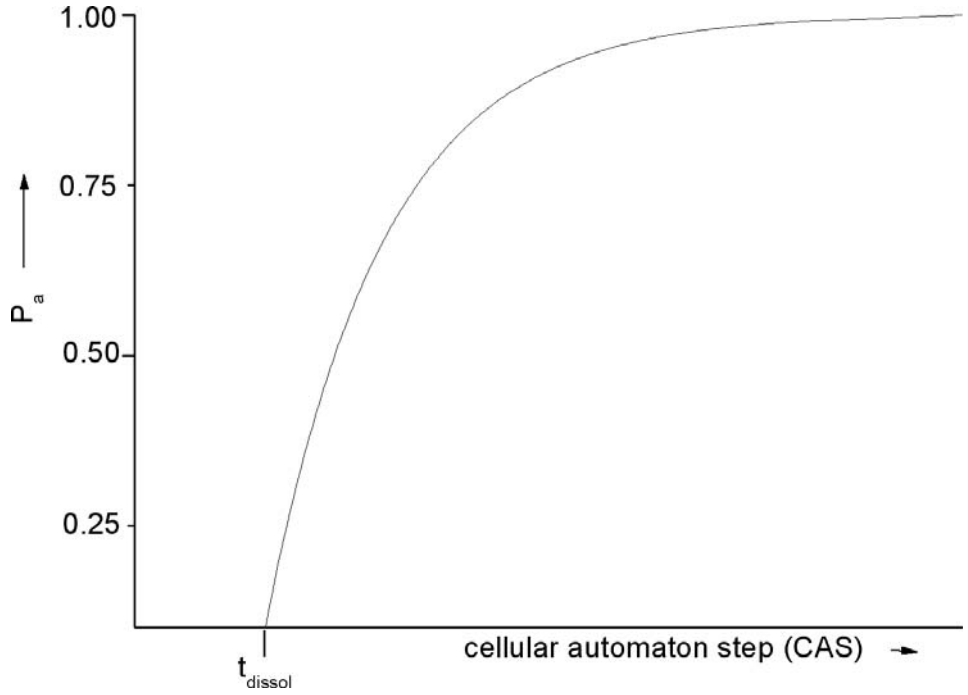

Figure 4.20: A schematic showing the definition of P_a for the probabilistic model.

4.2.2 Shrinkage of a Circular Grain in a Matrix

For the validation of the model, a simple case of circular grain embedded in a matrix ($100x71$ cells) was used to validate the presented probabilistic cellular automaton model. The simulation results are depicted in the figure 4.21.

(a) t=5 (b) t=1000 (c) t=2000 (d) t=2500

Figure 4.21: Illustration of the simulation of a circular grain versus simulation time for the probabilistic model.

The evolution of a circular grain with a reorientation probability of 50 % showed that the circle maintained in a circle shape with some fluctuations, shrinking towards the center under its own curvature. While shrinking, the total energy of the system is decreasing

which proves that the grain boundary migration couples both curvature and energy. The reason for the fluctuation of a grain boundary is due to statistical perturbations.

4.2.3 Effect of Triple Junctions

The effect of a triple junction is an important part of grain growth. Two inclined grain boundaries and a connecting segment parallel to the free surfaces were chosen as starting configurations depicted in the figure 4.22. They will be called open-H and slant-H after distorted letters H [64].

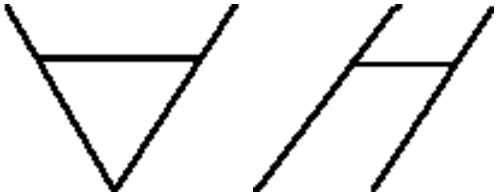

Figure 4.22: Initial structure to analyze the evolution of triple junctions a.) open-H and b.) slant-H configurations. The grid size contains $100x78$ cells.

This method provided the opportunity to study details of grain shape changes according to neighborhood rules in the probabilistic cellular automata model. The reorientation occurred with the probability of 50 % in order to prevent non-physical anisotropic growth reflecting the symmetry of the grid. The grid size is $100x78$ cells and no periodic boundaries were used. In every time step the entire grid of automata cells was updated simultaneously.

Simulation results of morphological changes are illustrated in figure 4.23 and 4.24 for the chosen open-H and slant-H starting configurations, respectively. The migration began at free surfaces where the straight boundary segments started to curve. Simultaneously, the triple junctions start to move to equilibrate the dihedral angles between the boundary planes. When curved segments are established they move towards their centers of curvature.

(a) t=2000 (b) t=5500 (c) t=10000 (d) t=13000

Figure 4.23: Development of microstructure for open-H configurations vs. simulation time.

(a) t=2000 (b) t=5500 (c) t=10000 (d) t=13000

Figure 4.24: Development of microstructure for slant-H configurations vs. simulation time.

This is an elementary topological event happening during the grain growth in polycrystalline materials, which comes out naturally in the used method.

4.2.4 Effect of Lattice Cell Number on Grain Growth

The CA approach has limitations, especially with regard to the length and time scale. The cellular automaton model strictly depends on the resolution of the microstructure, especially with models based on probabilistic transition rules (figure 4.25).

A high resolution of the grain structure led to very long simulation times (table 4.3) but a low resolution of grain structure led to inaccurate simulation results. Especially for high transformation probabilities, i.e. high annealing temperatures, a low grain structure resolution led to different grain structure statistics for the same simulation parameters.

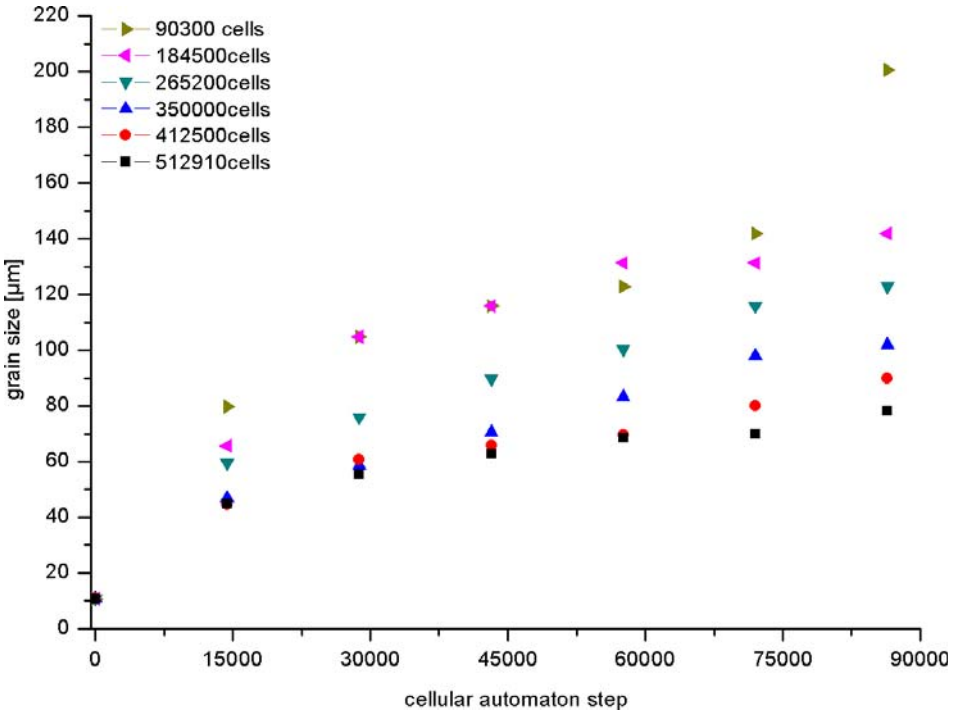

(a)

Figure 4.25: The impact of the resolution of grain structure on grain growth (probabilistic model). Average grain size vs. CAS.

dimensions	number of cells	$\Delta t_{simulation}[-]$
$350x258$	90300	1
$500x369$	184500	4
$600x442$	265200	9
$700x500$	350000	20
$750x550$	412500	31
$834x615$	512910	48

Table 4.3: Resolution of grain structure vs. simulation time (probabilistic model). $\Delta t_{simulation}$ is the normalized simulation time. For the comparison of the simulation times, the lowest calculated grain structure was defined arbitrary to have a simulation time of 1.

Due to the convergence of simulation results with higher grain structure resolutions and for an accurate simulation results of developing grain structures, the dimension $834x615$ (= 512910 cells) was chosen to resolve the grain structure of further simulation procedures of normal grain growth.

4.2.5 Simulation Results for Normal Grain Growth in the Presence of Second Phase Particles

In order to validate the influence of precipitates for the probabilistic CA model, starting at 900°C for 5h, a heating up with $10°C/h$ and a final solution annealing at 1000°C for 5h was experimentally conducted and compared to the simulation results. Calculation of precipitations kinetics by MatCalc® was used for the evaluation of simulation parameters in the probabilistic CA model. The probabilistic model needs a definition of time step where dissolution of second phase particles is started and ends, which is illustrated in the equation 4.21. For the comparison of probabilistic and deterministic model, the figure 4.26 also depicts the developing limiting grain size defined by Zener, which was used for the description of precipitation kinetics in the deterministic model.

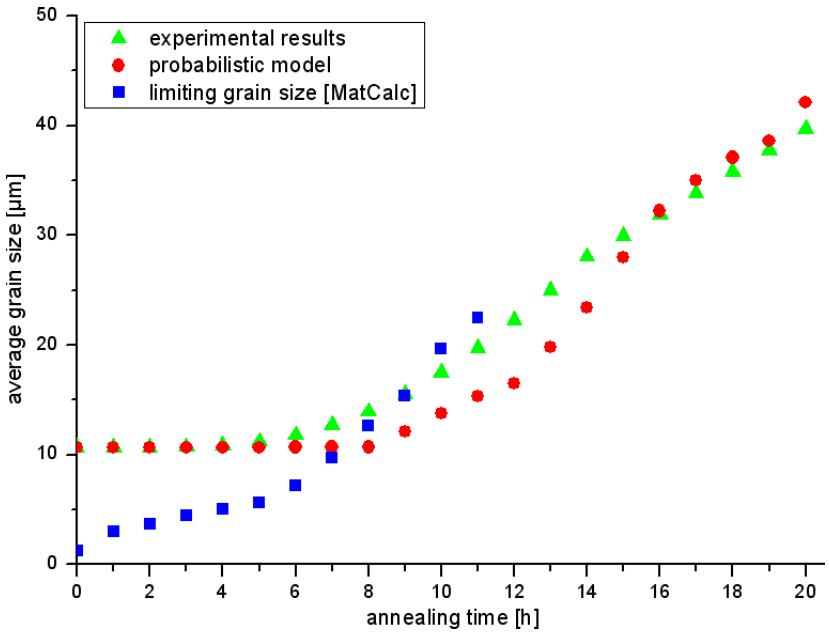

Figure 4.26: Grain growth in the presence of second phase particles: Comparison of probabilistic and deterministic model (limiting grain size) with experimental results.

The transition probability P_a describing the influence of precipitates in the probabilistic model (equation 4.21) was derived to be

$$P_a = 1 - exp\left(-2.4 \cdot 10^{-6} t\right) \tag{4.21}$$

The evaluated P_a development with simulation time influences strongly the total transition probability $P_{transition}$ of the grain growth process. Especially in the beginning of

the dissolution of precipitates, large differences between simulation and experimentally predicted average grain sizes were observed (figure 4.26). Therefore, it is stated that the influence of precipitates is better described by limiting grain size of the deterministic model.

4.2.6 Modelling Results for Normal Grain Growth

Considering the effect of lattice cell number on cell switching, discussed in chapter 4.2.4, the simulation of normal grain growth was performed at a grain structure resolution of 512910 (834x615) cells which represents an area of 650000 μm^2 and a grid size of 0.433 μm. The annealing experiments which should be simulated were already explained in chapter 3.5. Simulations of un-deformed specimens were performed at 900°C, 1000°C, 1100°C and 1200°C for up to 144000 seconds (40h) of annealing time. For the analysis of the simulation results only normal grains were considered.

The grains in the starting grain structure were relatively uniform in size with an average value of about 10.6 μm, but there were clusters of fine grains in some regions, as depicted in figure 4.27.

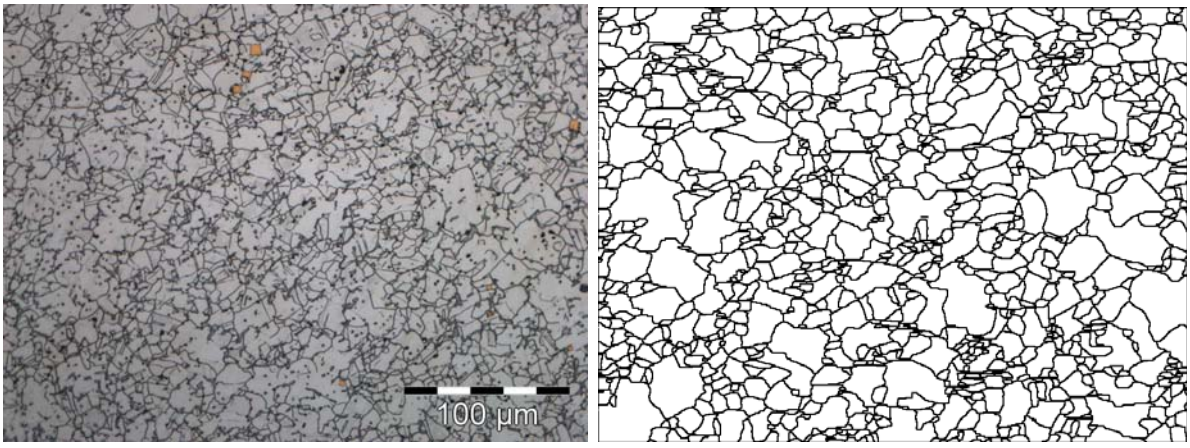

(a) initial micrograph (b) implemented grain structure

Figure 4.27: Micrograph of the initial grain structure (a) and (b) implemented initial grain structure for the modelling of normal grain growth in the probabilistic model.

The characteristic of grain growth strongly depends on the annealing temperature. The developing grain structures from the probabilistic CA model for normal grain coarsening are exemplarily shown in figure 4.28 for 1200°C. The increase of the grain size, the growth

of larger grains at the cost of smaller ones and the evolution of grains towards stable six sided configurations were the main topological results of the probabilistic CA model.

It can be observed from the simulated grain structures that curved boundaries tend to form a straight line with increasing computational time, which reflects the curvature as a driving force for migration. The results showed a tendency to form 120° dihedral angle between grain boundaries and the characteristics of topological requirement of the grain side distribution, e.g. six side neighborhood [31, 36, 111].

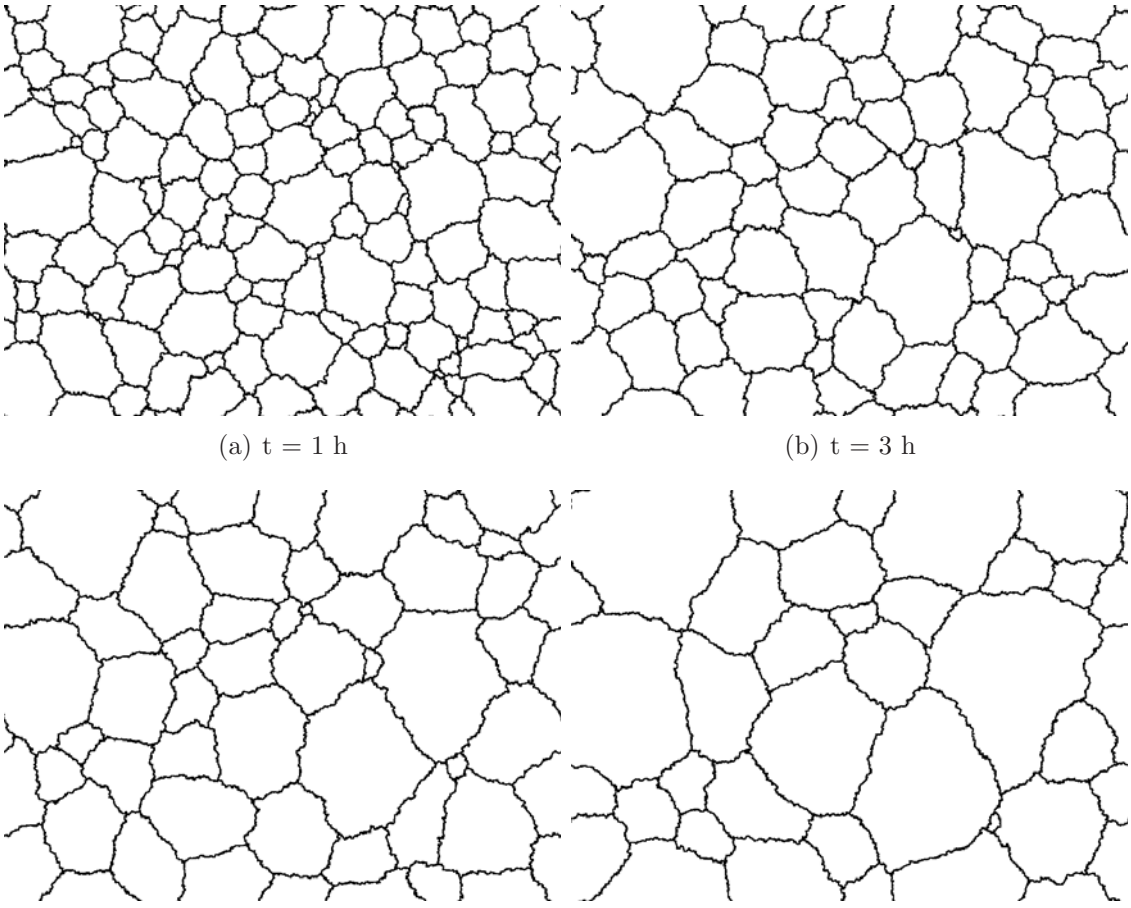

(a) t = 1 h (b) t = 3 h

(c) t = 5 h (d) t = 10 h

Figure 4.28: Simulated grain structures of normal grain growth for the annealing process at 1200°C for annealing time steps of (a) 1, (b) 3, (c) 5 and (d) 10 hours (probabilistic model).

The mean grain diameter at a given time step was then obtained by averaging over all grains in the system, assuming that each grain had a circular shape. The evolution of the grain size is depicted in the figure 4.29.

Comparing the results at 900°C, the simulation results of the deterministic model for normal grain growth (chapter 4.1.4) showed a strong impeding of grain growth by precipitations. The probabilistic model is based on the dissolution of precipitations. At 900°C, the description of grain growth impeding, as explained in the deterministic model, is not possible for the probabilistic model, yet. In contrast to that, a good correspondence of average grain size could be predicted for long annealing times at 900°C.
For higher annealing temperatures, an appropriate definition of transition probabilities resulted in a good correspondence between simulated and measured average grain size, presented in figure 4.29. The grain size distributions are discussed in the chapters 4.2.8 and 4.2.9.

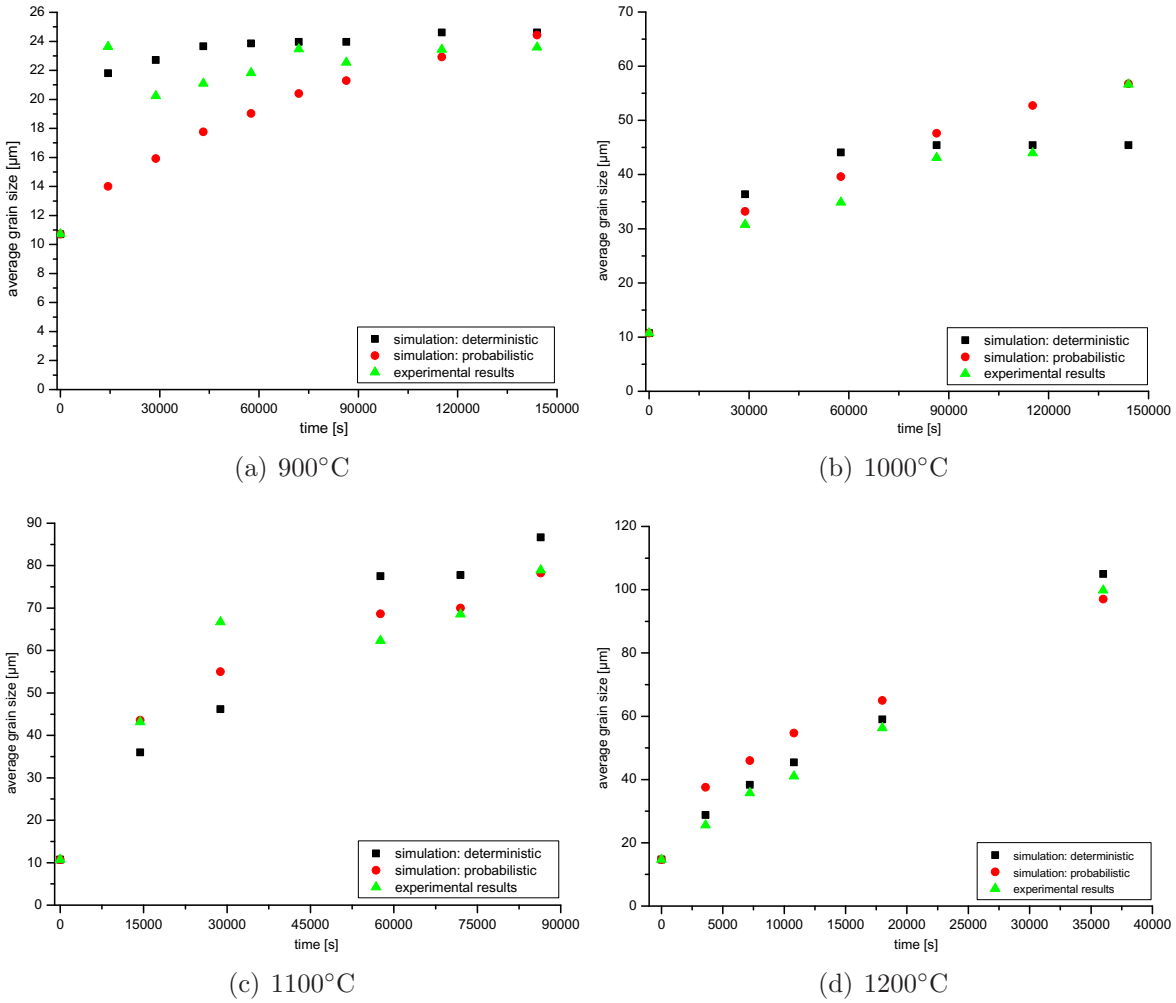

(a) 900°C (b) 1000°C

(c) 1100°C (d) 1200°C

Figure 4.29: Normal grain growth as a function of annealing times at (a) 900°C, (b) 1000°C, (c) 1100°C and 1200°C: comparison of experimental and simulation results. Both probabilistic and deterministic simulations are plotted.

Temperature is the most important parameter affecting the behavior of the grain coarsening process. The basic process during the migration of a grain boundary is the transfer of atoms to and from the grains which are adjacent to the grain boundary. The mechanism of grain boundary migration depends on several parameters including the boundary structure, temperature and point defects such as solutes and vacancies. The boundary structure and point defects are linked to the material's internal conditions while the temperature is related to the external condition. In general, the higher the temperature, the higher the frequency that the boundary energy barrier must be overcome, and thus the higher the boundary velocity.

The temperature dependence for normal grain growth was regressed as

$$P_{temp} = 17490.8 * e^{-\frac{125570}{R_{gas}T}} \tag{4.22}$$

and depicted in figure 4.30.

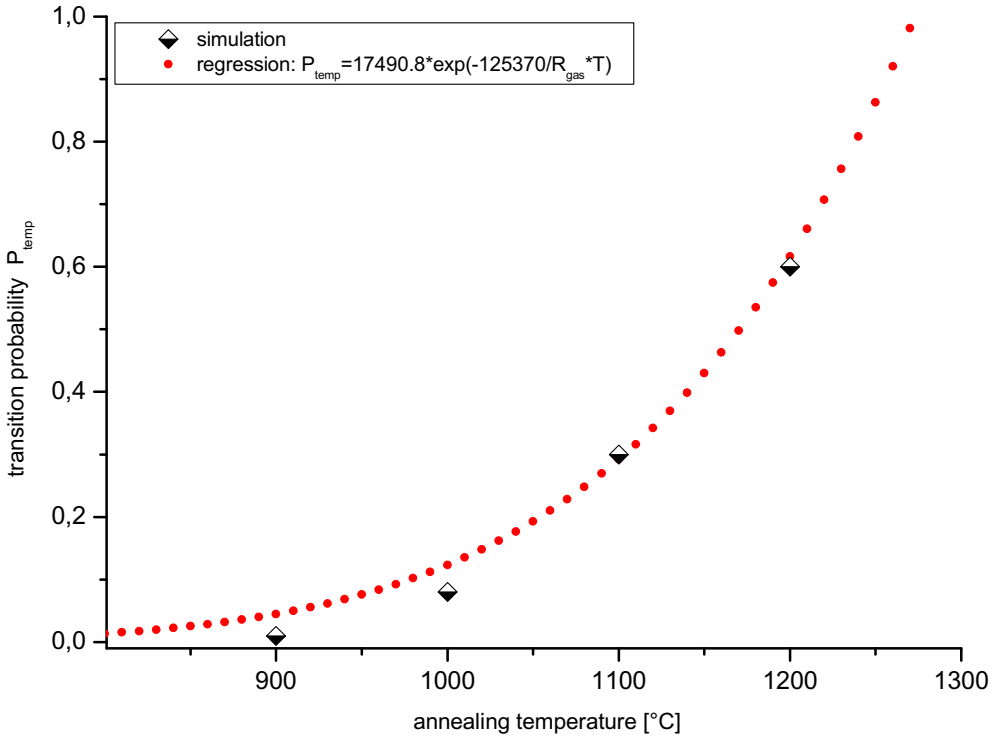

Figure 4.30: P_{temp} vs. annealing temperature for normal grain growth.

4.2.7 Simulation Results for Normal Grain Growth in the Presence of Deformation Energy

For considering the deformation energy, as already applied for the validation of the deterministic model (chapter 4.1.6), the same one-hit upsetting tests were carried out, followed by solution annealing at 1000°C for 1h.
The deformation energy was evaluated by EBSD measurements followed by the calculation of corresponding CD, MCD, and M_{aver} values, presented already in chapter 4.2 for the deterministic model. By using the M_{aver} values, an approximately 4.7 times higher stored energy term of the deformed specimen compared to the homogenized un-deformed specimen could be defined. Therefore, the input of deformation energy ($P_{\Delta\rho}$) comprised a 4.7 times higher transition probability at least in the beginning of the simulation. Due to the decrease of the stored deformation energy during the solution annealing process, it was assumed that the influence of deformation energy declined exponentially.
Starting from an elongated initial grain size of 13 μm (figure 4.31a), the average grain size of deformed specimen led to a more exquiaxed average grain size of 25 μm after annealing at 1000°C for 1h. Here, the same simulation parameters (grain structure resolution, description of P_{temp}) evaluated for normal grain growth (chapter 4.2.6) were used. The developing grain structures of the simulation are depicted in figure 4.31.

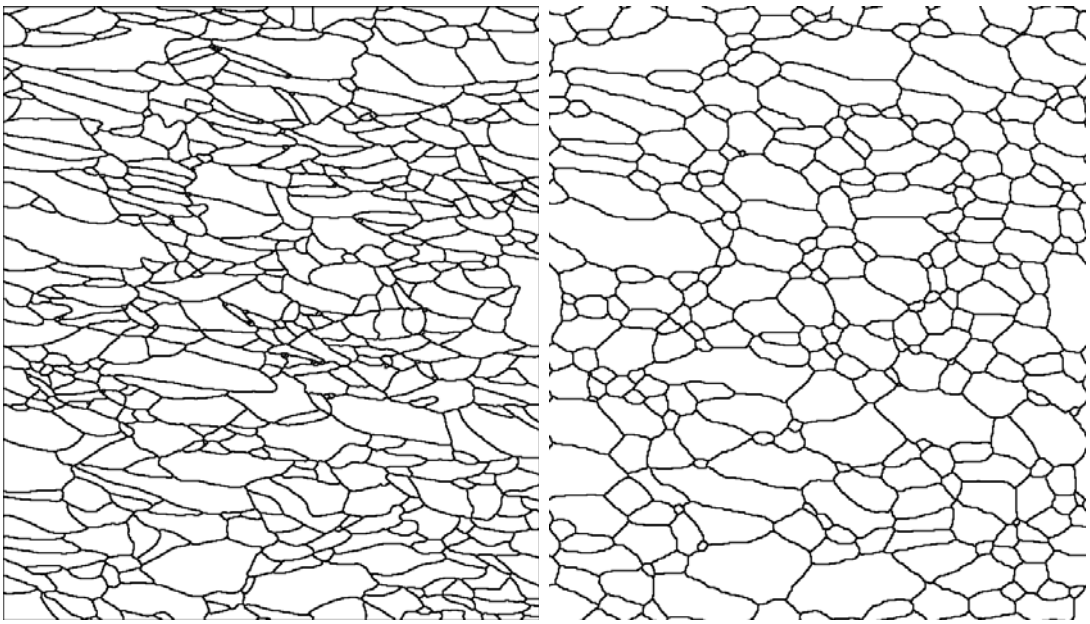

(a) 0 min (b) 60 min

Figure 4.31: Simulation of normal grain growth in the presence of deformation energy: grain structure development for (a) 0 and (b) 60 minutes.

Simulation without considering deformation energy resulted in a lower average grain size then evaluated in experiments (figure 4.32). Incorporating an exponential declination of $f(\Delta\rho)$ from 4.7 at 0 minutes to 1 at 60 minutes, which is defined in equation 4.17, led to the simulation results depicted in figure 4.32.

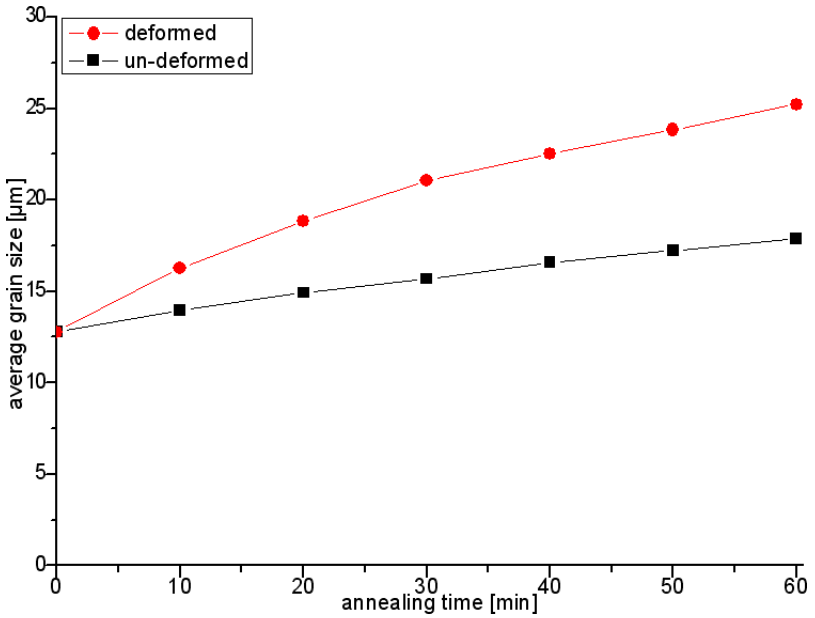

Figure 4.32: Prediction of normal grain growth for deformed and un-deformed specimens during the annealing process at 1000°C and 60 minutes in the probabilistic model.

4.2.8 Modelling Results for Abnormal Grain Growth

The procedure employed in the simulation of abnormal grain growth was nearly identical to that of normal grain growth, described in the chapter 4.2.6. The main difference was that a lower number of cells, and due to the experimental results evaluated, a larger domain area was needed. Additionally, three different simulation parameters defining abnormal and normal grain growth and low simulation times were required.
The grain structure mapped on a two-dimensional lattice contained 71100 cells (300x237), a grid size of 3.9 μm and a calculation domain of 1171x925 μm^2. It was assumed that the grain boundary energy was distributed heterogeneously, where a grain boundary between normal and abnormal grain had different grain boundary energy or grain boundary mobility.
In order to reflect abnormal grain coarsening, from the beginning on of the simulation, a selected fraction of abnormal grains got a higher transition probability reflecting higher grain boundary mobility compared to the fraction of normal grains with lower grain

boundary mobility. The prediction of grain structure aimed for an experimentally evaluated average grain size of normal and abnormal grains, and a corresponding fraction of abnormal grains. The modelling procedure allows a mixed grain structure evolution where all matrix grains are consumed by the abnormal grains, shown exemplarily in the figure 4.33 for the annealing process at 1200°C.

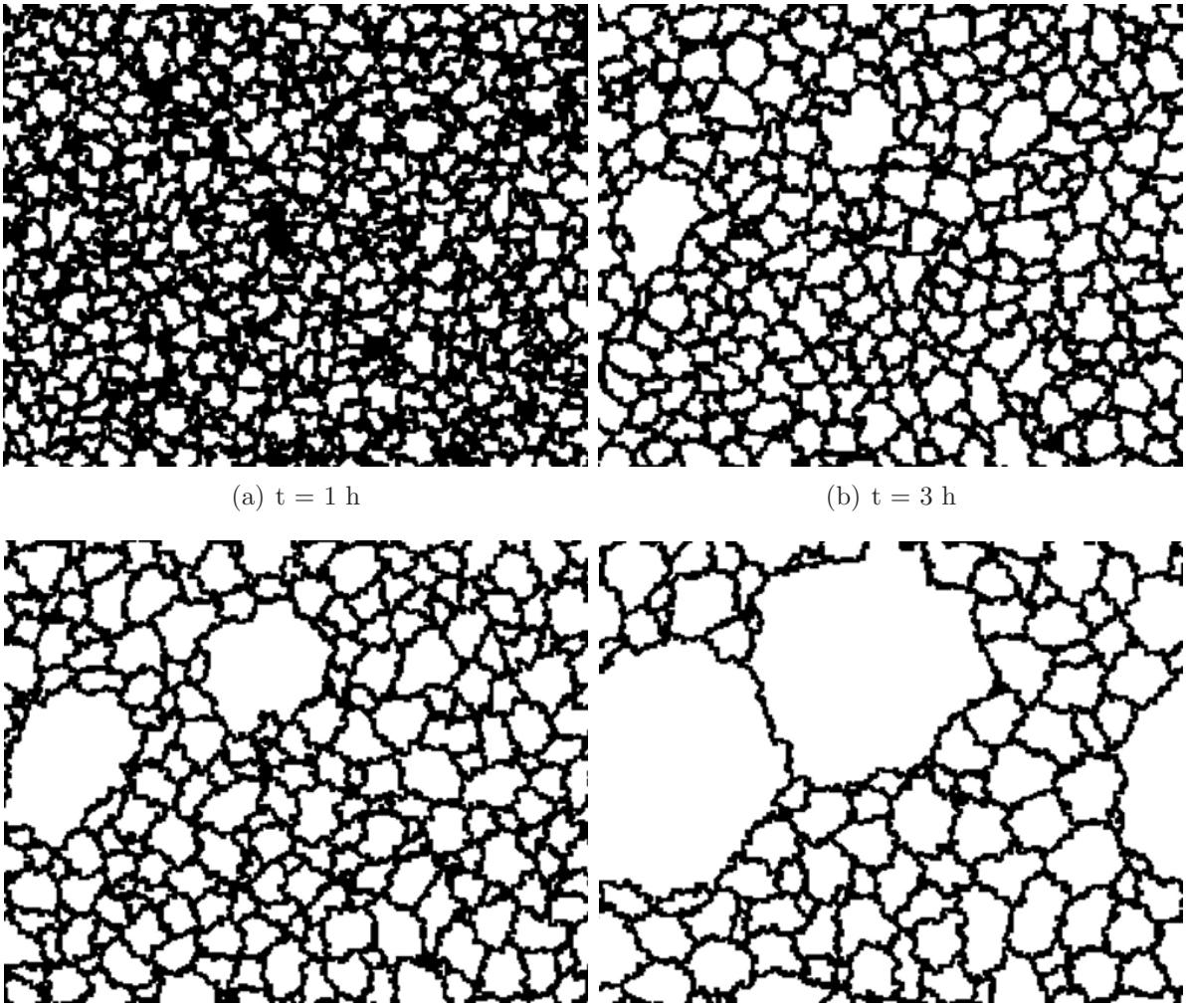

(a) t = 1 h (b) t = 3 h

(c) t = 5 h (d) t = 10 h

Figure 4.33: Simulated microstructure of normal and abnormal grain growth for the annealing process at 1200°C (probabilistic model).

The results of annealing experiments and simulation for temperatures between 1000°C and 1200°C showed a good correspondence of average grain sizes for normal and abnormal grains (figure 4.34).

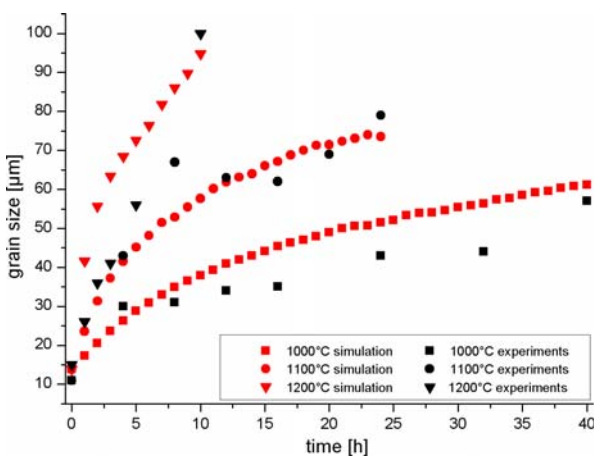

(a) Normal grain growth at different temperatures

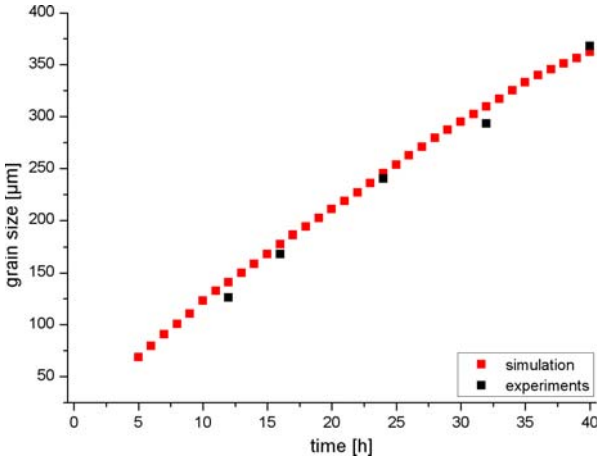

(b) Abnormal grain growth at 1000°C

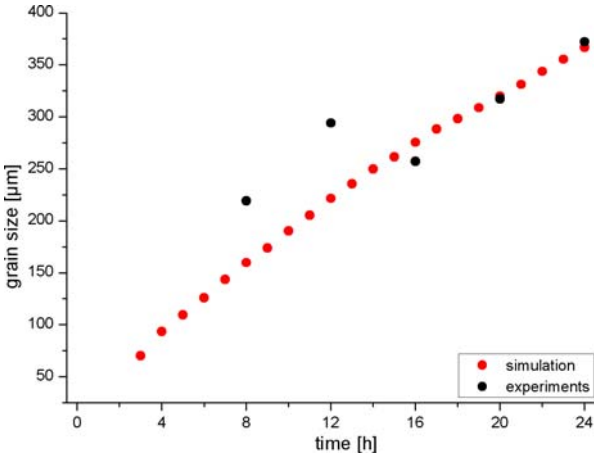

(c) Abnormal grain growth at 1100°C

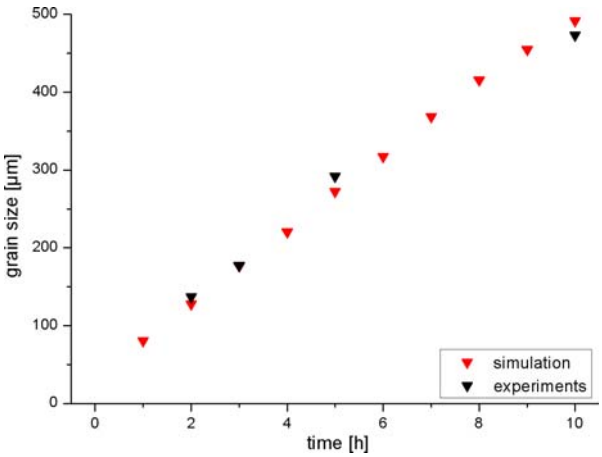

(d) Abnormal grain growth at 1200°C

Figure 4.34: Comparison between simulation and experiments for the normal and abnormal grain growth (average grain sizes) at different annealing temperatures. (a) Normal grain growth for different annealing temperatures and abnormal grain sizes at (b) 1000°C, (c) 1100°C and (d) 1200°C (probabilistic model).

Simulation results of the grain size distributions obtained at 1000°C, 1100°C and 1200°C, depicted in figures 4.35, 4.36 and 4.37, illustrate a deviation when compared to the experimental results, at least for long annealing times. The probabilistic cellular automata set-up depends strongly on the neighborhood configuration. At the beginning of the simulation the neighborhood switching frequency is higher than at the end of the simulation, due to the number of different orientations, i.e. grains, present. Thus, the small grains are vanishing very quickly in the beginning of the simulation resulting in an overestimation of the transition probability.

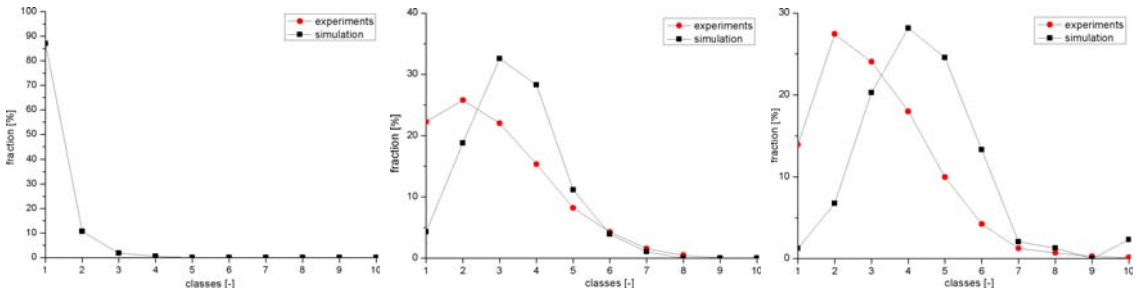

(a) reference specimen (b) t = 4 h (c) t = 8 h

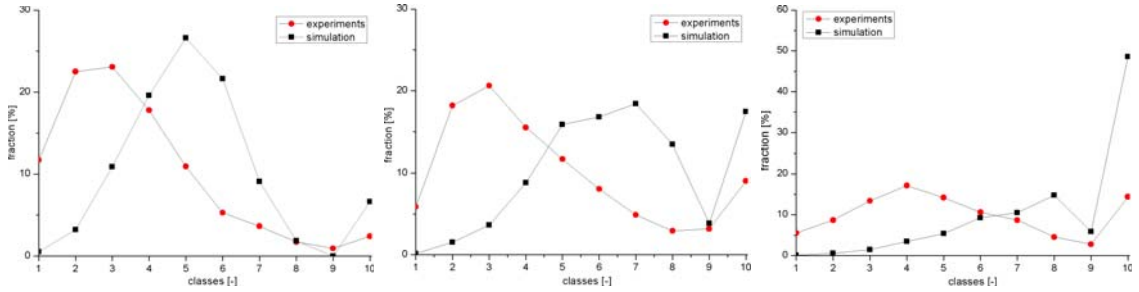

(d) t = 12 h (e) t = 24 h (f) t = 40 h

Figure 4.35: Grain size distribution for the annealing process at 1000°C and annealing times of (a) 0, (b) 4, (c) 8, (d) 12, (e) 24 and (f) 40 hours: simulation vs. experiments.

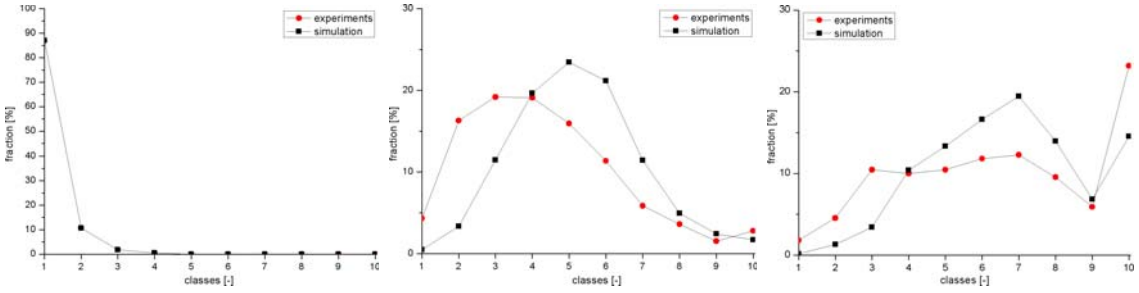

(a) reference specimen (b) t = 4 h (c) t = 8 h

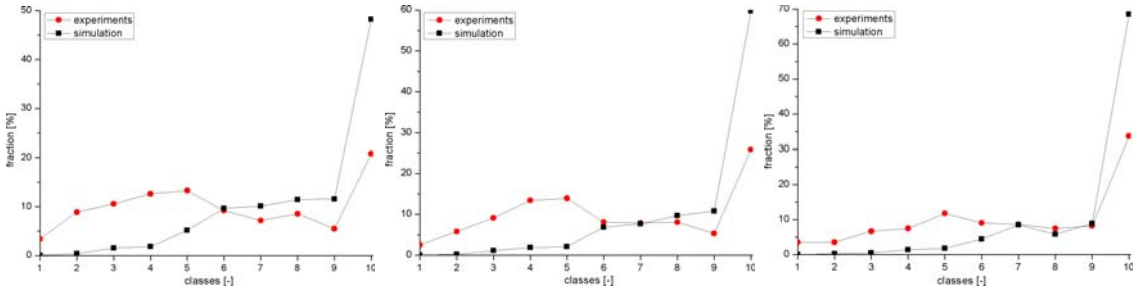

(d) t = 16 h (e) t = 20 h (f) t = 24 h

Figure 4.36: Grain size distribution for the annealing process at 1100°C and annealing times of (a) 0, (b) 4, (c) 8, (d) 16, (e) 20 and (f) 24 hours: simulation vs. experiments.

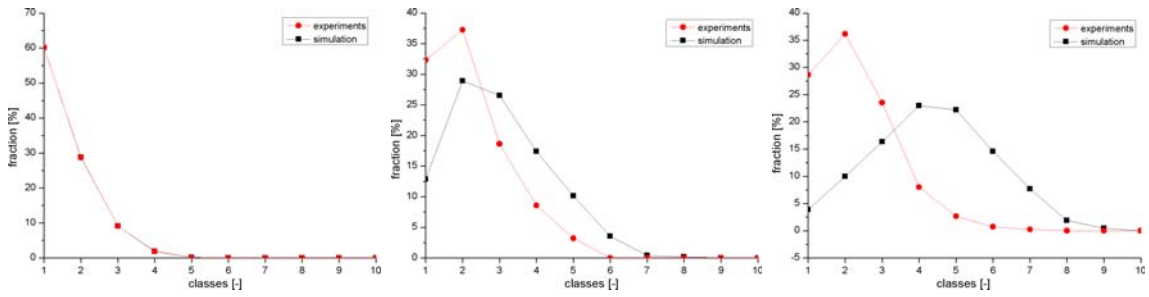

(a) reference specimen (b) t = 20 min (c) t = 40 min

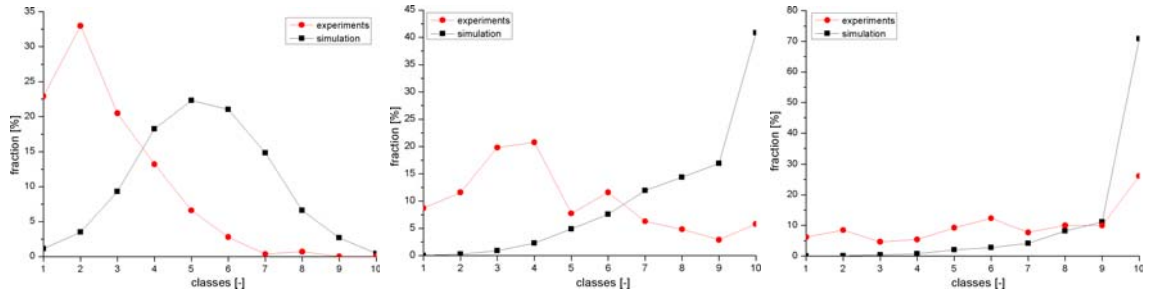

(d) t = 60 min (e) t = 300 min (f) t = 600 min

Figure 4.37: Grain size distribution for the annealing process at 1200°C and annealing times of (a) 0, (b) 20, (c) 40, (d) 60, (e) 300 and (f) 600 minutes: simulation vs. experiments (probabilistic model).

Grain sizes separating normal and abnormal grains, and the fractions of abnormal grains for different solution annealing temperatures, namely at 1000°C, 1100°C and 1200°C, and times are depicted in the figure 4.38.

In contrast to the simulation results of normal and abnormal grain sizes (figure 4.34), the fraction of abnormal grains did not correspond to the evaluated experimental results. This can be explained by the fact that the simulation procedure aimed for an appropriate average normal grain size, average abnormal grain size and fraction of abnormal grains only for the last time step of experimental results at congruent annealing temperature. The simulation results for grain size separating normal and abnormal grains corresponded to the experimental results only in the beginning of the simulation, which can be explained by the deviation of grain size distributions and the fraction of abnormal grains.

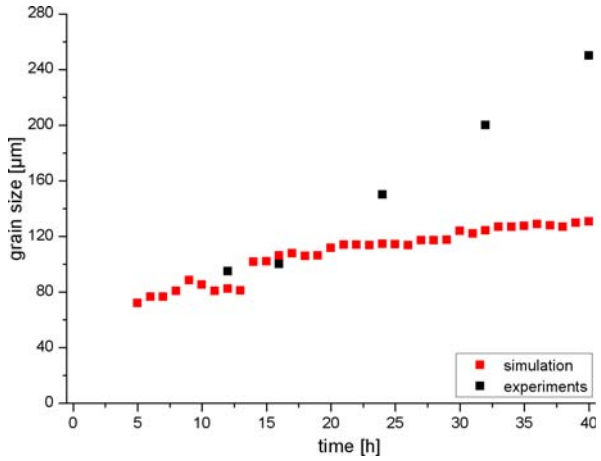

(a) Grain size separating normal and abnormal grains at 1000°C

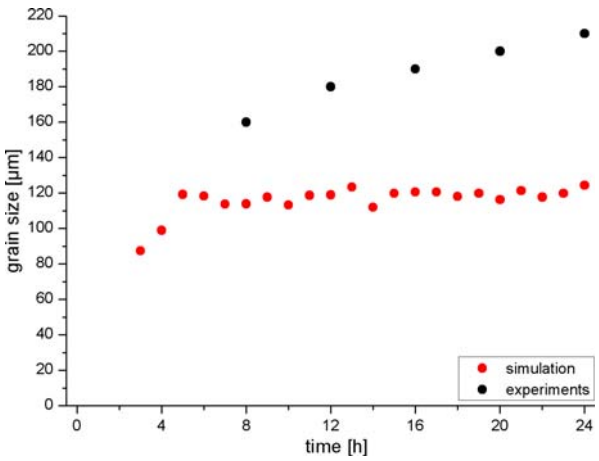

(b) Grain size separating normal and abnormal grains at 1100°C

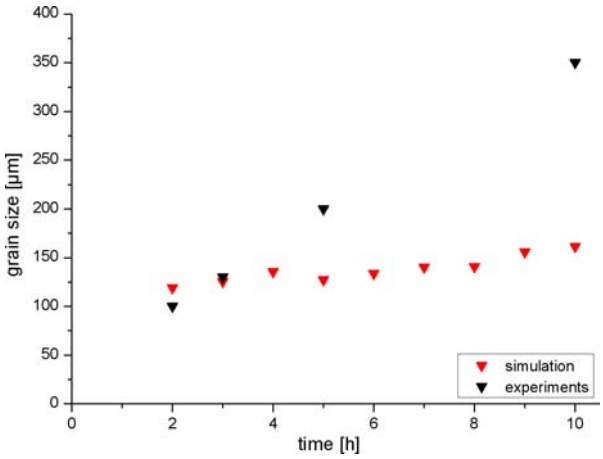

(c) Grain size separating normal and abnormal grains at 1200°C

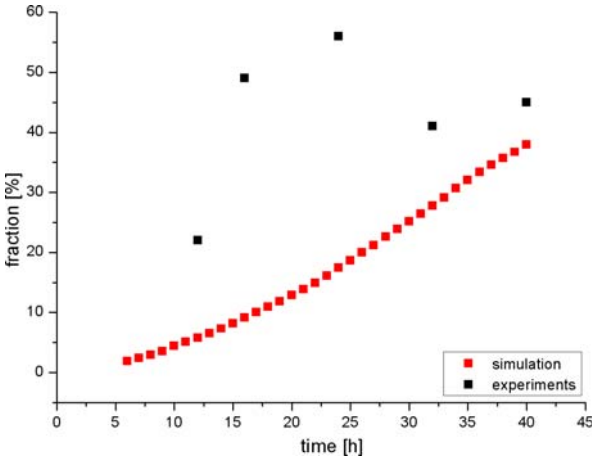

(d) Fraction of abnormal grains at 1000°C

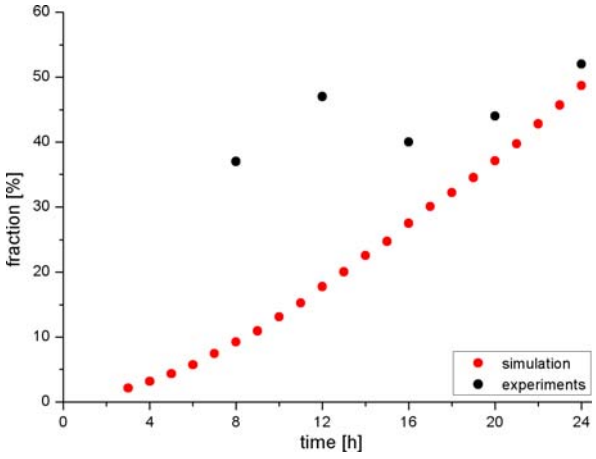

(e) Fraction of abnormal grains at 1100°C

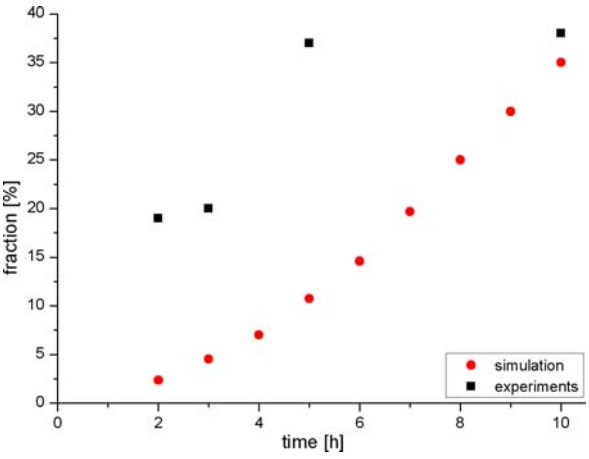

(f) Fraction of abnormal grains at 1200°C

Figure 4.38: Comparison of simulation and experiments for grain sizes separating normal and abnormal grains and fraction of abnormal grains at different annealing temperatures. (a) Grain size separating normal and abnormal grains at 1000°C, (b) grain size separating normal and abnormal grains at 1100°C, (c) grain size separating normal and abnormal grains at 1200°C, (d) fraction of abnormal grains at 1000°C, (e) fraction of abnormal grains at 1100°C and (f) fraction of abnormal grains at 1200°C .

The grain structure evolution with different transition probabilities for normal (P_{temp}^{NGG}) and abnormal (P_{temp}^{AGG}) grain growth (table 4.4) depends strongly on the difference between P_{temp}^{NGG} and P_{temp}^{AGG}. If the transition probabilities are equal, grain structure solely reflects normal grain growth and no abnormal grain growth can be observed. If the transition probabilities are not equal, then abnormal grain growth can be observed. The larger the difference between P_{temp}^{NGG} and P_{temp}^{AGG}, the sooner the developing abnormal grains consume the primary normal grains. The boundaries between the abnormal grains and primary normal grains are not in balance, where cells of normal grains have a higher chance to become part of abnormal grains than vice versa.

temperature [°C]	$\mathbf{P}_{temp}^{NGG}$[%]	$\mathbf{P}_{temp}^{AGG}$[%]	**fraction of** $\mathbf{P}_{temp}^{AGG}$ [%]
1000	04.20	06.20	00.07
1100	17.50	21.50	00.09
1200	81.00	91.00	00.05

Table 4.4: The definition of the simulation parameters used for the simulation of abnormal grain growth at different annealing temperatures. P_{temp}^{NGG} and P_{temp}^{AGG} stands for the different transition probabilities. Fraction defines the percentage of grains with the transition probability P_{temp}^{AGG}.

The fraction of abnormal grains was approximately 0.1 % and almost equal for all annealing temperatures simulated. Therefore, only a very low fraction (0.1 %) of grain boundaries had a higher mobility for grain growth, resulting in abnormal grain growth.

The total transition probability was fitted for the normal grain growth and defined as

$$P_{temp}^{NGG} = 873374exp\left(-\frac{171032}{R_{gas}T}\right) \tag{4.23}$$

and for the abnormal grain growth as

$$P_{temp}^{AGG} = 1036253exp\left(-\frac{171032}{R_{gas}T}\right) \tag{4.24}$$

resulting in a a 20 % higher grain boundary mobility of grain boundaries belonging to abnormal grains (figure 4.39).

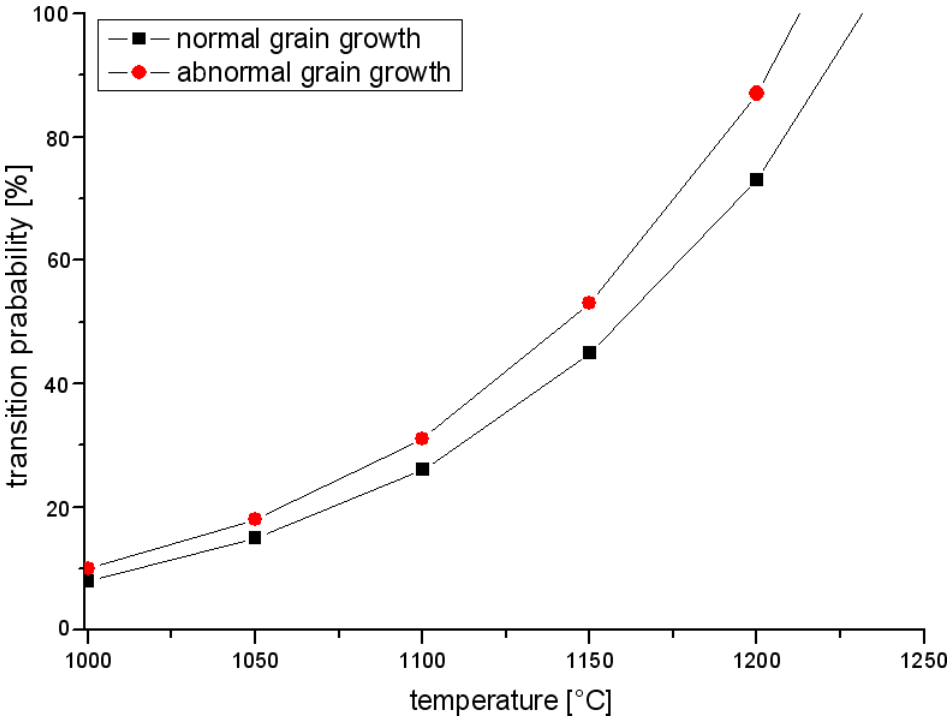

Figure 4.39: Definition of P_{temp}^{NGG} (black rectangle) and P_{temp}^{AGG} (red circles) at corresponding annealing temperatures describing normal and abnormal grain growth.

4.2.9 Modelling Results for Grain Sizes Separating Normal and Abnormal Grains

If the normal grain growth is solely influenced by mobility of grain boundary and curvature, then the probabilistic model initially defines one transition probability for the whole annealing process simulation and aims for an equivalent average grain size at corresponding annealing time, which is then compared to the results evaluated by experiments.

Due to the nonconformity of experiments and simulations for the prediction of separating grain size between normal and abnormal grains (figure 4.38), a so called 2-parameter approach was applied. The 2-parameters approach defines two different transition probabilities in the beginning of the simulation and aimed for the adjustment of normal grain size distributions at corresponding annealing time steps, depicted in table 4.5.

temperature [°C]	P_1[%]	P_2[%]	fraction of P_2 [%]
1000	100	5.0	90
1100	100	17.0	90
1200	90	2.5	65

Table 4.5: The definition of the simulation parameters used for the 2-parameter approach at different annealing temperatures. P_1 and P_2 stands for two different transition probabilities. Fraction defines the percentage of grains using the transition probability P_2.

In contrast to low annealing temperatures, the 2-parameters approach could describe normal grain growth very accurately at 1200°C due to the high mobility of grain boundaries. For the slow grain boundary migration at low annealing temperatures, a multi-parameters approach would be needed which was not performed in this work. The simulation results of grain size distributions and developing grain structures at 1200°C and different time steps are shown in the figures 4.40 and 4.41.

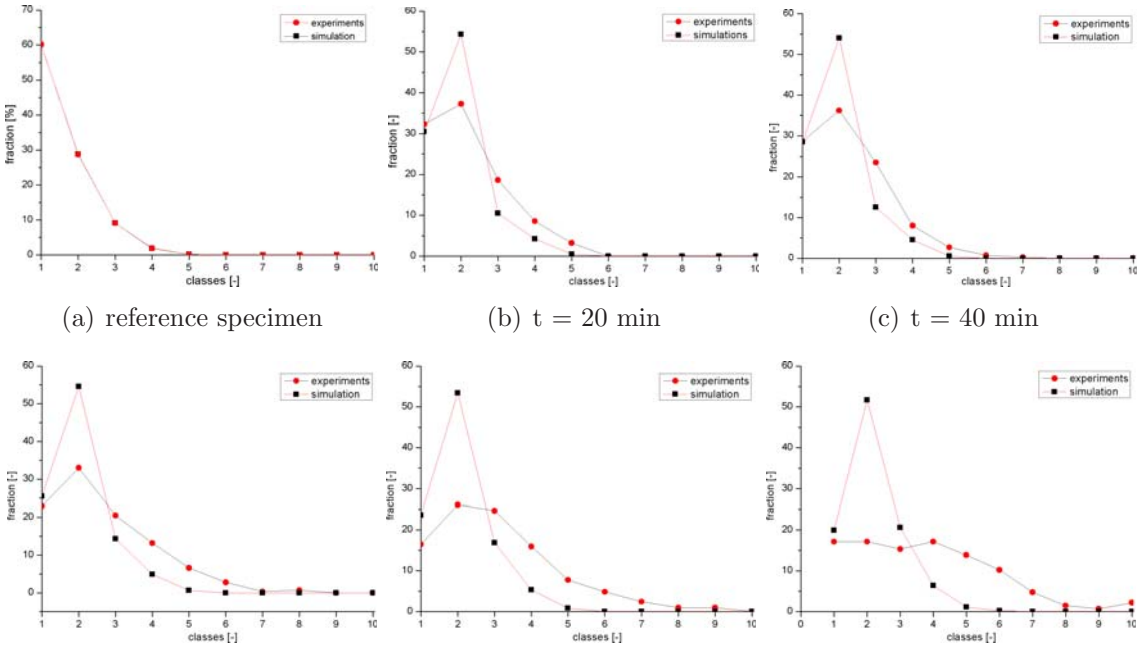

(a) reference specimen (b) t = 20 min (c) t = 40 min

(d) t = 60 min (e) t = 80 min (f) t = 120 min

Figure 4.40: Illustration of the simulation results of grain size distributions of the annealing process at 1200°C evaluated by a probabilistic 2-parameters approach: simulation vs. experiments for the annealing times of (a) 0, (b) 20, (c) 40, (d) 60, (e) 80, (f) 120 minutes.

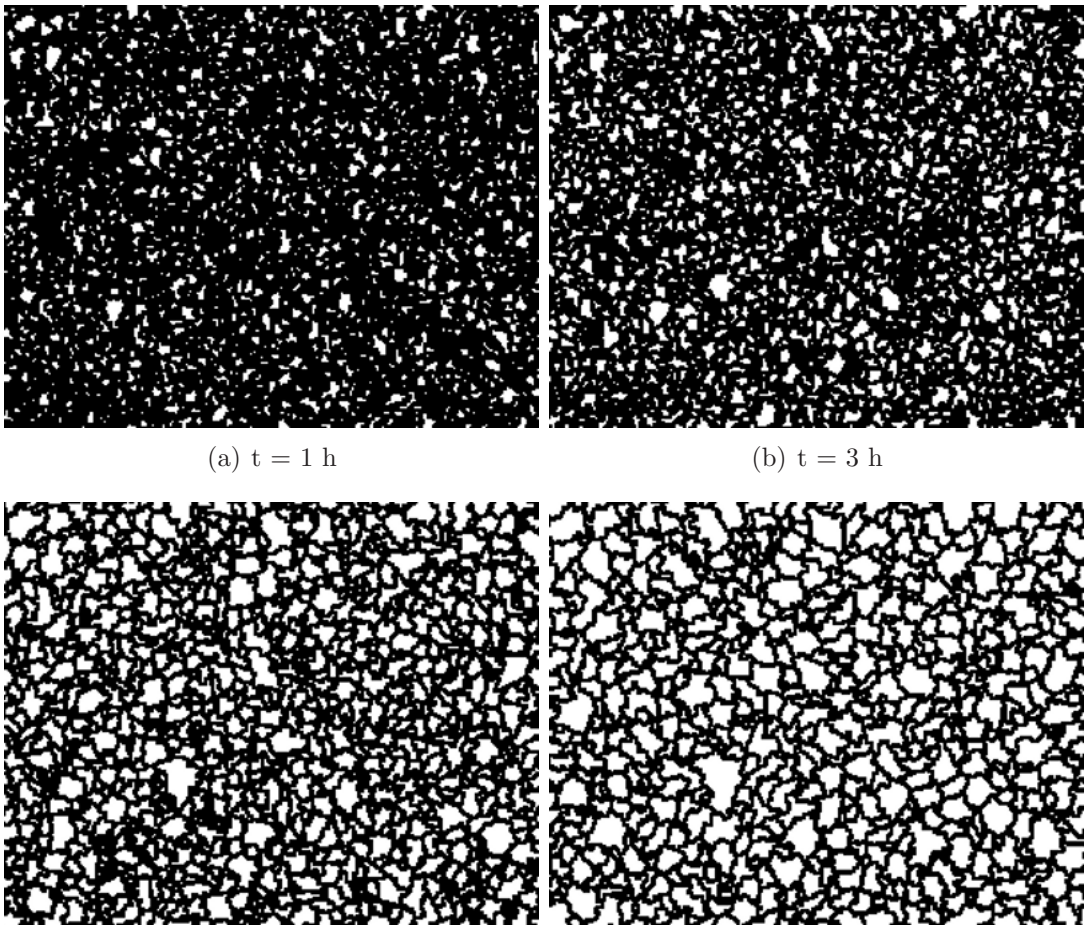

(a) t = 1 h (b) t = 3 h

(c) t = 5 h (d) t = 10 h

Figure 4.41: Results of the 2-parameters approach for the simulation of normal grain growth for the annealing process at 1200°C at (a) 1h, (b) 3h, (c) 5 and (d) 10h of solution annealing time.

Two parameters (i.e. transition probabilities) were defined and the grain size distributions in the beginning of the annealing procedure were adjusted to the experimental results. Exemplarily, for the simulation at 1200°C the first abnormal grains occurred after 120 minutes of annealing time (see chapter 3.5). It was assumed that the simulated results of grain size distributions after 20 minutes, 40 minutes, 60 minutes and 80 minutes only describe normal grain growth (figure 4.40). Therefore, the simulation parameters used for low solution annealing times describing normal grain growth, might also be the right simulation parameters for description of normal grain growth at long annealing times where abnormal grains occurred.

The adjustment of grain size distributions for normal grain growth led to the evalua-

tion of the largest grain size in the grain structure and thus the grain size separating normal and abnormal grains. The evaluated modified separating grain sizes and corresponding results for upgraded average normal grain sizes, average abnormal grain sizes and the fractions of abnormal grains are shown in the figure 4.42.

A lower grain size separating normal and abnormal grains resulted in a lower average normal and abnormal grain size whereas the fraction of abnormal grains was increasing steeper compared to the results obtained by experiments.

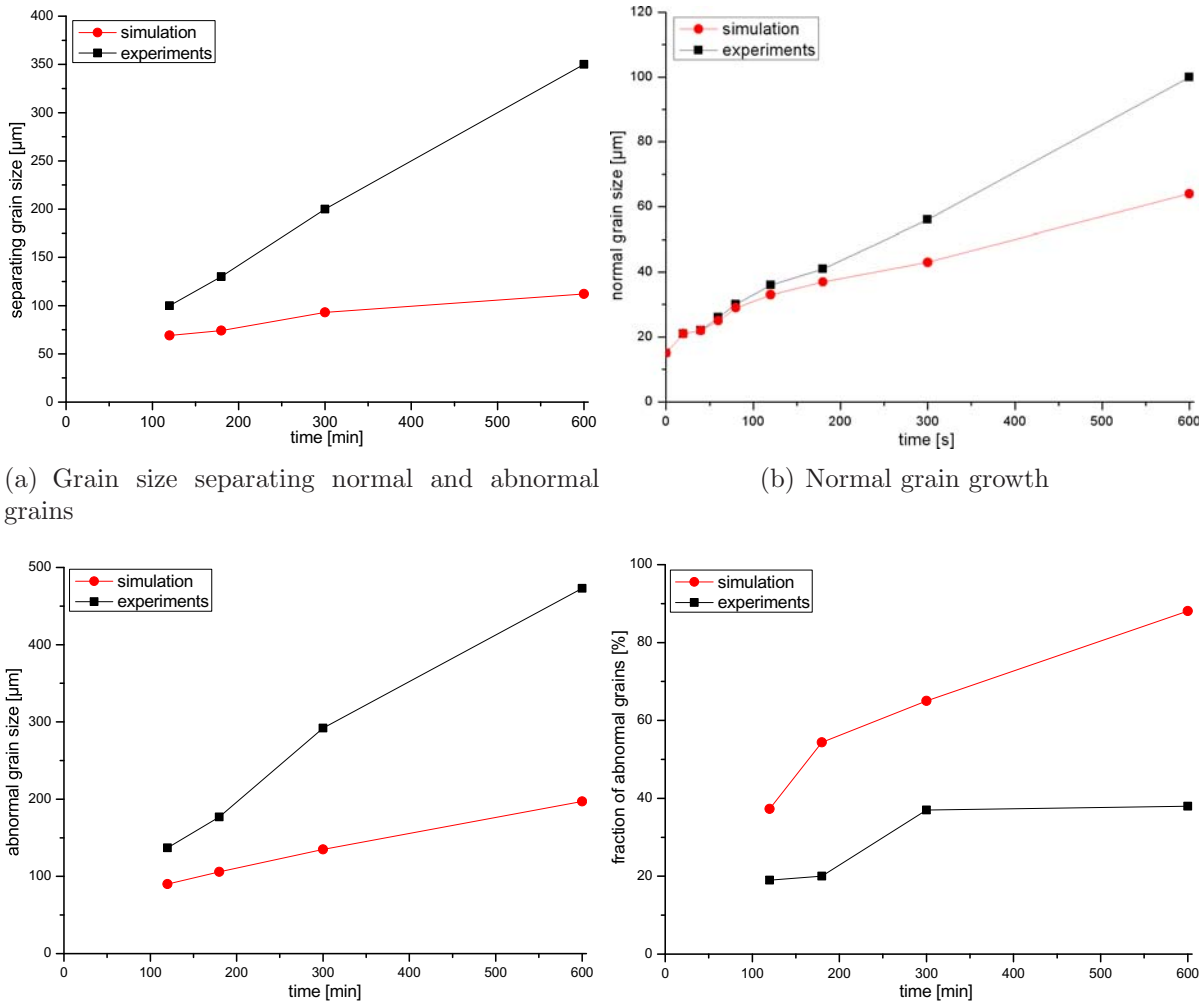

(a) Grain size separating normal and abnormal grains

(b) Normal grain growth

(c) Abnormal grain growth

(d) Fraction of abnormal grains

Figure 4.42: Results for the evaluation of separating grain size for solution annealing at 1200°C by 2-parameter approach: simulation vs. experiments. (a) Grain size separating normal and abnormal grains, (b) normal grain growth, (c) abnormal grain growth and (d) fraction of abnormal grains.

The prediction of separating grain size at 1000°C and 1100°C could not be performed by using the 2-parameters approach, where the results of the adjustment of grain size distributions are depicted in figure 4.43 and figure 4.44. In contrast to the grain structure results of 1200°C explained above, the first abnormal grains occurred after 8 hours of annealing, which led to very long simulation times. Comparing the results of grain size distribution at 1100°C and 4h, a huge deviation between simulation and experimental results can be stated. A 2-parameters approach is therefore not sufficient to describe grain size distributions at 1100°C or 1000°C.

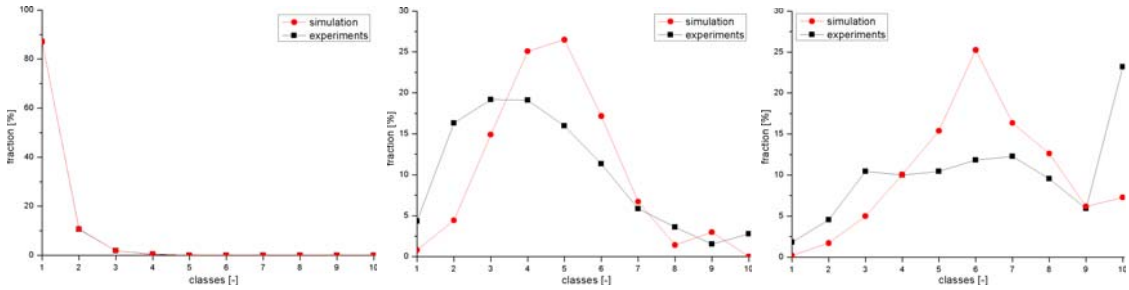

(a) reference specimen (b) t = 4 h (c) t = 8 h

Figure 4.43: 2-parameters approach for the description of the grain size distribution of the annealing process at 1100°C: simulation vs. experiments for the annealing times of (a) 0, (b) 4 and (c) 8 hours.

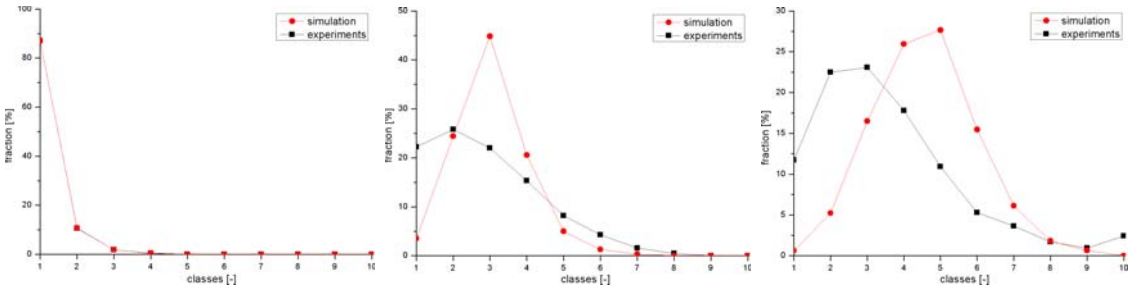

(a) reference specimen (b) t = 4 h (c) t = 12 h

Figure 4.44: 2-parameters approach for the description of the grain size distribution of the annealing process at 1000°C: simulation vs. experiments for the annealing times of (a) 0, (b) 4 and (c) 12 hours.

4.3 Discussion of Modelling Results

A deterministic cellular automata model for grain growth with a precise estimation of curvature has been developed. The model is able to simulate experimentally observed topological arrangements during grain growth. Therefore, several expected features such as growth of larger grains at the expense of smaller ones, evolution of grain structure towards stable six-sided grains, curvature driven switching of neighboring grains and shrinkage of three and four-sided grains are the main topological characteristics of the model. The results proved the stability of six-sided grains, although the 120° rule in the case of triple junctions is not implemented.

The grain growth kinetics predicted by the deterministic CA model corresponded well to the evaluated experimental results, even for a deformed and thus elongated grain structure. Incorporating deformation energy in grain growth simulation, the elongated grain structure resulted in an exquiaxed grain structure. A close observation exhibited that the aspect ratio decreases with annealing time. It is also evident that the definition of limiting grain size during simulation enabled the prediction of grain growth in the presence of second phase particles.

Due to the complex evaluation of the grain boundary curvature, the deterministic model requires long simulation times. In order to reduce the simulation time, a lower cell resolution was defined, thus a low calculation domain. Therefore, simulation of abnormal grain growth was difficult to be processed. Even though, the simulation results showed that a low fraction of grain boundaries (0.1 %) move with an approximately 35-times higher mobility, resulting in abnormal grain growth. Nevertheless, the present deterministic CA model provides a robust and comprehensive method to describe the grain growth behavior in polycrystalline materials.

In the presented probabilistic CA model, every cell on the boundary has a probability to change its state according to the underlying transition rules. For a higher probability there is a higher frequency for cells on the grain boundary to change its state. The grain structure itself influences the grain growth kinetics by definition of Moore´s neighborhood, where the grain boundary movement is possible in any direction. Therefore, small grains grow faster than large grains, and the growth of grains is accommodated by shrinkage and disappearance of other grains. The reduction in grain boundary energy that accompanies the shrinkage in grain boundary area proves that this model has coupled the grain

boundary migration driven by both curvature and energy.

The major difficulty of the presented probabilistic CA model is the length-time scale combination. The total transition probability in the system can not be above the value one. Therefore, for certain lattice cell resolutions, the transition probability was chosen in that way that the highest probability represented the development of the largest average grain size. In the present work, considering transition probabilities a relationship based on experimental work and simulation results was established. The grain size in real materials is in μm, therefore the cells are representing only grains. For the definition of lower length scale factors, such as second phase particles, only rate equations were used. Exemplarily, in order to represent the influence of second phase particles on grain growth, an impeding factor that describes the transition probability considering the dissolution of second phase particles P_a was introduced and experimentally validated. Additionally, introducing two different switching probabilities, the average grain sizes and fractions of abnormal grown grains (approximately 0.1 %) could be predicted.

The probabilistic CA model does not end in the exact same results when repeated, but it indeed outputs close results at the same conditions. Over a statistically significant number of trials, it was obtained that the standard deviation of the average grain size was lower than 2 %. This proves that the model is reliable and accurate.

Incorporating EBSD measurements into both CA models allows to consider the influence of stored deformation energy on grain growth. Assuming that on average all cells of simulation area posses the same increase of grain boundary pressure when deformed, the incorporation of deformation parameters which represent the whole grain structure, and not a local cell, was used to predict the impact of stored deformation energy on normal grain growth. Modelling results of both CA models proved that an initially elongated grain structure of a deformed specimen resulted in an almost equiaxed or circle shaped grain structure after the annealing process. For a large area domain which was exemplarily used for modelling of abnormal grain growth, a high lattice cell number was needed which is difficult to be measured by EBSD. Due to the irregularity of EBSD scanning, the local evaluation of the deformation energy for every lattice cell in the grain structure was not possible, thus a global application of EBSD methods was used in the presented simulation procedure.

The indifference of grain growth kinetics between modelling and experimental results

comes from topological factors, which determine the grain growth. The grain boundary migration reduces boundary surface area, where grains with more than six sides grow because their boundaries are concave, and grains with less than six sides shrink. In the modelling, the factor that affects the movement of grain boundaries is determined from local area and not from the whole boundary. This is the major difference between CA model and topological constraints for grain growth.

The mathematical description of the grain boundary movement requires three parameters in the 2D case of the deterministic model, namely the energy, curvature and mobility of the grain boundary, which are classic basic impacts on the grain growth. In this work, the grain boundary energy was defined as a constant and the initial grain structure was implemented from micrographs defining the curvature of the matrix. Therefore, the deterministic model sensitively reacts on the definition of the grain boundary mobility in the system. Additionally, the probabilistic model defines only one parameter, the transition or switching probability, which is used to derive all other grain movement constants. The transition probability is very sensitive on the grain structure resolution, where faster grain growth kinetics are achieved with lower grain structure resolutions.

In contrast to the 2D modelling presented in this thesis, in a 3D case triple junction mobilities or quadruple points, which are dragging the grain boundary migration, play an important role. Thus the grain boundary movement becomes even more complex resulting in even more sensitive grain growth parameters. Exemplarily, a 3D model with implemented orientation data could be used to consider the faceting of the grain boundaries thus describe the anisotropy of the grain boundary energy. Faceting grain boundaries have been observed in the experimental part of this work and could be used to explain the occurrence of abnormal grains. Another important irregularity of the modelling and experimental part is that all grains were considered to have a circle shape, which would not be the case in a 3 dimensional CA model.

Both models do not depend on the material but both strongly depend on the grain structure resolution, especially the transition probabilities of the probabilistic model. Different materials lead to different grain growth kinetics where in the case of relatively fast grain growth kinetics, e.g. Nickel-based alloys, a high resolution of the grain structure must be used resulting in long simulation times. A simulation conducting on a large grid system needs a more powerful computer to process the large volume of data produced in the symulation

Due to the similarity of cell lattices there is a potential ability to couple the CA model and FEM, which enables a prediction of microstructural evolution after or during deformation. Incorporating temperature distributions or stored energy, the CA model may define additional arbitrary transition rules to be applied to the state variables, where recrystallization and phase transformation can be modelled. Moreover, a three dimensional CA model would highlight the effect of local grain boundary properties and incorporate local crystallographic impacts on the microstructural changes of heterogenous materials.

5 Conclusions

Based on an extensive literature survey, a deterministic and a probabilistic Cellular Automata (CA) Model have been developed to reflect the grain growth process for solution annealing of austenitic stainless steel 304L (18-9 Cr-Ni, balance Fe).

Developed CA models are capable of accounting for spatial and temporal descriptions of grain growth on a fine scale and at a high computational efficiency. Both the deterministic and probabilistic model couple the impact of the grain boundary curvature, annealing temperature, deformation energy, precipitates and grain boundary mobility on the grain growth process. The presence of precipitates is described either by using the limiting grain size defined by Zener in the deterministic model or by the dissolution of precipitates, influencing transition probabilities in the probabilistic model. Different methods for the description of stored energy, namely CD, MCD and M_{aver} values, incorporating crystal orientations are applied to predict normal grain growth in the presence of stored deformation energy. Depending on the grain structure resolution, the simulated and experimental micrographs are comparable from the topological viewpoint with evolution of grains towards stable six sided configurations and preferred tendency to form 120° dihedral angles between grain boundaries.

The un-deformed homogenized initial grain structures investigated by transmission electron microscopy proved the occurrence of faceted grain boundaries during annealing, explaining higher mobilities of a small part of grain boundaries assuming to result in abnormal grain growth. The annealing cycles were carried out at 900°C, 1000°C, 1100°C and 1200°C for annealing times of up to 40 hours where the average grain sizes, fraction of abnormal grains and grain size distributions were analyzed. Abnormal grain growth started at 1200°C after 120 minutes, at 1100°C after 8 hours, at 1000°C after 12 hours and at 900°C never due to the grain boundary pinning resulting from precipitations at grain boundaries.

Regression analysis of normal grain sizes showed that the grain growth exponents n depends strongly on the annealing temperature and rises from 0.31 at 1000°C to 0.43 at 1200°C defining an activation energy of 62.3 kJ/Kmol. For abnormal grain growth, n rises from 0.75 at 1000°C to 0.89 at 1200°C and defines a much lower activation energy of 33.7 kJ/Kmol. This decline of Q_{act} allows abnormal grains to grow faster.

The simulated results were very close to the underlying physical system. The quantitative analysis of grain growth phenomena started with the predictions of average normal and abnormal grain sizes. In accordance with experimental results, the simulated grain growth kinetics increase with temperature, which was described either by higher mobilities or higher transition probabilities. Assuming an heterogenous distribution of grain boundary mobilities or grain boundary energies in the evaluated physical system, the prediction of abnormal grain growth was possible. A very low fraction (0.1 %) of grain boundaries posses a higher mobility or transition probability resulting in abnormal grain growth. The CA simulations define a lower activation energy for abnormal grain growth, which was in accordance to the experimental results.

Due to the nonconformity of experiments and simulations for the prediction of separating grain size between normal and abnormal grain growth, a two-parameters approach was applied to predict normal grain size distributions. In the analysis of the simulated grain structures an improved definition of the fraction of abnormal grains was evaluated.

Further research should be done on the development of CA models on the grain structure evolution under complex deformation conditions, e.g. recovery and recrystallization. In order to do this, the CA model must couple the deformation parameters with Finite Elements Methods. A progressive 3D modelling set-up would decisively increase the accuracy of the modelling results.

List of Figures

List of Tables

Bibliography

[1] G. Gottstein: *Physikalische Grundlagen der Materialkunde*, vol. 2, Springer Berlin Heidelberg New York, 2001, ISBN 9783540711049.

[2] Wikipedia: *http://en.wikipedia.org* .

[3] P. Marshall: *Austenitic stainless steels: Microstructure and mechanical properties*, Springer, Elsevier Applied Science Publishers, Ripple Road, Barking, Essex, England, 1984, ISBN 0853342776.

[4] S. P. Products: *http://www.sppusa.com* .

[5] S. Jaiswal, D. Farrugia, Z. Husain, P. Ingham, J. Wilkinson and P. Morris: "Modelling of microstructure in rod rolling of alloy and stainless steels", *Technical steel research*, British Steel, Swinden technology centre, Moorgate, GB Rotherham S60 3AR, UK, 1992. Final report, Europian Commision.

[6] D. Lober: *http://www.metallograf.de* .

[7] M. E. Wahabi, J. Cabrera and J. Prado: "Hot working of two AISI 304 steels - a comparative study", *Materials Science and Engineering* **A 343**:116–125, 2003.

[8] H. Hong, B. Rho and S. Nam: "Correlation of the $M_{23}C_6$ precipitation morphology with grain boundary characteristics in austenitic stainless steel", *Materials Science and Engineering* **A 318**:285–295, 2001.

[9] H. Atkinson: "Theories of normal grain growth in pure single phase systems", *Acta Metallurgica* **36**(3):469–491, 1988.

[10] R. Bürgel: *Handbuch Hochtemperatur-Werkstofftechnik: Grundlagen, Werkstoffbeanspruchungen, Hochtemperaturlegierungen- und beschichtungen*, vol. 3, Fried. Vieweg & Sohn, Wiesbaden, 2006, ISBN 9783528231071.

[11] P. Flewitt and R. Wild: *Grain boundaries: Their microstructure and chemistry*, vol. 1, Wiley-VCH Verlag GmbH, Weinheim, Germany, 2001, ISBN 0471979511.

[12] M. Winning: *Grain boundary mechanics: Interactions between mechanical stresses and grain boundaries – New approaches to microstructure control and materials design*, Vuvillier Verlag Goettingen, Aachen, 2007, ISBN 3867271860.

[13] J. Hirth and J. Lotte: *Theory of dislocations*, vol. 2, Wiley, ISBN 0471091251, New York, 1982.

[14] S. Chan and R. Balluffi: "Study of energy vs misorientation for grain boundaries in gold by crystallite rotation method—II. Tilt boundaries and mixed boundaries", *Acta Metallurgica* **34**:2191–2199, 1986.

[15] J. Burke and D. Turnball: "Recrystallization and grain growth", *Progress in Metal Physics* **3**:220–292, 1952.

[16] P. Beck, J. Kremer, L. Demer and M. Holzworth: "Grain growth in high purity aluminium and in aluminium-magnesium alloys", *Transcriptions of AIME* **175**:372–380, 1949.

[17] N. Gao and T. Baker: "Real time-temperature models for monte carlo simulations of normal grain growth", *ISIJ International* **38**(7):744–751, 1998.

[18] C. Sellars and J. Whiteman: "Recrystallisation and grain growth in hot rolling", *Metal Science* **13**:187–194, 1979.

[19] A. Yoshi, M. Fujioka and Y. Watanabe: "Modelling of microstructural evolution and mechanical properties of steel plates produced by thermo-mechanical control process", *ISIJ international* **32**:3395–3404, 1992.

[20] P. Manohar, D. Dunne, T. Chandra and C. Kilmore: "Continuous Cooling Transformation Behavior of Microalloyed Steels Containing Ti, Nb, Mn and Mo", *ISIJ international* **36**:194–200, 1996.

[21] H. Hu: "Grain growth in zone-refined iron", *Canadian Metallurgical Quarterly* **13**(1):275–286, 1974.

[22] F. Humphreys: "A network model for recovery and recrystallisation", *Scripta Metallurgica et Materialia* **27**(11):1557–1562, 1992.

[23] M. Anderson, D. J. Srolovitz, G. S. Grest and P. Sahni: "Computer simulations of grain growth-I. Kinetics", *Acta Metallurgica* **32**(5):783–791, 1984.

[24] D. Srolovitz, M. Anderson, P. Sahni and G. Grest: "Computer simulation of grain growth-II. Grain size distribution, topology, and local dynamics", *Acta Metallurgica* **32**(5):793–802, 1984.

[25] D. Srolovitz, M. Anderson, G. Grest and P. Sahni: "Computer simulation of grain growth-III. Influence of a particle dispersion", *Acta Metallurgica* **32**(9):1429–1438, 1984.

[26] G. Grest, D. Srolovitz and M. Anderson: "Computer simulation of grain growth-IV. Anisotropic grain boundary energy", *Acta Metallurgica* **33**(5):509–520, 1985.

[27] D. Srolovitz, G. G.S. and M. Anderson: "Computer simulation of grain growth-V. abnormal grain growth", *Acta Metallurgica* **33**(12):2233–2247, 1985.

[28] D. Fan and L. Chen: "Computer simulation of grain growth using a continuum field model", *Acta Materialia* **45**(2):611–622, 1997.

[29] D. Fan, C. Geng and L. Chen: "Computer simulation of topological evolution in 2D grain growth using a continuum diffuse-interface field model", *Acta Materialia* **45**(3):1115–1126, 1997.

[30] Y. Liu, T. Baudin and R. Penelle: "Simulation of normal grain growth by cellular automaton", *Scripta Metallurgica* **34**:1679–1683, 1996.

[31] C. Smith: "Grain, phases and intefaces: an interpretation of microstructure", *Transcription of AIME* **175**:15–51, 1948.

[32] T. Gladman: "On the theory of the effect of precipitate particles on grain growth in metals", *Processing of Royal Society* **A294**:298–308, 1966.

[33] T. Gladman and F. Pickering: "Grain coarsening of austenite", *Journal of the Iron and Steel Institute* **6**:653–664, 1967.

[34] P. Rios: "Abnormal grain growth in materials containing particles", *Acta Metallurgica et Materialia* **42**(3):839–843, 1994.

[35] R. Elst, J. V. Humbeeck and L. Delaey: "Evaluation of grian growth criteria in particle-containing materials", *Acta Metallurgica* **36**(7):1723–1729, 1988.

[36] C. Smith: "Microstructure", *Transcription of American Society for Metals* **45**:533–575, 1953.

[37] J. Burke: "Some factors affecting the rate of grain growth in metals", *Transcript of Metallurgical Society AIME* **180**:73–91, 1949.

[38] V. Voort: *ASM Handbook Volume 9 - Metallography and Microstructures*, ASM International, george f. vandervoort ed., 2004, ISBN 0871707063.

[39] S. Kurtz and F. Carpay: "Microstructure and normal grain growth in metals and ceramics. Part I. Theory", *Jornal of Applied Physics* **51**(11):5725–5744, 1980.

[40] D. Quidort and Y. Brechet: "A Model of Isothermal and Non Isothermal Transformation Kinetics of Bainite in 0.5C Steels", *ISIJ International* **42**:1010–1017, 2002.

[41] P. Rios: "A theory of grain boundary pinning by particles", *Acta Metallurgica* **35**(12):2805–2814, 1987.

[42] P. Rios: "Abnormal grain growth in pure materials", *Acta Metallurgica et Materialia* **40**(10):2765–2768, 1992.

[43] P. Rios: "Abnormal grain growth in the presence of coarsening particles", *Acta Metallurgica et Materialia* **40**(4):649–651, 1992.

[44] P. Rios: "Abnormal growth and abnormal coarsening with a quasi-stationary distribution", *Materials Science and Engineering* **A165**:L5–L8, 1993.

[45] P. Rios: "On the relationship between pinning force and limiting grain radius", *Scripta Materialia* **34**(8):1185–1188, 1996.

[46] P. Rios: "Abnormal grain growth development from uniform grain size distribution", *Acta Materialia* **45**(4):1785–1789, 1997.

[47] P. Rios: "Abnormal grain growth development from uniform grain size distribution due to mobility advantage", *Scripta Materialia* **38**(9):1359–1364, 1998.

[48] P. Rios, G. Fonseca, J. Lins and F. Augusto: "Grain curvature measurements: A comparison with geometrical models", *Scripta Materialia* **57**:727–730, 2007.

[49] J. L. Walter and C. G. Dunn: "Impurity Atoms and Energy Relationship of Surfaces", *Acta Metallurgica* **8**:497–503, 1960.

[50] R. Cahn and P. Haasen: *Pysical Metallurgy*, North Holland, Amsterdam, Netherlands, 4th ed., 1996, ISBN 0444898751.

[51] S. Lee, J. Choi and D. Y. Yoon: "The dependence of abnormal grain growth on initial grain size in 316 L stainless steel", *Zeitschrift für Metallkunde* **92**(7):655–662, 2001.

[52] H. Gleiter: "The mechanism of grain boundary migration", *Acta Metallurgica* **17**(5):565–573, 1969.

[53] S. Lee, N. Hwang, D. Yoon and M. Henry: "Grain boundary faceting and abnormal grain growth in nickel", *Metallurgical and Materials Transactions A* **31A**(3):985–994, 2000.

[54] J. Koo and D. Yoon: "The Dependence of Normal and Abnormal Grain Growth in Silver on Annealing Temperature and Atmosphere", *Metallurgical and Metarials Transactions A* **32A**:469–475, 2001.

[55] J. Choi and D. Yoon: "The temperature dependence of abnormal grain growth and grain boundary faceting in 316 L stainless steel", *ISIJ International* **41**(5):478–483, 2001.

[56] J. Koo and D. Yoon: "Abnormal grain growth in bulk Cu-The dependence on initial grain size and annealing temperature", *Metallurgical and Metarials Transactions A* **32A**(8):1911–1926, 2001.

[57] H. Gleiter: "Theory of grain boundary migration rate", *Acta Metallurgica* **17**(7):853–862, 1969.

[58] Y. Saito and M. Enomoto: "Using Monte Carlo methog for simulating grain growth", *ISIJ International* **32**:267–274, 1992.

[59] Y. Saito: "Monte Carlo simulation of grain growth in three dimensions", *ISIJ International* **38**:559–566, 1998.

[60] H. Frost, C. Thompson and D. Walton: "Simulation of thin films grain structure -II. Abnormal grain growth", *Acta Metallarugica et Materialia* **40**(4):779–793, 1992.

[61] F. Humphreys: "A unified theory of recovery, recrystallization and grain growth, based on the stability and growth of cellular microstructures. The effect of second-phase particles", *Acta Materialia* **45**(12):5031–5039, 1997.

[62] M. Rappaz and C. Gandin: "Probabilistic modelling of microstructure formation in solidification processes", *Acta Materialia* **41**:345–360, 1993.

[63] S. Wolfram: *A new kind of science*, Wolfram Media, USA, 2002, ISBN 9781579550080.

[64] J. Koc and V. Paidar: "Modelling of the efect of tripple junctions on grain boundary migration by a cellular automaton", *Journal de Physique IV* **11**(5):585–592, 2001.

[65] D. Raabe: "Intorduction of a scaleable three-dimensional cellular automaton with a probabilistic switching rule for the discrete mesoscale simulation of recrystallization phenomena", *Philosophical Magazine A* **79**(10):2339–2358, 1999.

[66] A. Rollet and D. Raabe: "A hybrid model for mesoscopic modelling of recrystallization", *Computational Materials Science* **21**(1):69–78, 2001.

[67] H. Hasselbarth and I. Goebel: "Simulation of recrystallisation by cellular automata", *Acta materialia* **39**:2135–2143, 1991.

[68] C. Gandin, M. Rappaz and R. Tintillier: "Three-Dimensional Probabilistic Simulation of Solidification Grain Structures : Application to Superalloys Precision Castings", *Metallurgical Transactions* **24**:467–479, 1993.

[69] C. Gandin, M. Rappaz and R. Tintillier: "3-Dimensional Simulation of the Grain Formation in Investment Casting", *Metallurgical Transactions* **25**:629–635, 1994.

[70] C. Gandin and M. Rappaz: "A Coupled Finite Element - Cellular Automaton Model for the Prediction of Dendritic Grain Structures in Solidification Processes", *Acta Materialia* **42**:2233–2246, 1994.

[71] J. Gawad, M. Paszynski, P. Matuszyk and L. Madej: "Cellular automata coupled with hp-adaptive finite element method applied to simulation of austenite-ferrite phase transformation with a moving interface", in: "The 12th International Conference on Metal Forming 2008 (Krakow Poland)", vol. 2, pp. 579–586, Steel research international, Verlag Stahleisen GmbH, 2008.

[72] W. Yu, S. Banks and E. Palmiere: "Cellular automata modelling of austenite grain coarsening during reheating", *Thermomechnical Processing of Steel* pp. 186–193, 2000.

[73] W. Yu: *Cellular automata modelling of austenite grain coarsening during reheating*, Ph.D. thesis, The University of Sheffield, Department of Engineering Materials, 2002.

[74] W. Yu, C. Wright, S. Banks and E. Palmiere: "Cellular automata method for simulating microstructure evolution", *IEE Processing, Science, Measurement and Technology* **150**(5):211–213, 2003.

[75] W. Yu, E. Palmiere, S. Banks and J. Han: "Cellular automata modelling of austenite grain coarsening during reheating-I. Normal grain coarsening", *Journal of University of Science and Technology, Beijing* **11**(6):517–523, 2004.

[76] W. Yu, E. Palmiere, S. Banks and J. Han: "Cellular automata modelling of austenite grain coarsening during reheating-I. Abnormal grain coarsening", *Journal of University of Science and Technology, Beijing* **12**(1):26–32, 2005.

[77] S. Raghavan and S. Sahay: "Modeling the grain growth kinetics by cellular automaton", *Materials Science and Engineering A* **A 445-446**:203–209, 2007.

[78] S. Raghavan and S. Sahay: "Modeling of topological features during grain growth by cellular automaton", *Computational Material Science* **46**:92–99, 2009.

[79] Y. Lan, D. Li, C. Huang and Y. Li: "A cellular automaton model for austenite to ferrite transformation in carbon steel under non-equilibrium interface conditions", *Modelling and Simulation in Materials Science and Engineering* **12**:719–729, 2004.

[80] Y. Lan, D. Li and Y. Li: "A mesoscale cellular automaton model for curvature driven grain growth", *Metallurgical and Materials Transactions B* **37**(2):119–129, 2006.

[81] N. Yazdipour, C. Davies and P. Hodgson: "Microstructural modeling of dynamic recrystallization using irregular cellular automata", *Computational Materials Science* **44**:566–576, 2008.

[82] K. Jannsens: "Random grid, three-dimensional, space-time coupled cellular automata for the simulation of recrystallization and grain growth", *Modelling and Simulation in Material Science and Engineering* **11**:157–171, 2003.

[83] H. Schumann and H. Oettel: *Metallographie*, vol. 14, Wiley-VCH Verlag, 2005, ISBN 352730679X.

[84] Struers: *http://www.struers.com* .

[85] G. Winter: *Grain growth in dependence of different annealing times and temperatures in a austenitic stainless steel*, Master's thesis, University of Leoben, 2009.

[86] R. Djaic and J. Jonas: "Static recrystallization of austenite between intervals of hot working", *Journal of the Iron and Steel Institute* pp. 256–261, 1972.

[87] H. Hu and B. Rath: "On the time exponent in isothermal grain growth", *Metallurgical Transactions* **01**:3181–3184, 1970.

[88] M. Candic, B. Tian, M. Kamaya, G. Winter and C. Sommitsch: "Simulation of the microstructure evolution by cellular automaton", in: "Conference on Hot Forming and Steel Properties, Grado, Italy", September, 2009.

[89] M. Candic, G. Winter, B. Tian and C. Sommitsch: "Cellular automaton modelling of grain growth during annealing of alloy Fe-19Cr-8Ni", in: "TMS, San Francisco, California, USA", March, 2009.

[90] C. Zener and C. Smith: "Private communications", *Transaction of American Institute for Mining and Metallurgical Engeners* **175**:15–25, 1949.

[91] MatCalc: *http://www.matcalc.com* .

[92] S. Cummins, M. Francois and D. B. Kothe: "Estimating curvature from volume fractions", *Computers and structures* **83**:425–434, 2005.

[93] M. Kamaya, A. Wilkinson and J. Tichmarsh: "Quantification of plastic strain of stainless steel and nickel alloy by electron backscatter diffraction", *Acta Meterialia* **54**:539–548, 2006.

[94] M. Kamaya: "Measurement of local plastic strain distribution of stainless steel by electron backscatter diffraction", *Materials Characterization* **60**(2):125–132, 2008.

[95] A. Wilkinson and D. Dingley: "Quantitative deformation studies using electron back scatter patterns", *Acta Metallurgica et Materialia* **39**:3047–3055, 1991.

[96] A. Sutton: "Statistical representations and analysis of orientation data", *Philosophical Magazine Letters* **74**:389–394, 1996.

[97] A. Wilkinson: "A new method for determining small misorientations from electron back scatter diffraction patterns", *Scripta Materialia* **44**:2379–2385, 2001.

[98] M. Kamaya: "Measurement of crystal misorientation distribution by electron backscatter diffraction", *Transactions of Japan Society of Mechanical Engineering A* **74**(3):315–322, 2007.

[99] M. Kamaya, J. D. Fonseca, L. Li and M. Preuss: "Local Plastic Strain Measurement by EBSD", *Applied Mechanics and Materials* **7-8**:173–179, 2007.

[100] M. Kamaya, J. Q. D. Fonseca, L. Li and M. Preuss: "Local Plastic Strain Measurement by EBSD", in: "The 5th BSSM International Conference on Advances in Experimental Mechanics, Manchester", pp. 137–179, 2007.

[101] M. Kamaya: "Measurement of local plastic strain distribution of stainless steel by electron backscatter diffraction", *Materials Characterization* **60**:125–132, 2009.

[102] A. Arsenlis and D. M. Parks: "Crystallographic aspects of geometrically-necessary and statistically-stored dislocation density", *Acta Materialia* **47**:1597–1611, 1999.

[103] F. Humphreys and M. Hatherly: *Recrystallization and related annealing phenomena*, vol. 2nd Edition, Elsevier Ltd, Oxford, UK, 2003, ISBN 0080441645.

[104] M. Candic, B. Tian, S. Kleber and C. Sommitsch: "Entwicklung der Gefuegestruktur und Beurteilung der effektiven Dehnung bei der Warmumformung", in: "XXVI. Verformungskundliches Kolloquium, Planneralm/Donnersbach", pp. 151–157, 2007.

[105] M. Candic, B. Tian, S. Kleber, S. Mitsche and C. Sommitsch: "Investigation of retained deformation energy after hot forming and its influence on the abnormal grain growth of the nickel based alloy 80a", in: "TMS 2008", New Orleans, Louisiana, USA, 2008.

[106] M. Candic, B. Tian, M. Wießner, M. Kamaya and C. Sommitsch: "On the retained strain during multipass deformation for the austenitic stainless steel 304L", in: "2nd Steelsim Conference, Graz", March, 2007.

[107] G. Rathenau and J. Custers: "Secondary recrystallization of face-centred Ni-Fe alloy", *Philips Research Reports* **4**:241–260, 1949.

[108] C. Antonione, G. Gatta, G. Riontino and G. Venturello: "Grain growth and secondary recrystallization in iron", *Journal of Materials Science* **8**:1–10, 1973.

[109] C. Antonione, F. Marino, G. Riontino and M. Tabasso: "Effect of slight deformations on grain growth in iron", *Journal of Materials Science* **12**:747–750, 1977.

[110] J. Zauner: *Herstellung und Analyse des abnormalen Kornwachstums für den austenitischen Stahl 304L nach der Warmumformung*, Master's thesis, Chair of Metal Forming, Department Product Engineering, University of Leoben, 2009.

[111] W. Mullins: "Estimation of the geometrical rate caonstant in idealized three dimensional grain growth", *Acta Metallurgica* **37**(11):2979–2984, 1989.